RIVELATORI A CONTEGGIO DI SINGOLO FOTONE E LORO APPLICAZIONI

Valeria Rosso
Universita' di Pisa, Dipartimento di Fisica "E. Fermi", INFN Sezione di Pisa

RIVELATORI A CONTEGGIO DI SINGOLO FOTONE E LORO APPLICAZIONI

- Introduzione alla Radiografia Digitale
- Un sistema di rivelazione a conteggio di singolo fotone
  - Mammografia Digitale
  - Altre applicazioni
- Il progetto MATISSE

The beginning

- 1895 Prof. Wilhelm Conrad Roentgen discovers X-rays
- Phosphor screens introduced early 20th century
- In the ‘70 years routine use of fluoroscopy with image intensifiers coupled to TV cameras
- In the ‘80 years 'the radiography becomes digital (imaging plates, CCDs, flat-panels, semiconductor detectors both amorphous and crystalline)

M. Hoheisel, NIM A563 (2006) 215–224

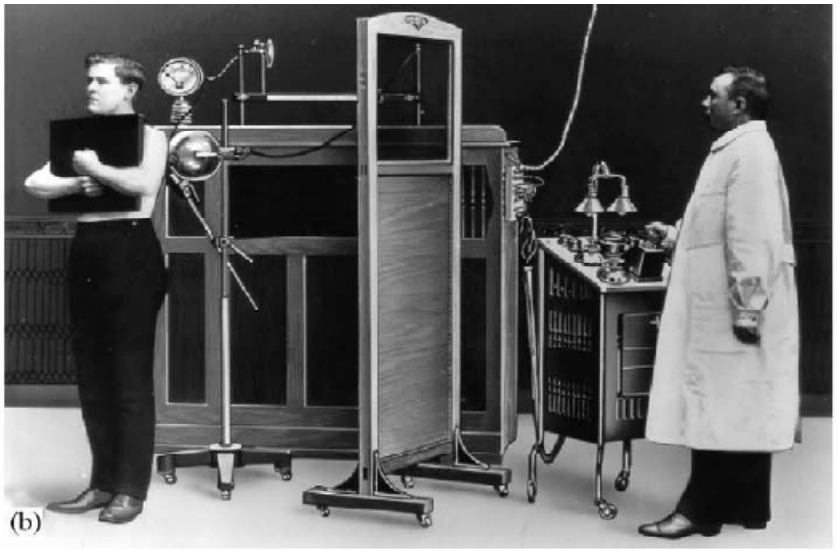

Digital Radiographic Imaging

- Film-screen systems:
  - detection and display on the same medium
- Digital radiography features:
  - transmitted intensity pattern sampling
  - spatial sampling

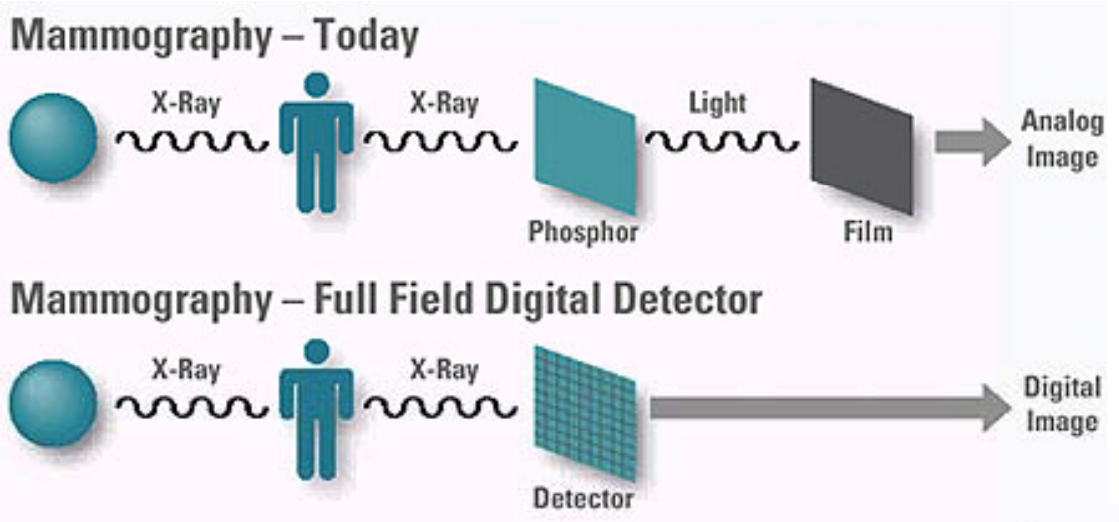

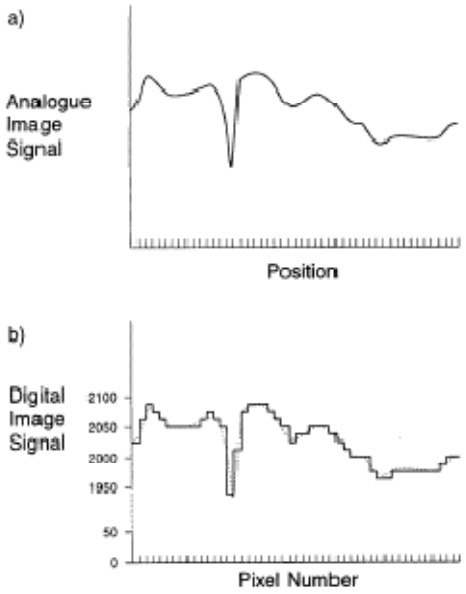

X-ray film: dynamic range

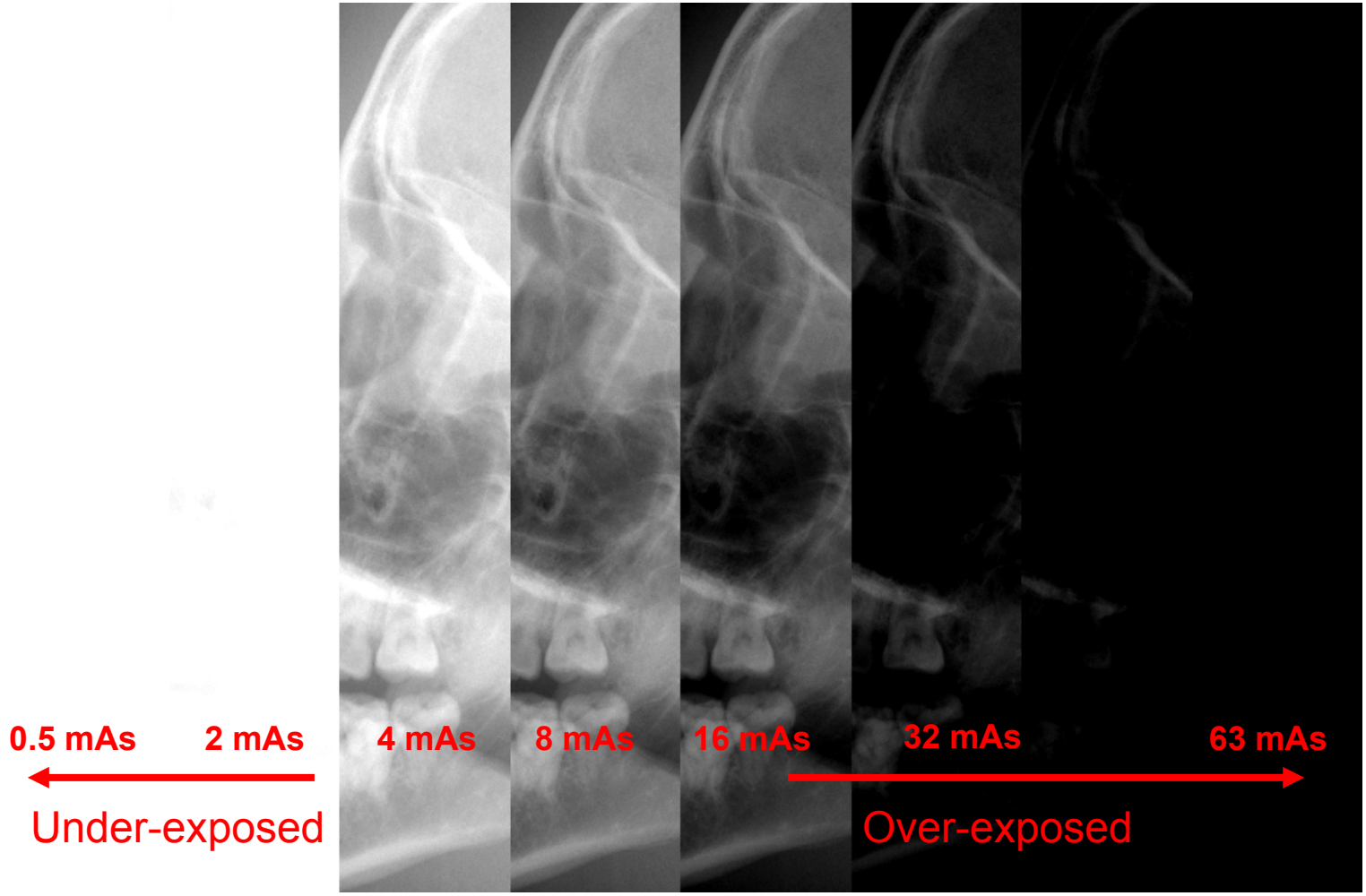

Flat panel detector: dynamic range

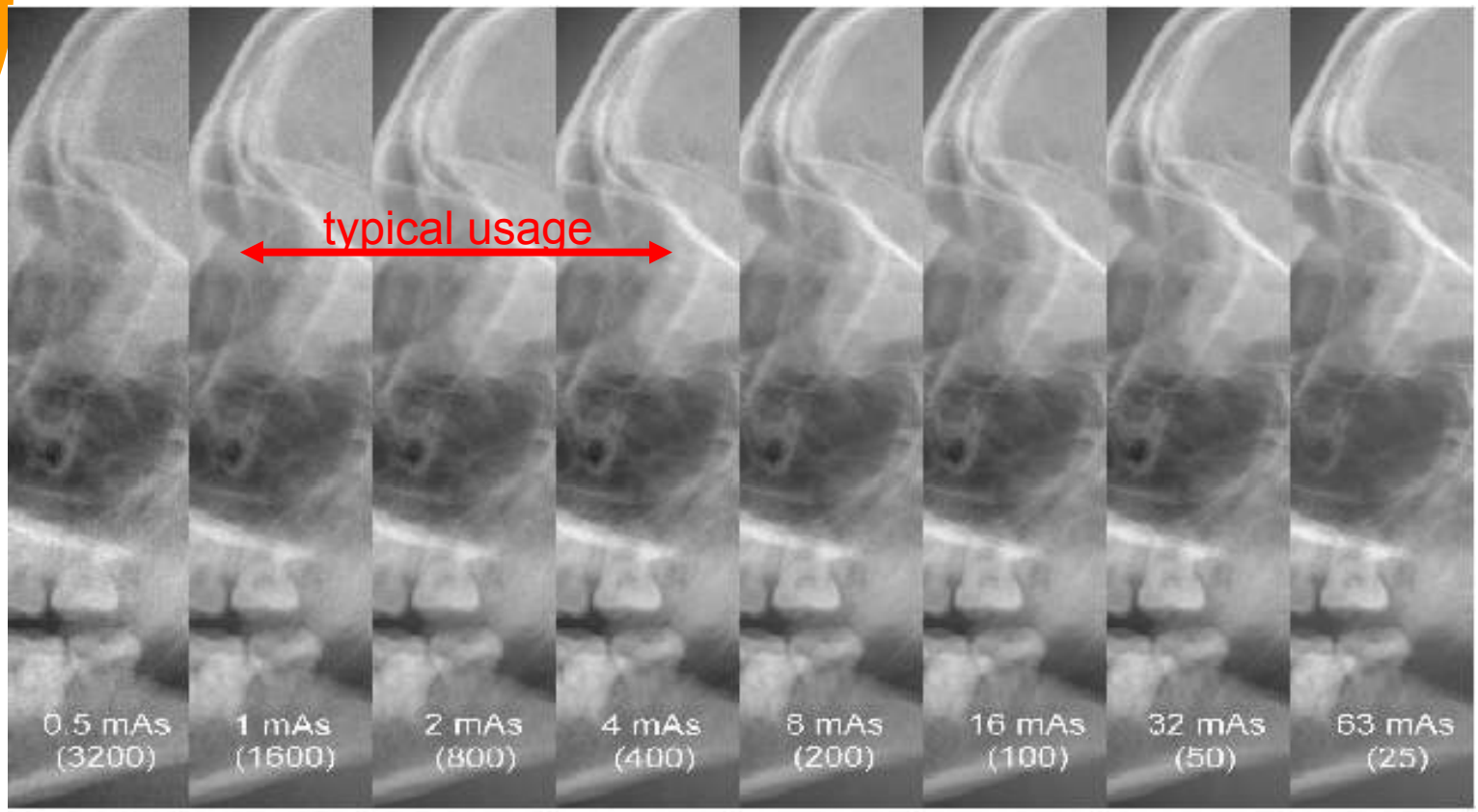

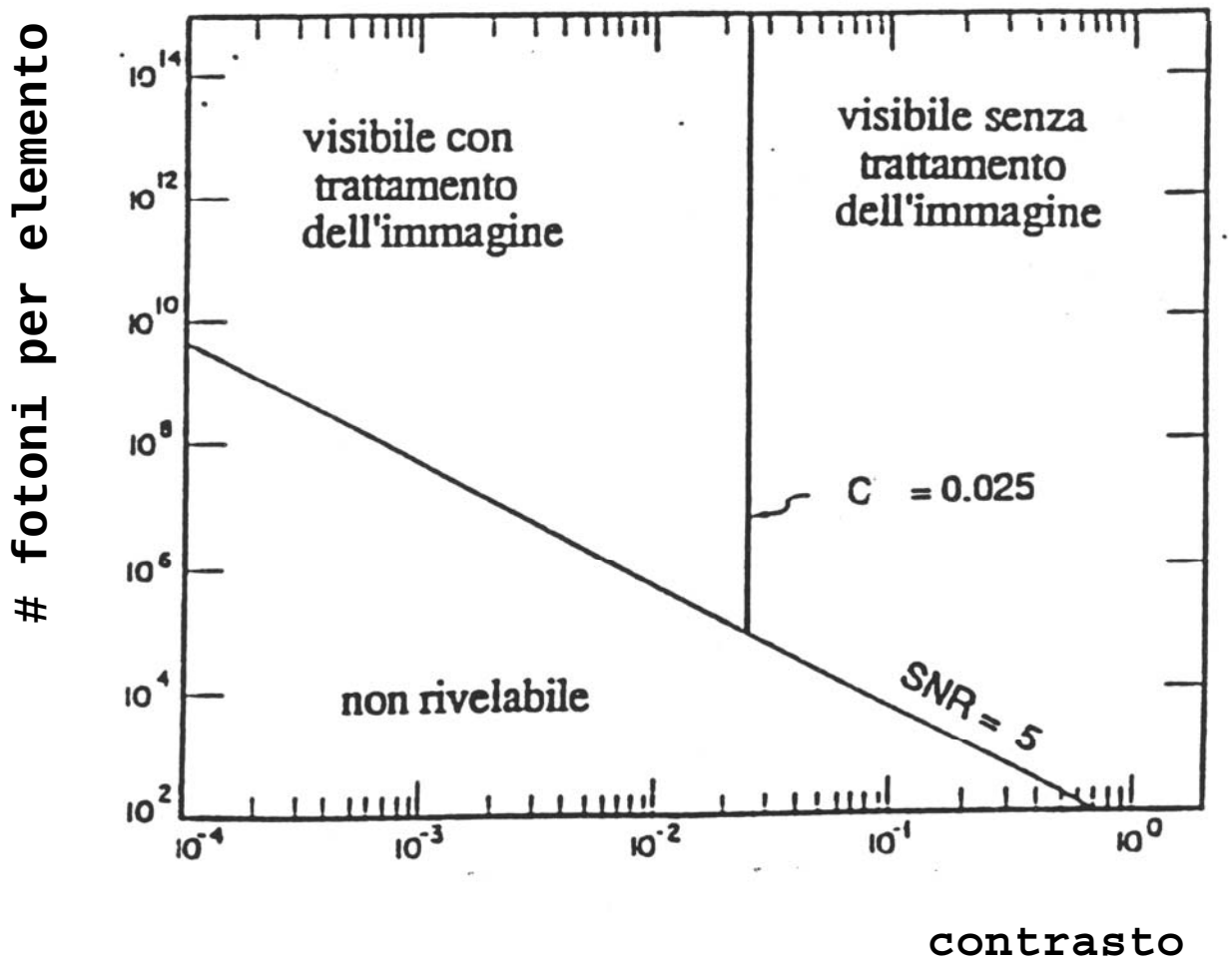

Albert Rose- Vision: human and electronic

Physical Parameters

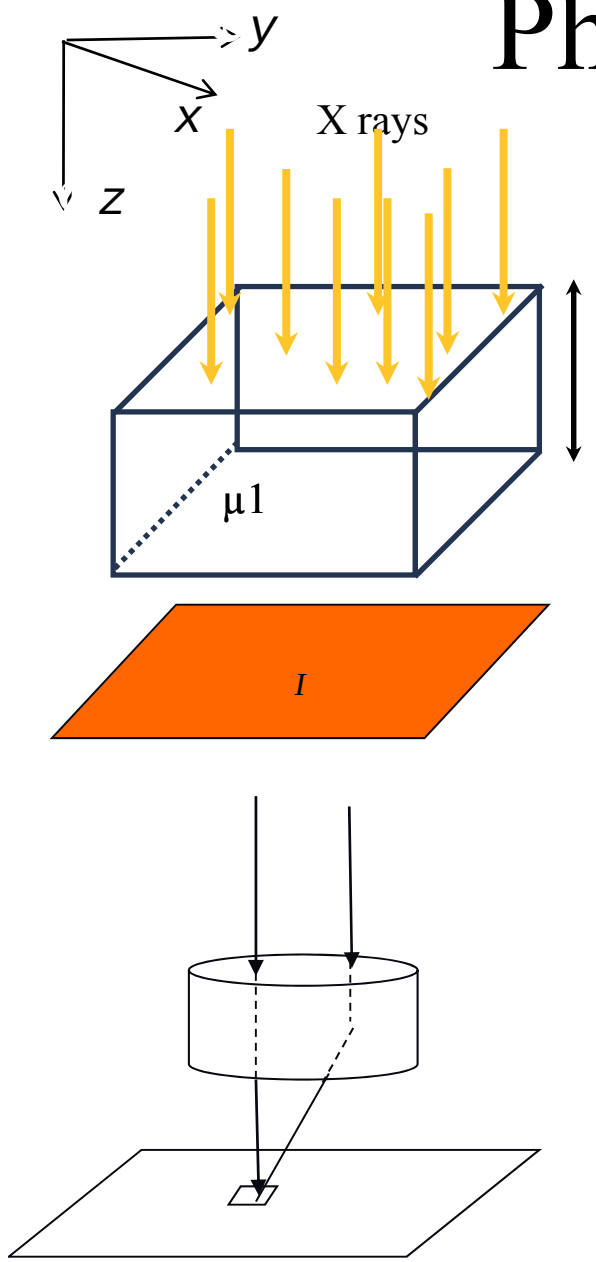

N incident photons per unit area

$I(x,y)$ dxdy energy absorbed in dxdy of detector

$$I(x,y) = \text{primary} + \text{secundary}$$

$$I(x,y) = N\varepsilon(E,0)Ee^{-\int \mu(x,y,z)dz} + \int \varepsilon(E_s,\theta)E_s S(x,y,E_s\Omega)d\Omega dE_s$$

S is slowly varing function: the integral can be sostituted with the value at the centre of the image

$$\bar{S} = \int S(0,0,E_s\Omega)d\Omega dE_s$$

$$\bar{\varepsilon}(E)E = \int \varepsilon(E_s,\theta)E_s S(0,0,E_s\Omega)d\Omega dE_s / \bar{S}$$

$$I(x,y) = N\varepsilon(E,0)Ee^{-\int \mu(x,y,z)dz} + \bar{S}\bar{\varepsilon}(E)E$$

R=scattered/primary

$$I(x,y) = N\varepsilon(E,0)Ee^{-\int \mu(x,y,z)dz}(1+R)$$

Physical Parameters

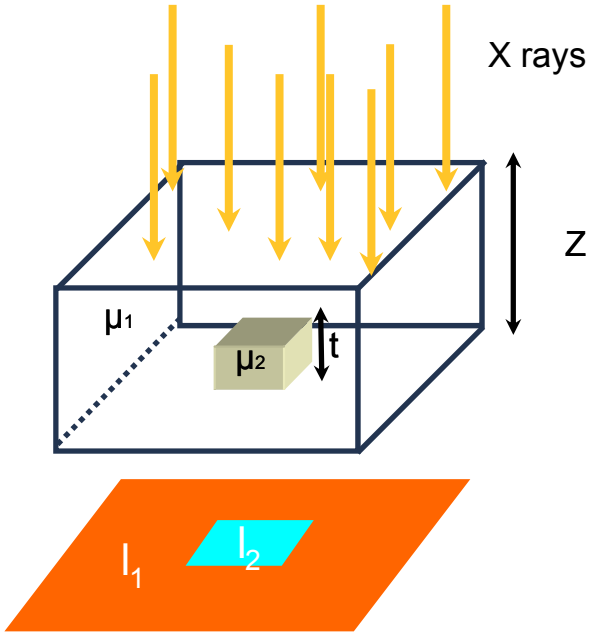

$$I_1 = N\varepsilon(E,0)Ee^{-\mu_1 z} + \overline{S}\overline{\varepsilon}(E)E$$

$$I_2 = N\varepsilon(E,0)Ee^{-\mu_1(z-t)-\mu_2 t} + \overline{S}\overline{\varepsilon}(E)E$$

CONTRAST

$$C = \frac{I_1 - I_2}{I_1} \qquad C = \frac{1 - e^{-(\mu_2 - \mu_1)t}}{1 + R}$$

SIGNAL

$$signal = (I_1 - I_2)A = ICA = CAN\varepsilon Ee^{-\mu_1 z}(1 + R)$$

Digital Mammography

Principal Mammography task:
✓Detection of the tumor masses (objects with contrast < 1% and diameter ≈ 1-5 mm)
✓Detection of the microcalcifications (objects with high contrast and small dimensions ≈ 100 μm)

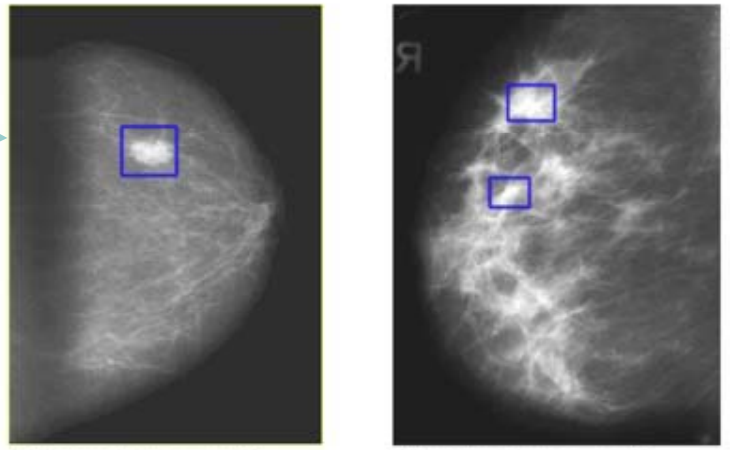

a) Breast carcinoma surrounded by adipose tissue

b) Breast carcinoma surrounded by fibroglandular tissue

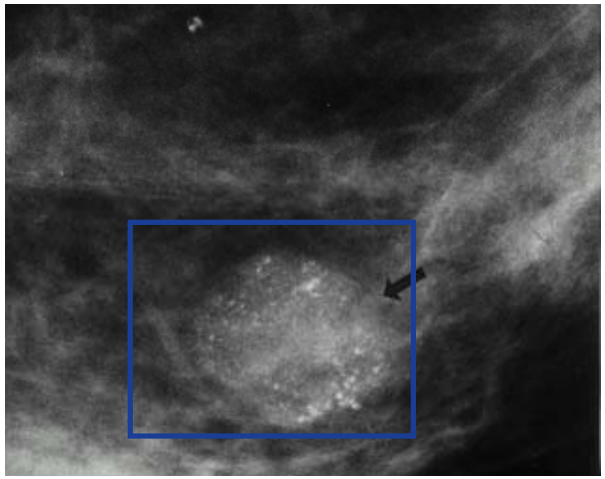

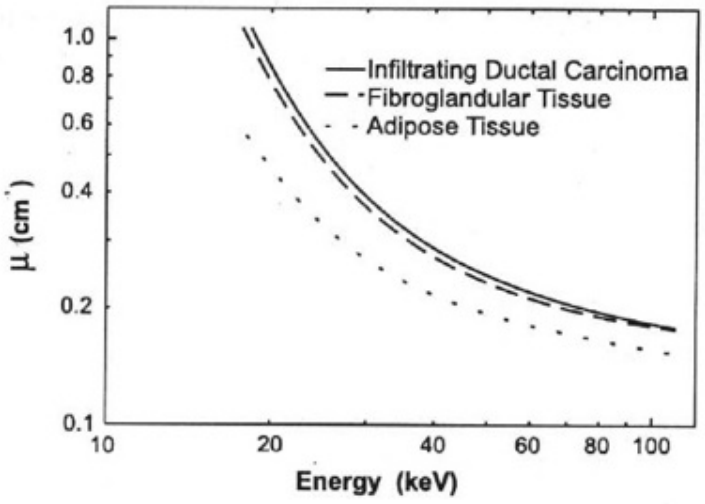

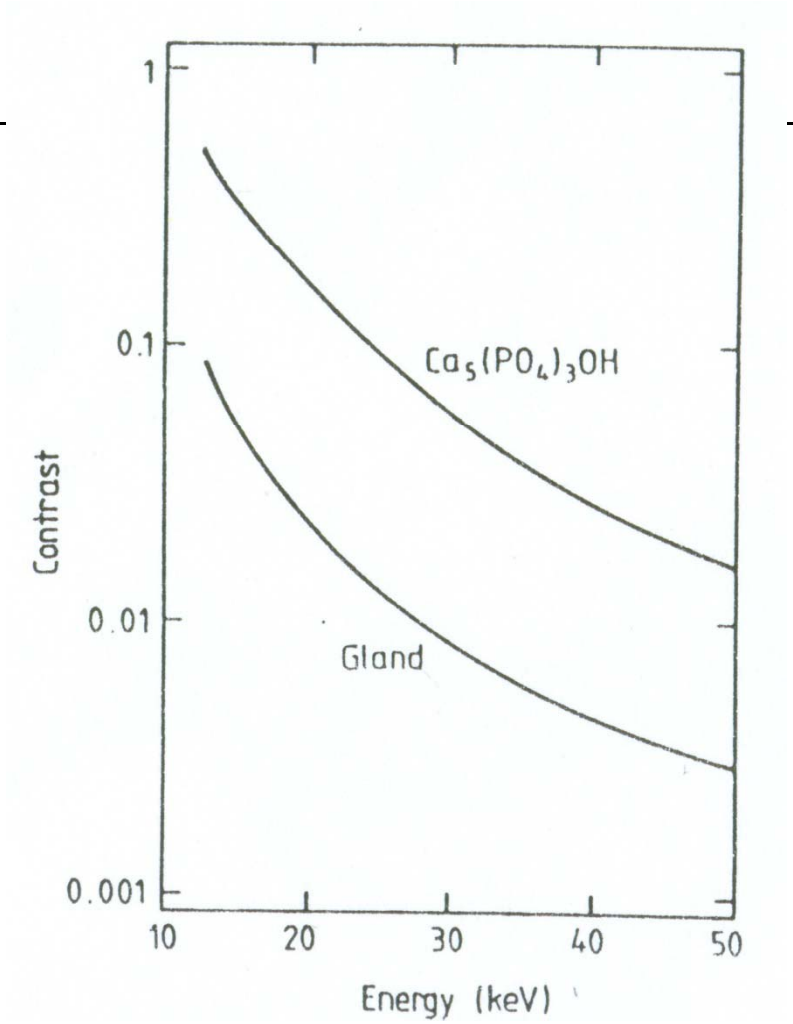

Dettagli immersi in tessuto mammario sano

100um di calcio

1mm tessuto ghiandolare

Requisiti per un sistema per la MD

Dobbiamo rivelare dettagli a basso contrasto

- C ~ alcuni %
- flusso: 10^5-10^6 $\gamma/(s\ mm^{-2})$

Scelta del rivelatore:

- geometria di lettura
- materiale

Scelta dell'electronica di read-out

Realizzare il sistema di rivelazione

Test del sistema di rivelazione

STRIP DETECTORS

n+n electronic channels

multiple hits problem

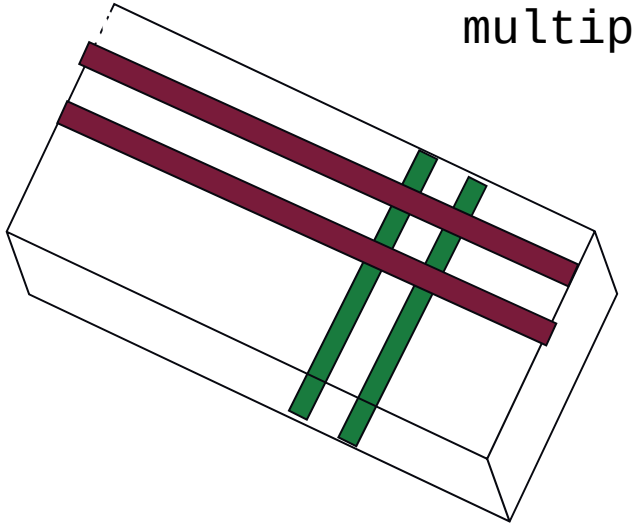

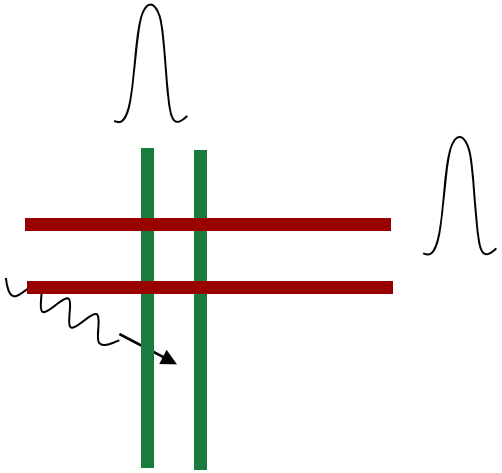

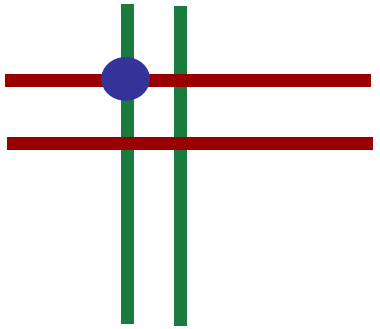

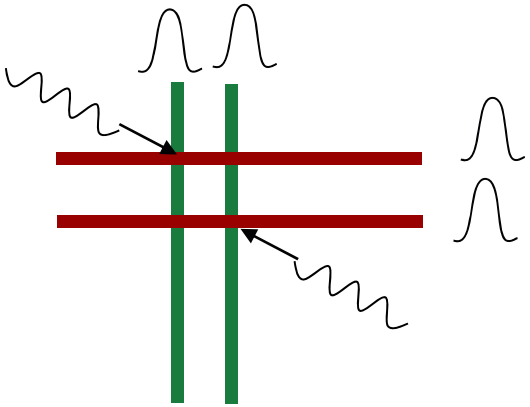

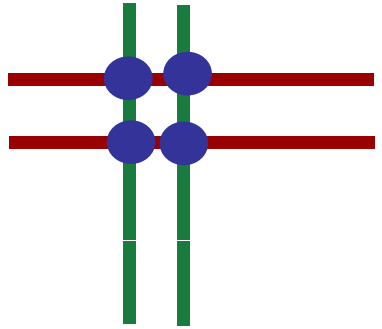

La probabilita' di avere **r** eventi in un intervallo **T** se gli eventi sono indipendenti e hanno un rate costante υ con $\tau=1/\upsilon$, e' calcolabile facendo uso della distribuzione di Poisson

$$P(r) = \frac{\mu^r e^{-\mu}}{r!} \qquad \mu = \frac{T}{\tau}$$

Considerando:

una superficie di 1.4x1.4 cm2, un tempo di campionamento T=25ns e un flusso di 5.10^4 $\gamma/(s\ mm^2)$

P(0)=78% P(1)=19% P(2)=2,4%

E' necessaria una geometria di elettrodi di lettura a pixels

Numero di canali di lettura n^2 contro i 2n di un rivelatore doppia faccia

Efficienze: GaAs 200µm Si 300µm

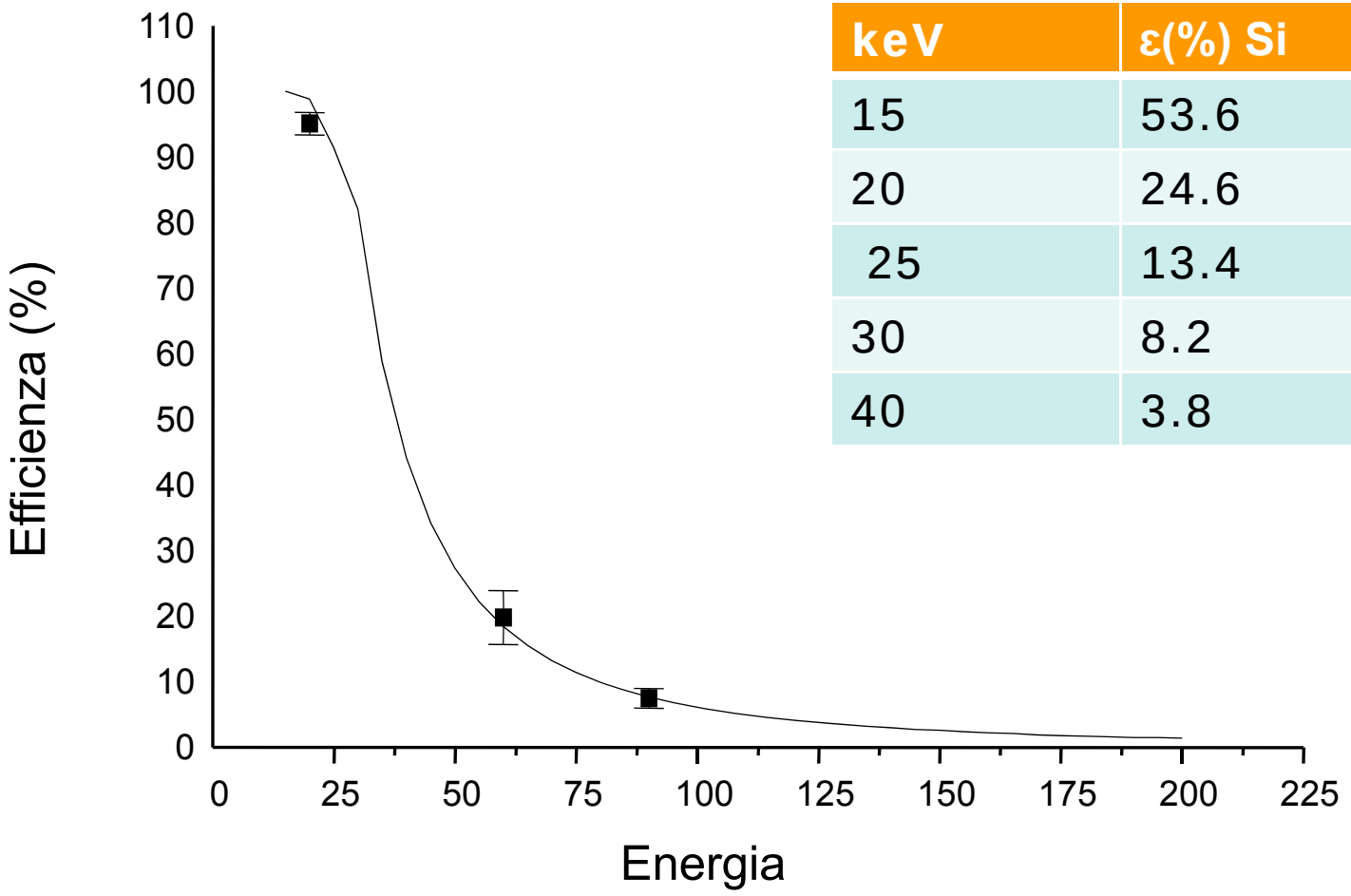

keV	ε(%) Si
15	53.6
20	24.6
25	13.4
30	8.2
40	3.8

GaAs : layout del wafer pisa2 e mappa delle matrici 64x64

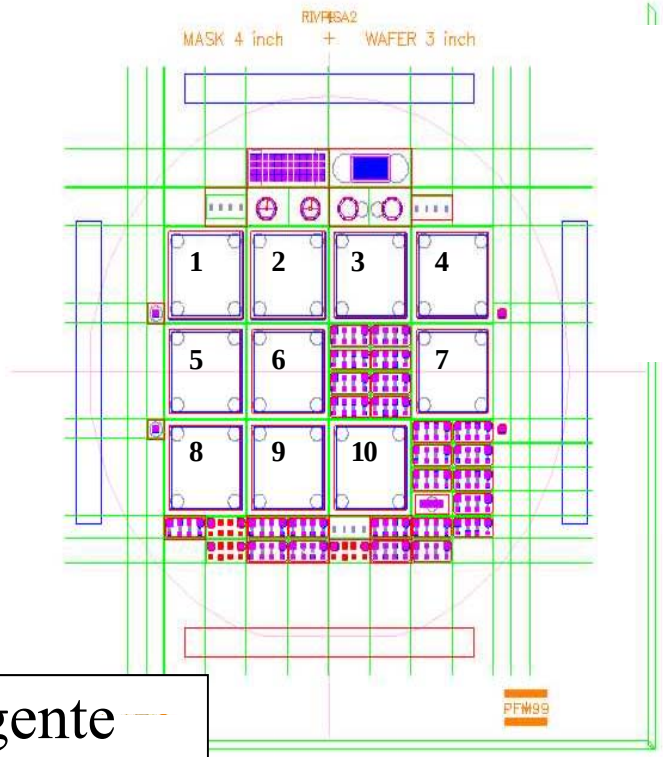

Commercial LEC grown GaAs
Carbon density: studied

Double Schottky barrier developed by AMS

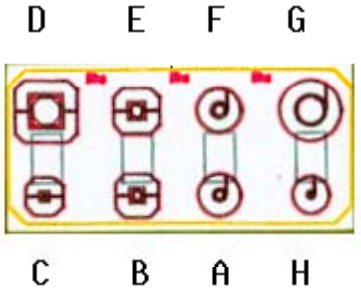

Struttura test

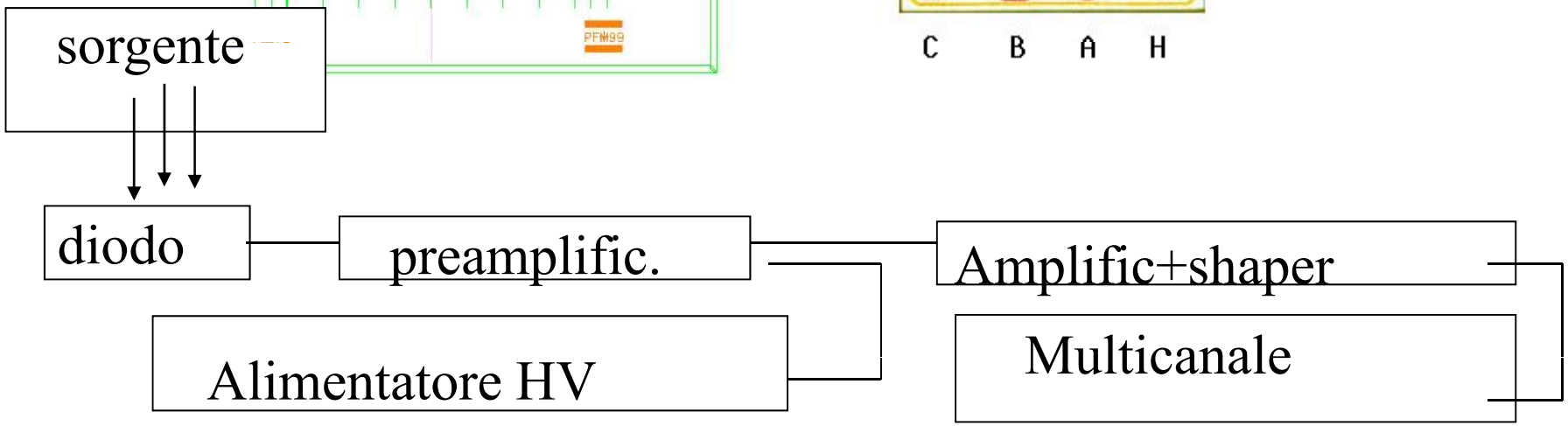

Pad di diametro 2 mm e spessore 200 um (ACR 68 [C] = 1.3 10^{15} cm^{-3})

sorgente ^{241}Am studio CCE

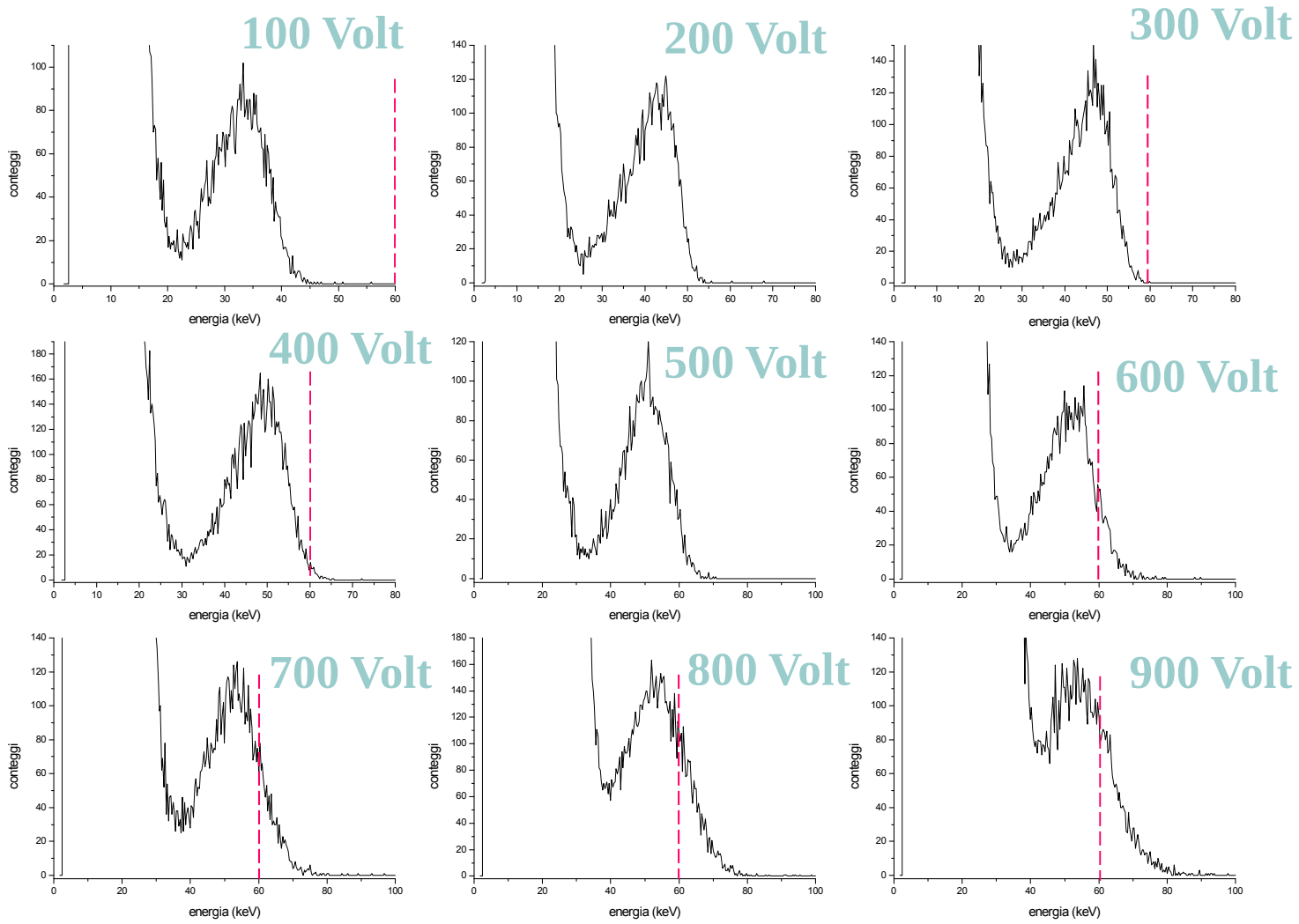

20 60 keV

ACR 68 [C] = 1.3 10^{15} cm^{-3}

sorgente ^{241}Am

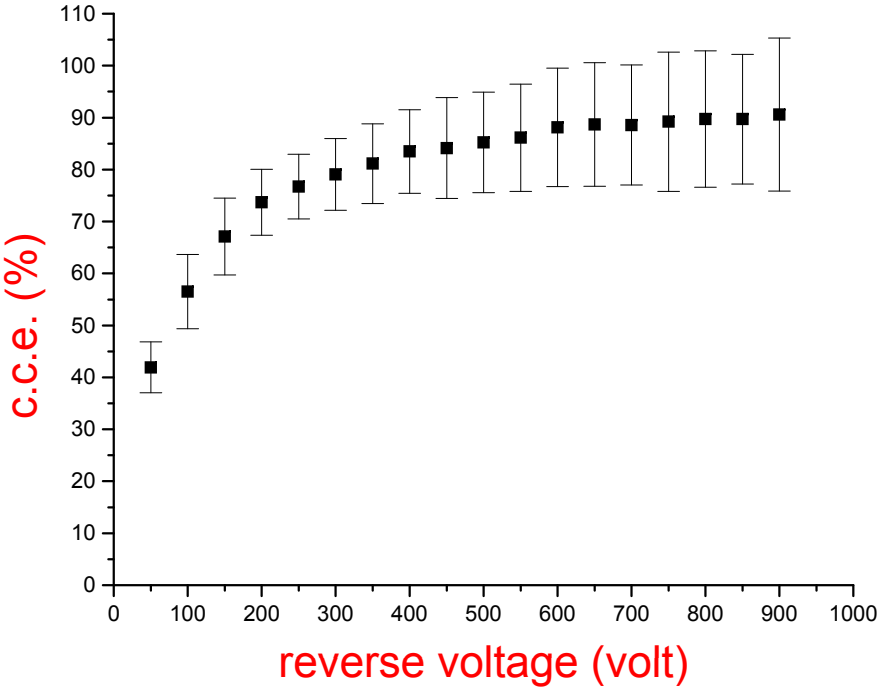

V_{bias}	c.c.e.(%)
100	56.5 ± 7.2
200	73.7 ± 6.3
300	79.1 ± 6.9
400	83.5 ± 8.0
500	85.2 ± 9.7
600	88.1 ± 11.4
700	88.6 ± 11.6
800	89.7 ± 13.1
900	90.6 ± 14.7

Spectroscopic Characterization

ACR 068

$[C] = 1.3\ 10^{15}\ cm^{-3}$

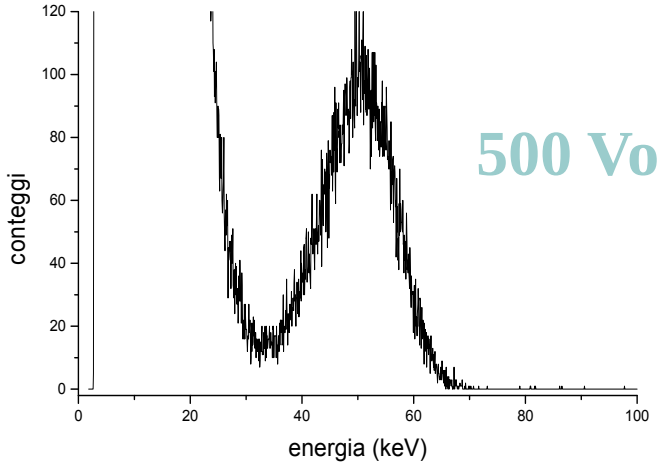

ACR 013

$[C] = 5\ 10^{15}\ cm^{-3}$

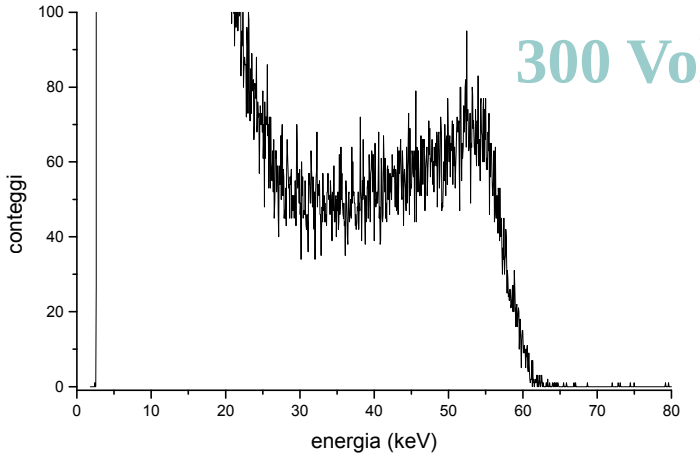

ACR 079

$[C] = 1\ 10^{16}\ cm^{-3}$

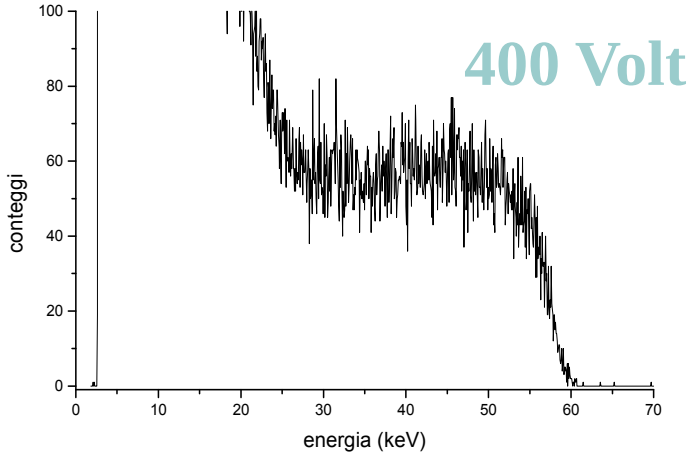

Irradiation with ^{231}Am Source (59,54 KeV)

Comparison of spectra acquired using diodes with the different Carbon concentrations

Electrical Characterization

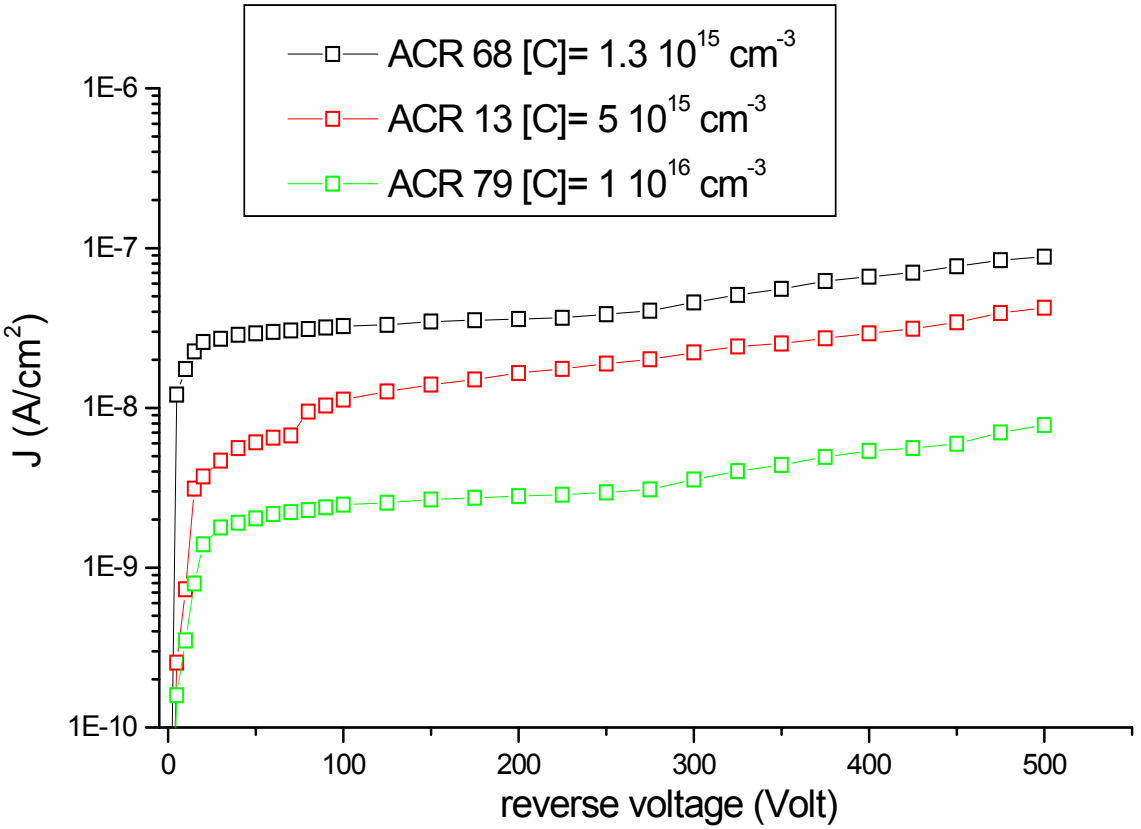

Current density decreases when Carbon concentration become higher.

GaAs pixel detectors

It' s important to define the optimal reverse voltage for the detector because :

Operating bias (V_{bias}) influences image quality

Increasing V_{bias} increase leakage current and noise
breakdown limit

in order to have response uniformity the detector must be overdepleted

Characteristics:

- Carbon density of 1.0-1.3 x $10^{15}cm^{-3}$
- Breakdown voltage > 500 Volt
- Current Density < 50 nA/mm^2 (@ 300 Volt)
- Charge Collection Efficiency > 75 % (@ 300 Volt)

We have observed that it's important to have a well defined concentration of Carbon in the bulk of GaAs so we have studied the behaviour of single diodes

S.R. Amendolia, Nucl Instr Meth, **A380**,(1996) 410-413

Confronto Immagini

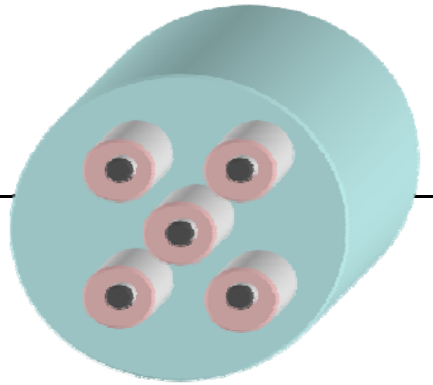

Si
300 μm

GaAs
200 μm

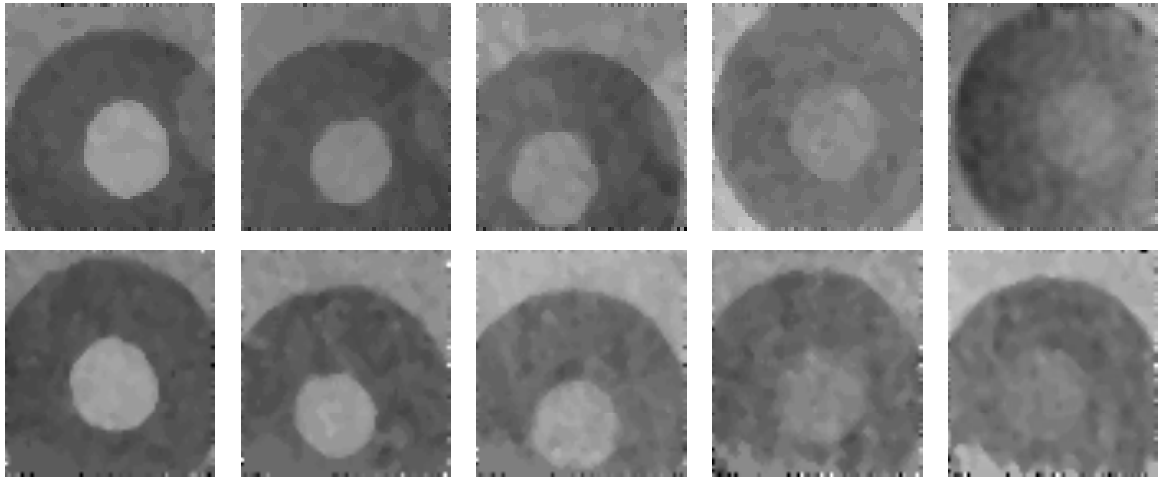

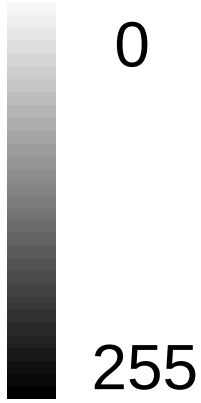

10.9 mm

Esposizione = 32 mAs
Tempo esposizione ~ 1 s
Dose = 6 mGy

Silicon detectors

- ✓Simulation of Silicon detectors to choose a structure to avoid the risk of electrical discharge between detector and electronic chip
- ✓Wafer production and electric tests

Simulation of Silicon detectors: ISE-TCAD

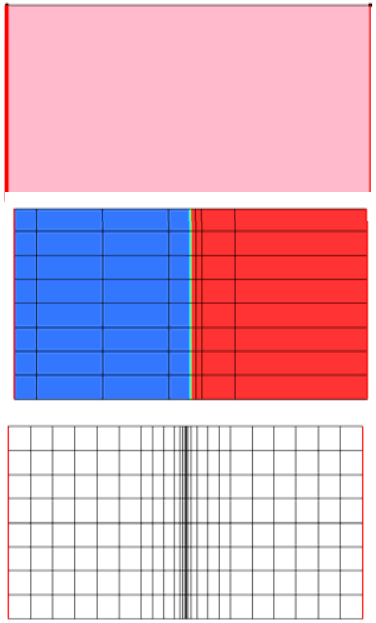

Creation of a geometry

↓

Creation of dopant distribution

↓

Creation of elementary domain

↓

Iterative Calculus

Physical Equation

$$\nabla \varepsilon \nabla \psi = -q(p - n + N_D - N_A)$$ Poisson Equation

$$\nabla J_{n/p} = \pm qR \pm q\frac{\partial (n/p)}{\partial t}$$ Continuity Equation

$$J_n = -n q \mu_n \nabla \Phi_n \, , \, J_p = -p q \mu_p \nabla \Phi_p$$

ψ electrostatic potential
ε electric permittivity
q elementary charge
n, p electron and hole densities
N_D, N_A donors and acceptors
J_n, J_p current densities
R recombination rate
μ mobility
Φ quasi-Fermi potential

Electric Potential at the cutting edge

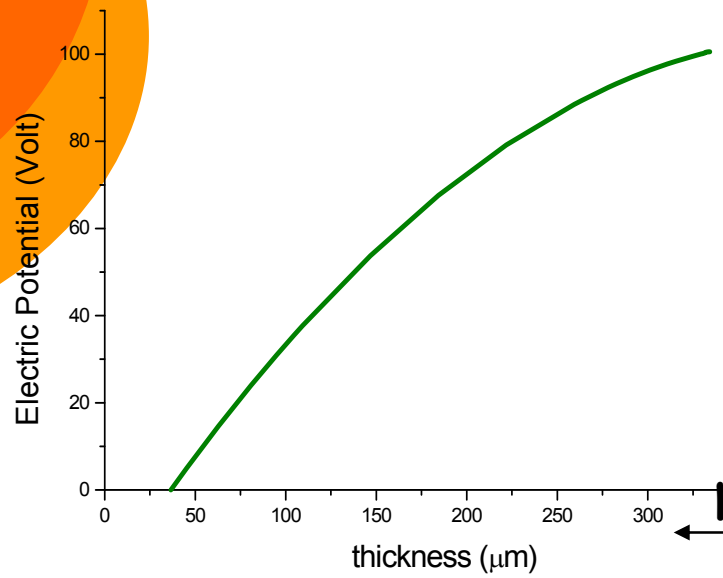

p+ contact	$N_B \sim 2\ 10^{19}\ cm^{-3}$
n+ contact	$N_P \sim 1\ 10^{20}\ cm^{-3}$
Bulk	$N_P \sim 5\ 10^{11}\ cm\text{-}3$
Scribe Line	$N_P \sim 1\ 10^{17}\ cm^{-3}$
Oxide	free charge ~ $4\ 10^{11}\ e^-$

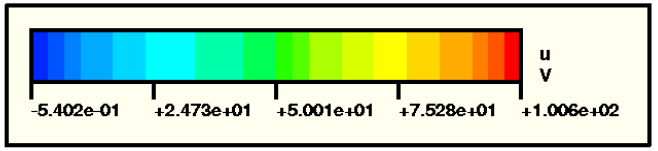

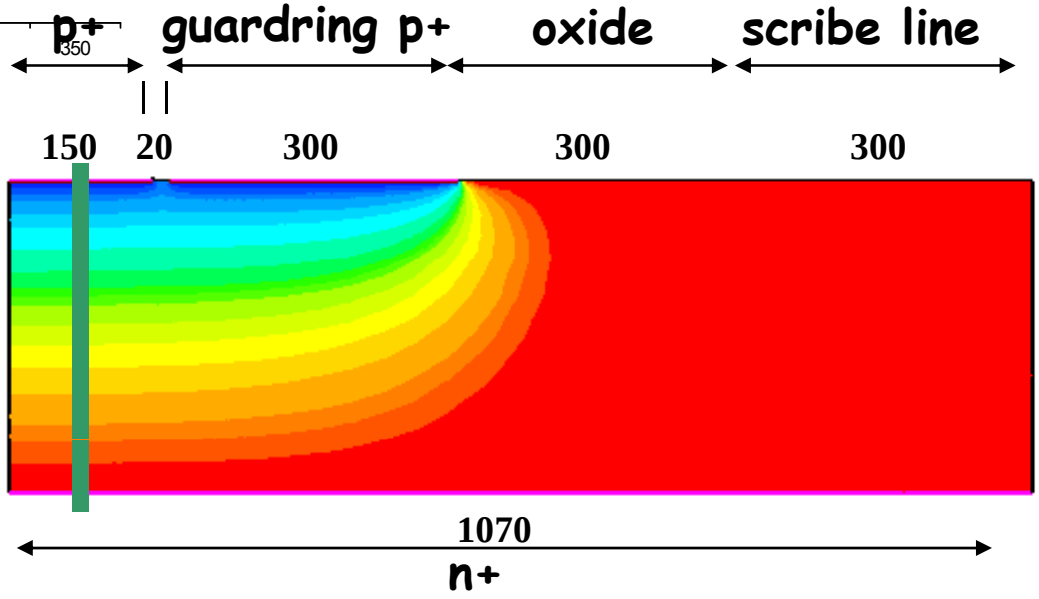

p+ Contact at ground
Guardring at ground
n+ Contact at 100 Volt

New structure: Electric Potential

Multiguardring (450 μm)

3 x (oxide 15 μm + p^+ 15 μm)
3 x (oxide 20 μm + p^+ 15 μm)
3 x (oxide 25 μm + p^+ 15 μm)
3 x (oxide 30 μm + p^+ 15 μm)

p+ contact	$N_B \sim 2\ 10^{19}$ cm^{-3}
n+ contact	$N_P \sim 1\ 10^{20}$ cm^{-3}
Bulk	$N_P \sim 5\ 10^{11}$ cm-3
p-stop	$N_B \sim 5\ 10^{17}$ cm^{-3}
scribe Line	$N_P \sim 1\ 10^{17}$ cm^{-3}
Oxide	free charge ~ $4\ 10^{11}$ e$^-$

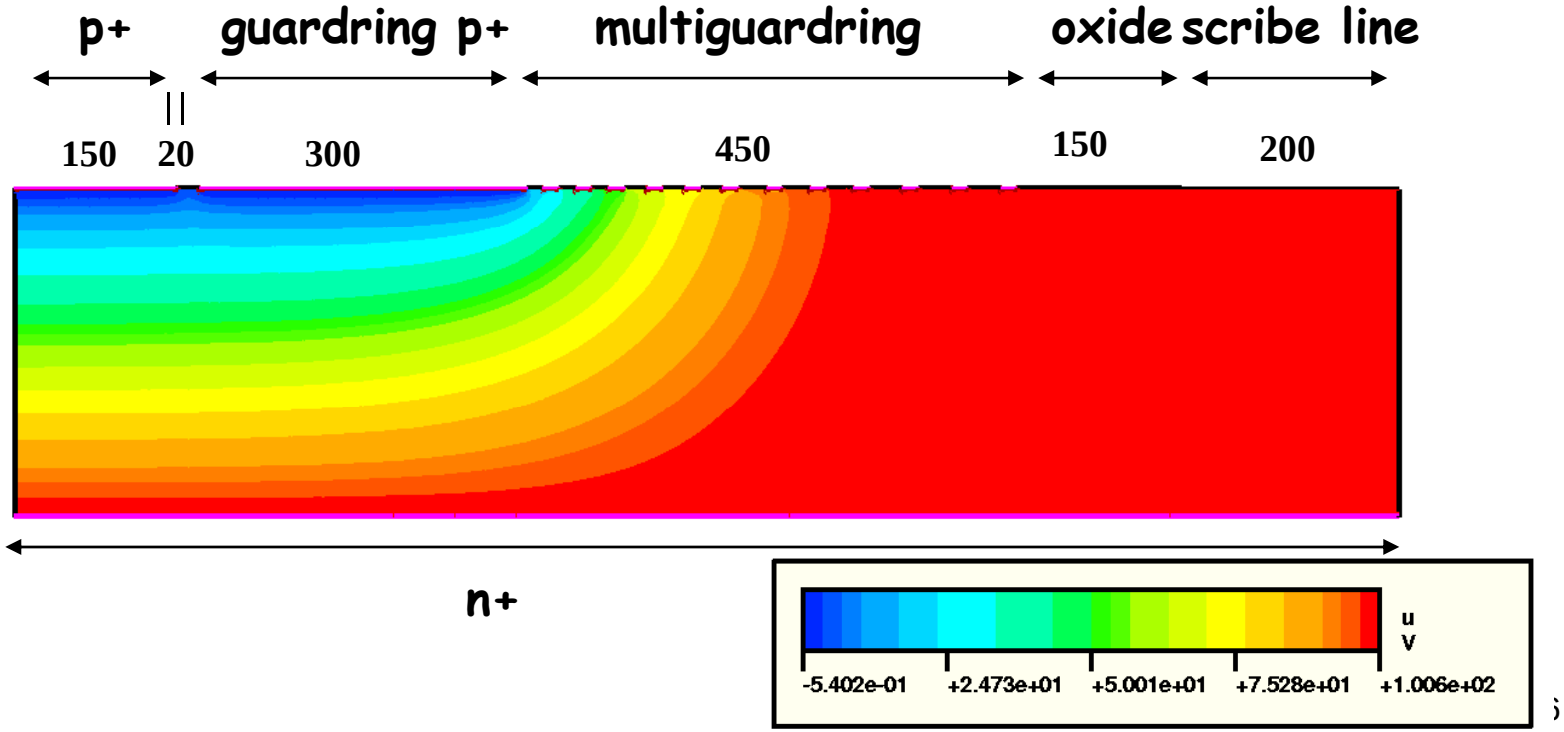

Electric Field and Potential

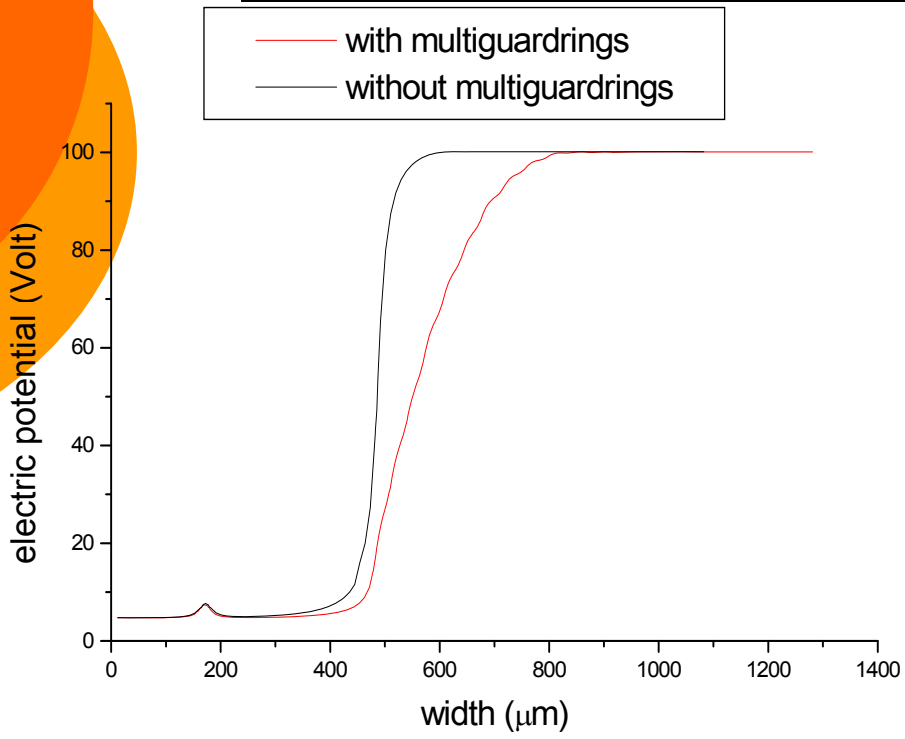

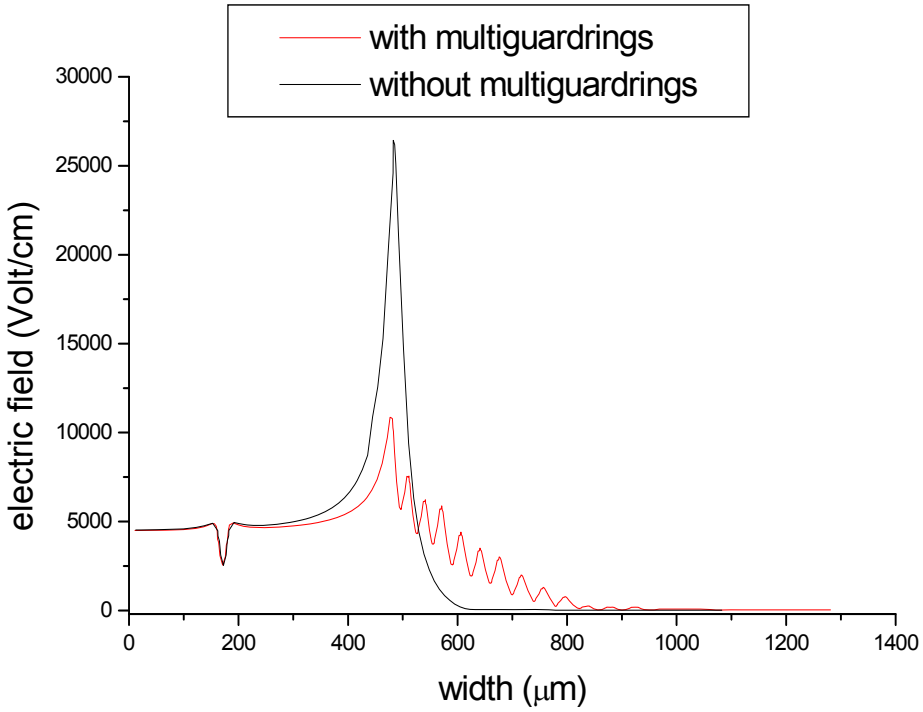

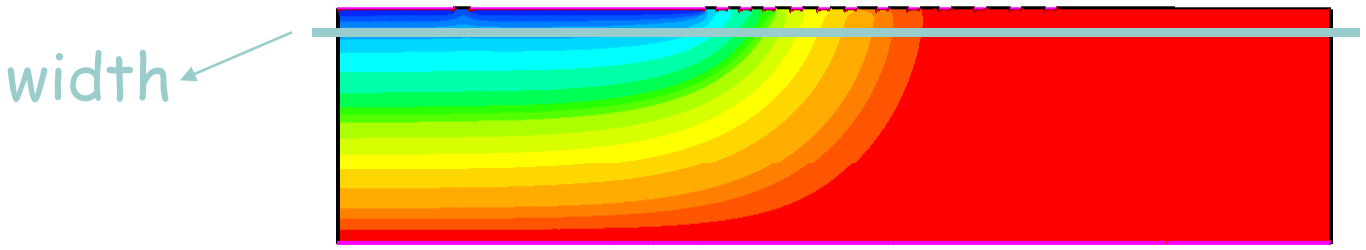

Wafer layout at ITC-IRST

12 wafers 4 inches in diameter

Thickness 300 μm, 525 μm and 800 μm

Type of production : p+/n

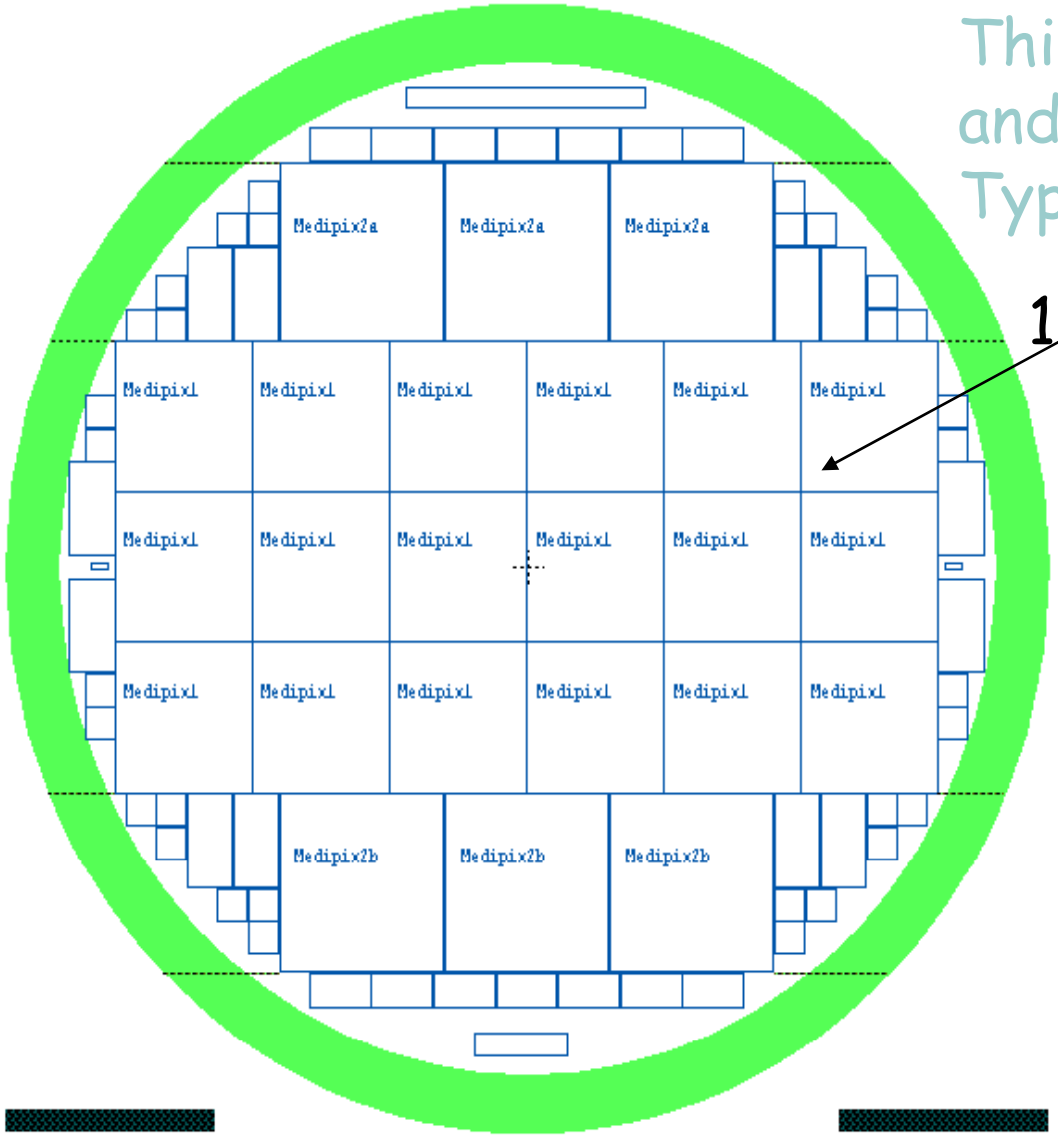

18 detectors for Medipix 1

Several test structures

Photos of some details

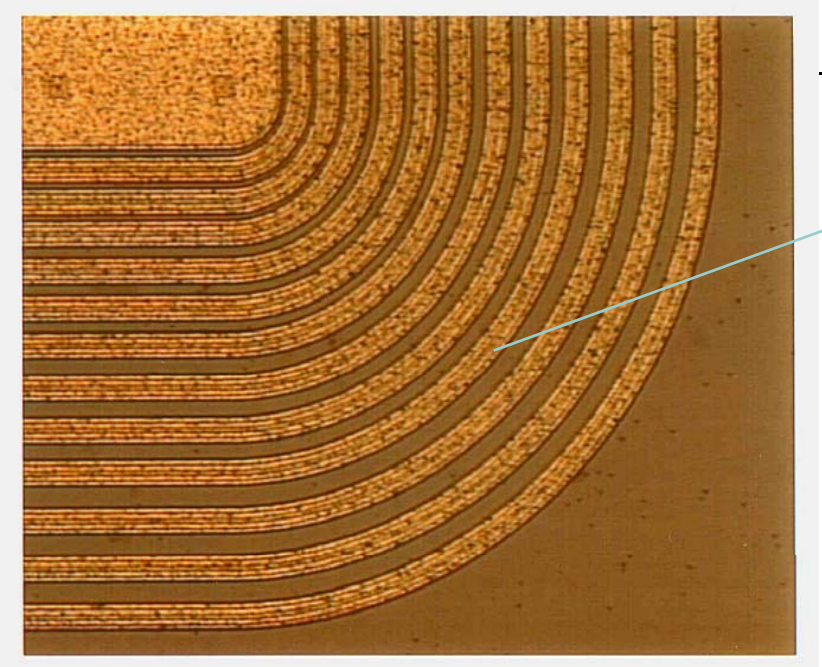

multiguardrings

multiguardrings

Pixel 150 μm x 150 μm

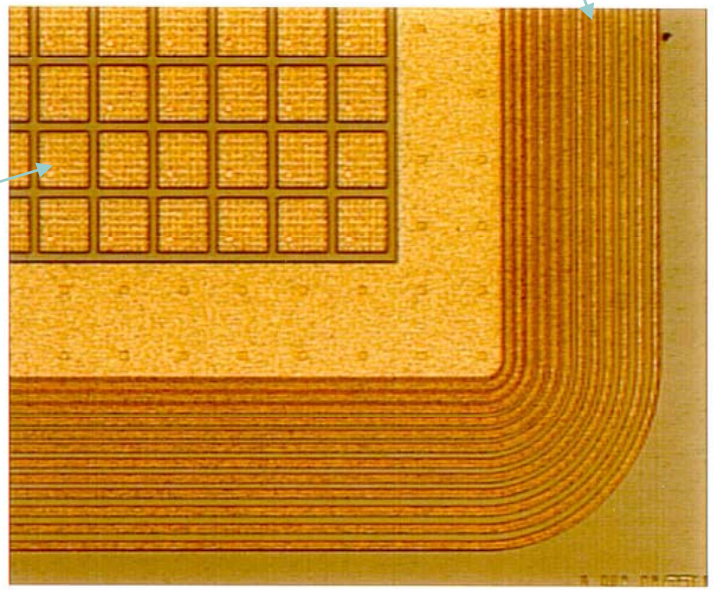

Test structure in the wafer

To check the properties of the wafers we have tested the electircal characteristic of some single diodes
(3 diode for each wafer always in the same position)

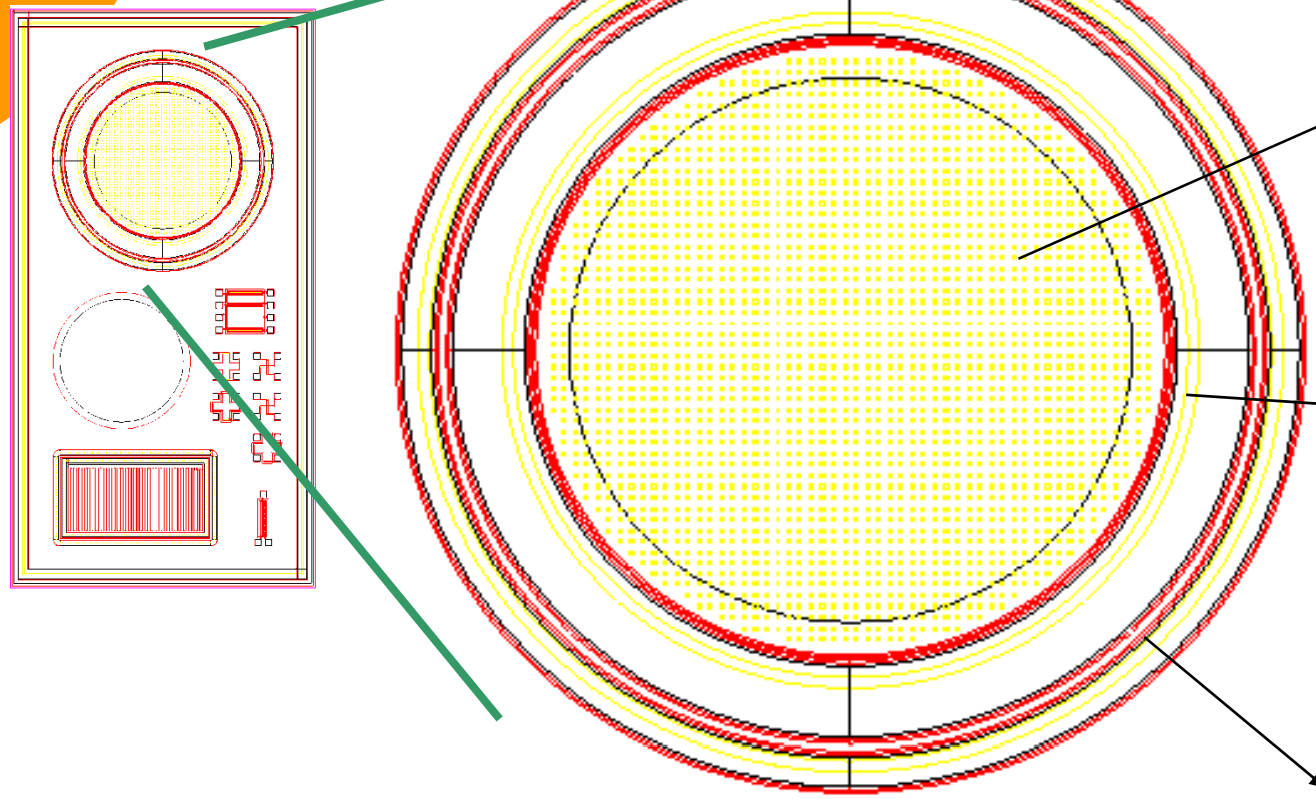

Electrical Characterization

T= 21.5 °C U=65 %

Thickness 300 μm

Current in the central diode with guardring at ground

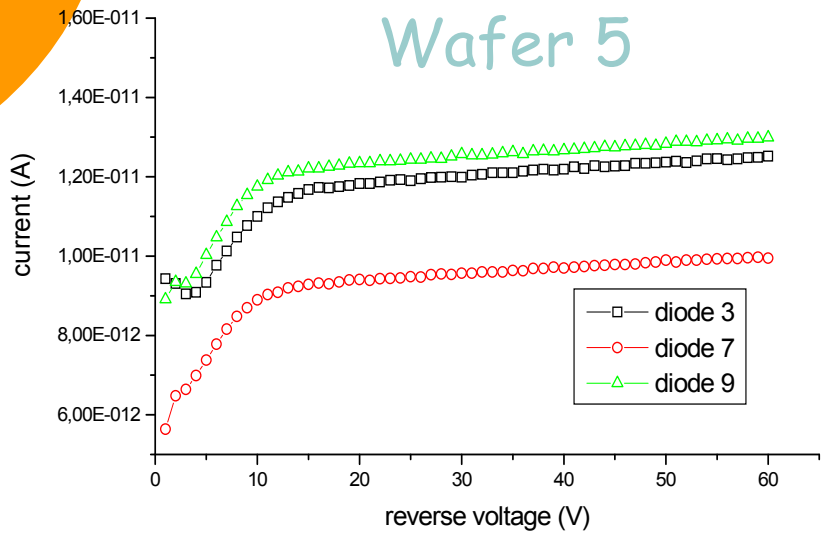

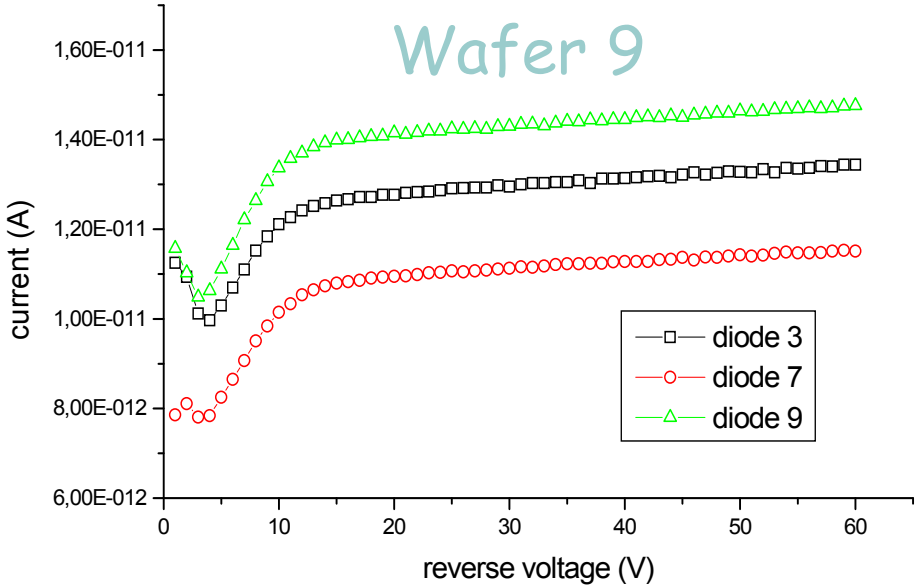

$1.2\ 10^{-11}$ A $\rightarrow$J= $3.8\ 10^{-10}$ A/cm^2 contro J= 10^{-8} A/cm^2 del GaAs

Electrical Characterization

Thickness 525 μm

T= 21.5 °C U=65 %

Current in the central diode with guardring at ground

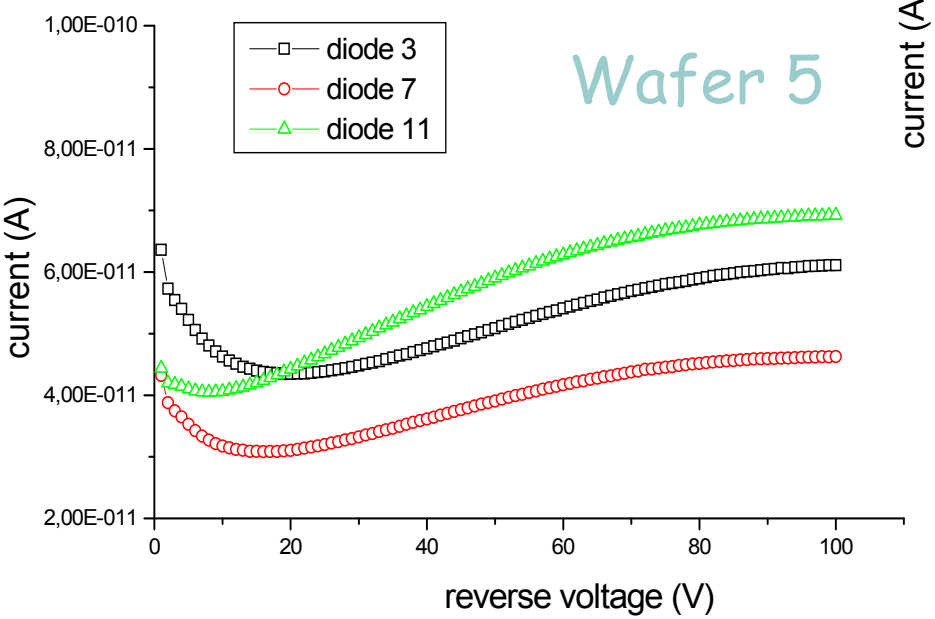

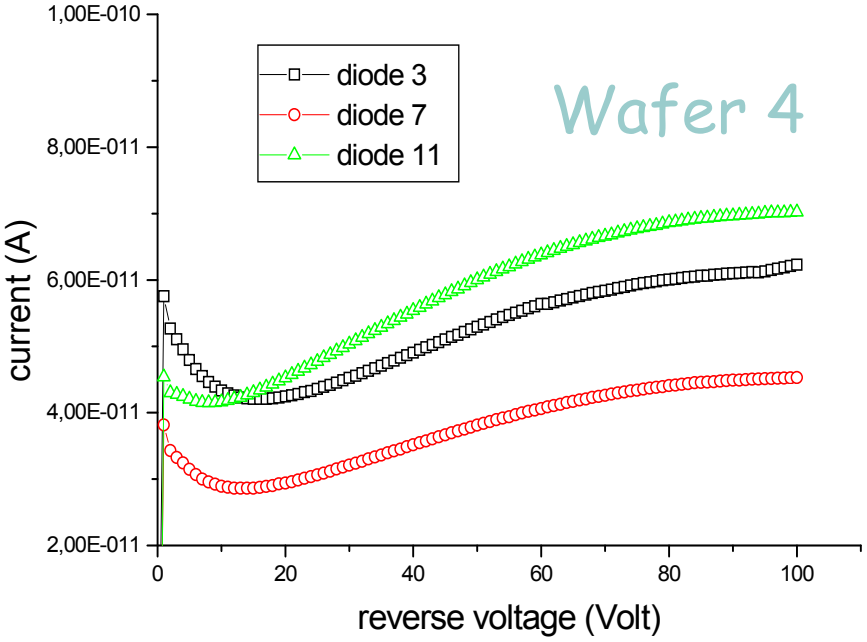

Image of different Al thickness

Exposure condition: W anode, 40 kV, 40 mA, 630 ms

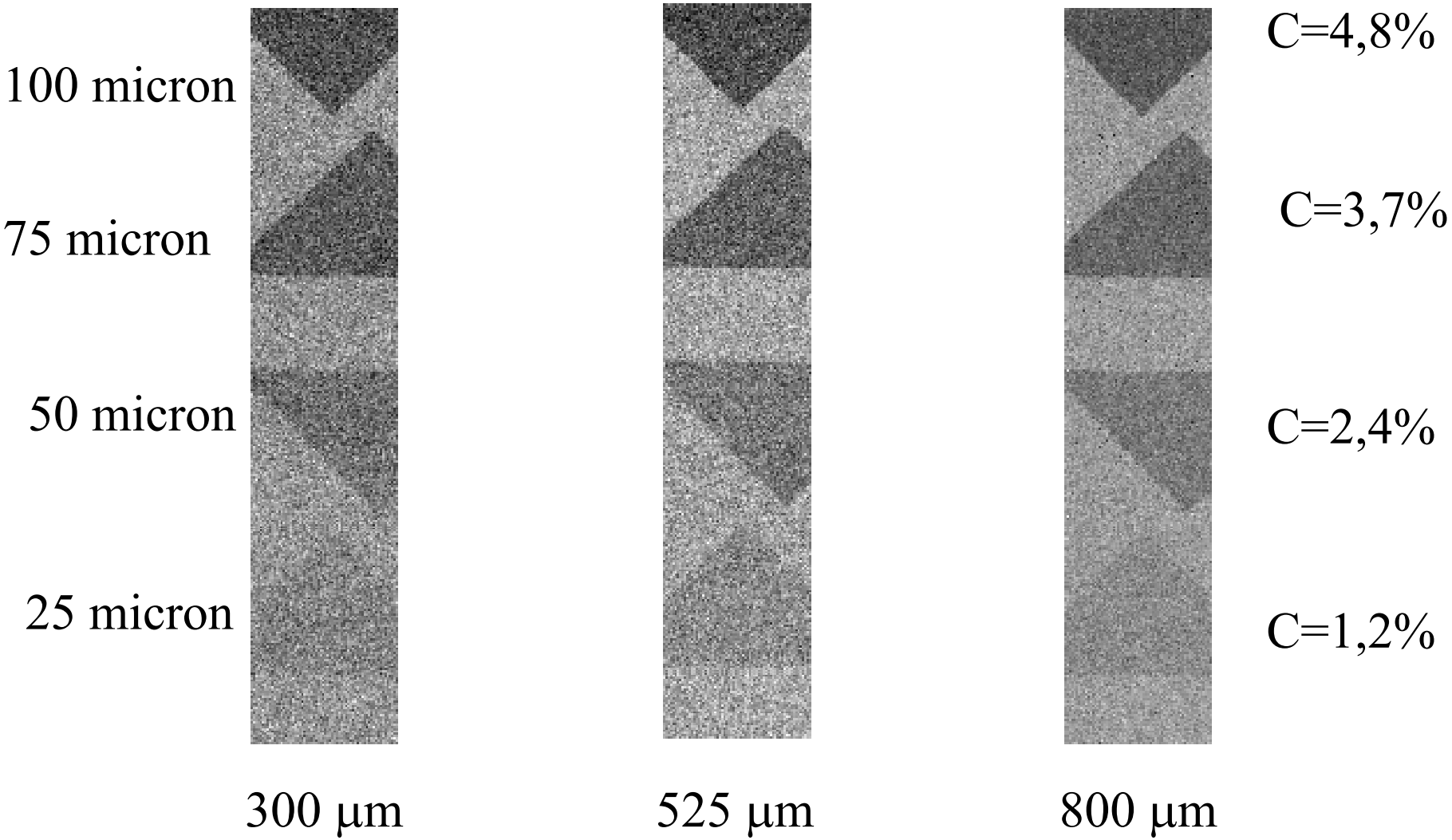

M.G. Bisogni et al.,IEEE Trans. Nucl. Science, **52**, (2005), 1989-1993

Scelta la configurazione degli elettrodi di lettura e il materiale del rivelatore occorre un asic per leggerlo

MPXI: a single photon counting chip

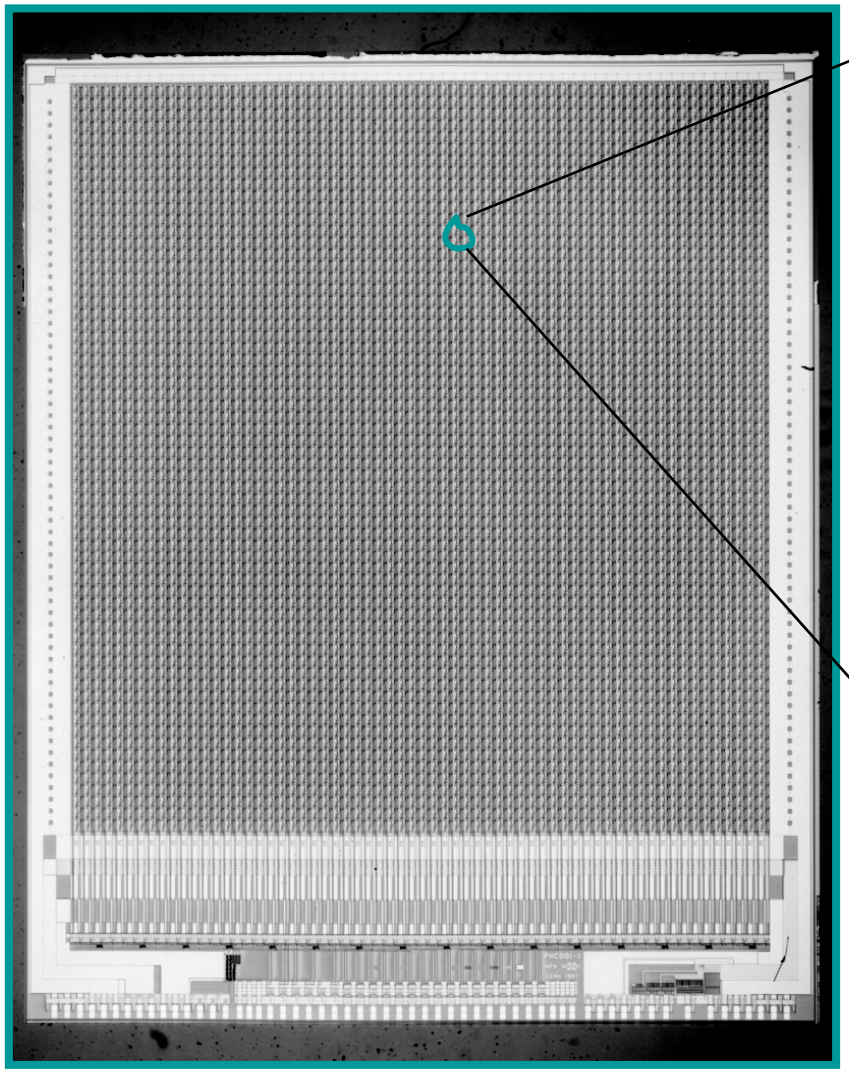

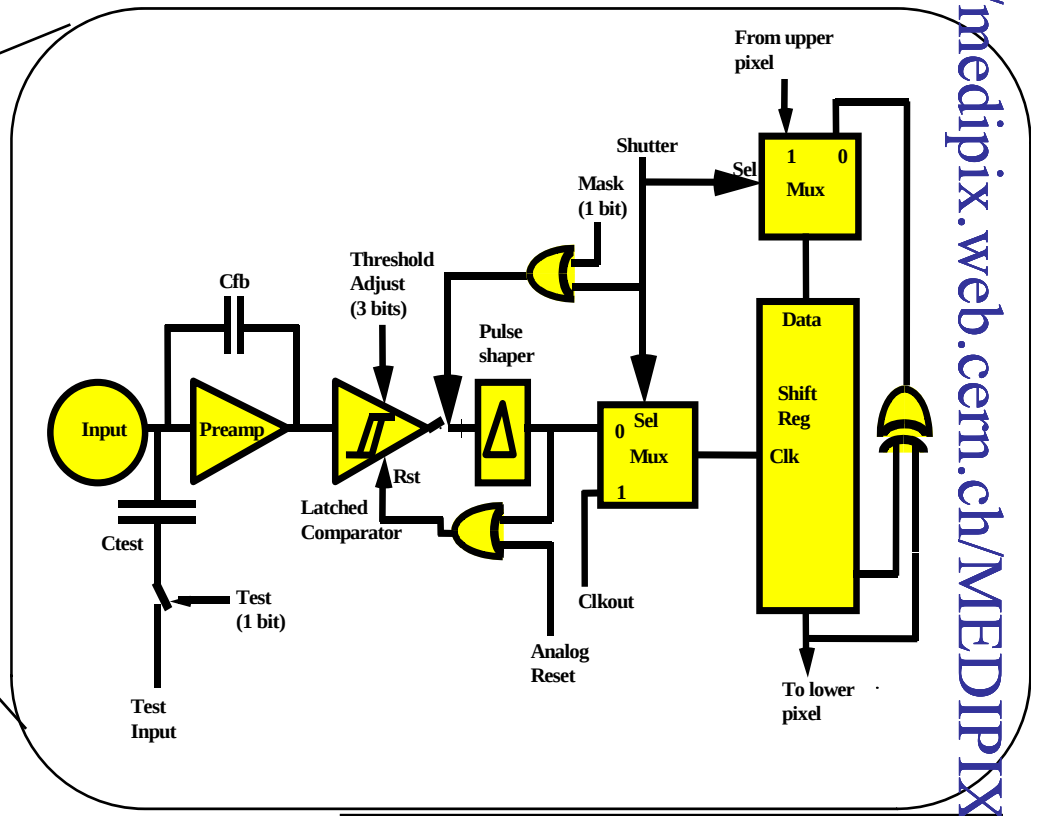

2 mm

12 mm

EP CERN SACMOS1
FASELEC Zurigo
pixel 170 x 170 μm^2
canali 64 x 64
area 1.7 cm^2
threshold adjust 3-bit
pseudo-random counter 15-bit

http://medipix.web.cern.ch/MEDIPIX/

TEST ELETTRICI

- Risposta di un singolo canale ad impulsi test
- Distibuzione di soglia media dei 4096 canali
- Costruzione della matrice di aggiustamento fine della soglia
- Misure di Cross-Talk
- Calibrazione elettrica del chip

Test elettrici

Risposta di un singolo canale ad un treno di 1000 impulsi

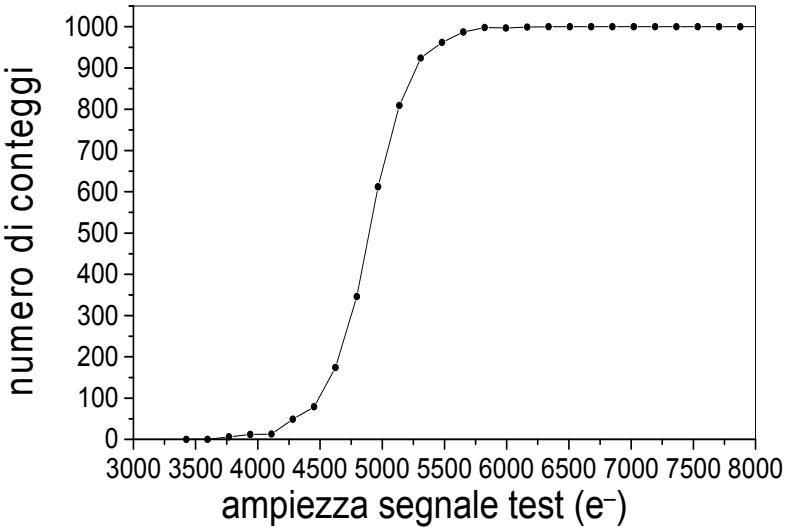

Distribuzione di soglia media per V_{th} = 1.2 volt

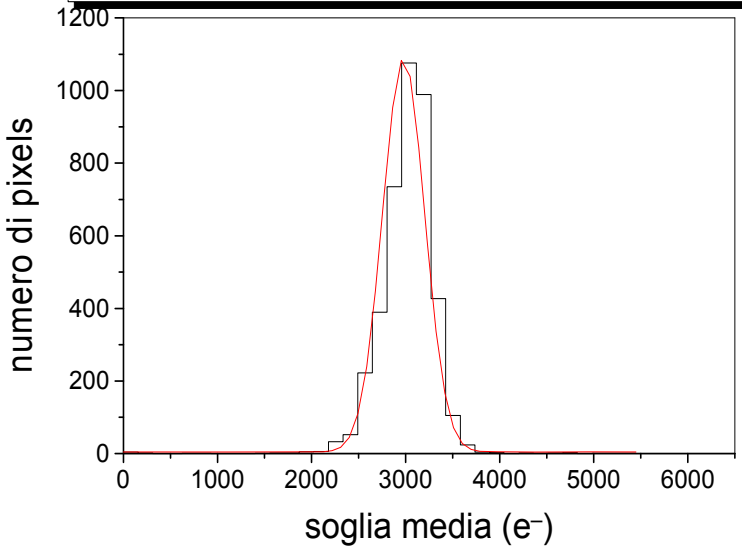

SOGLIA (e^-)	σ_{TH} (e^-)	ENC (e^-)	σ_{TOT} (e^-)
2950	450	350	570

Test elettrici

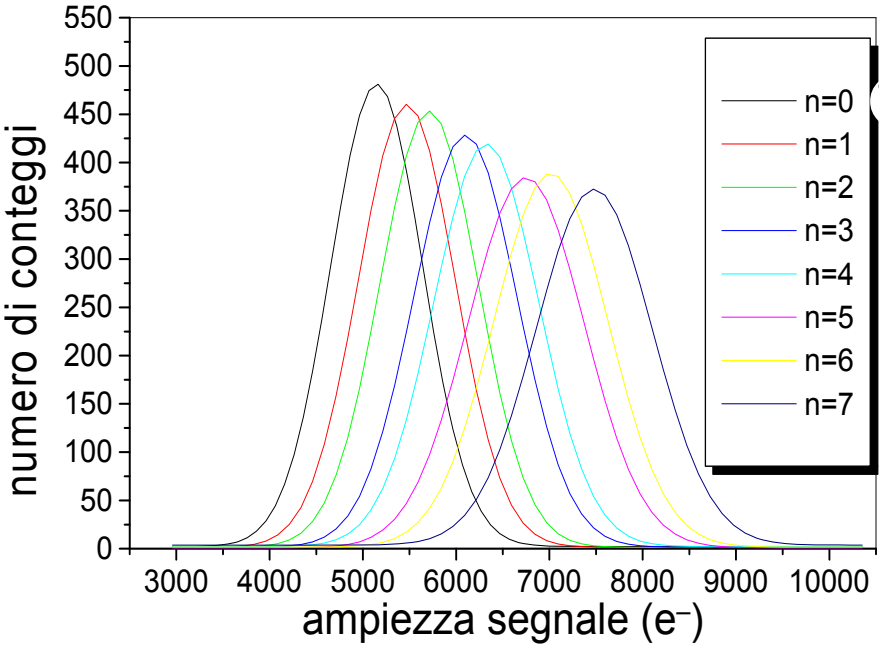

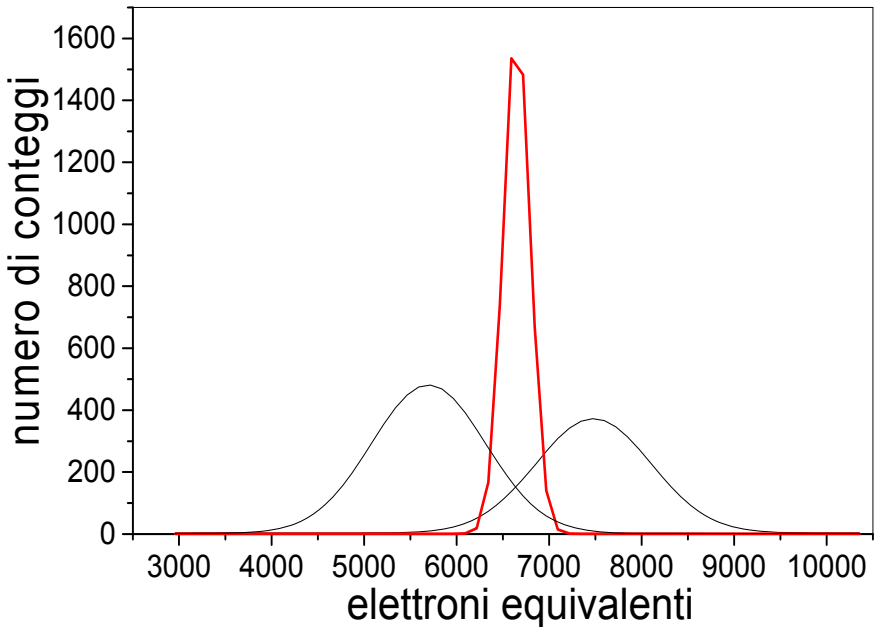

Aggiustamento fine della soglia

Tensione di soglia $= V_{th} + n \times (V_{tha}/8)$

$n = 0,\ldots\ldots,7$

Ad ogni pixel viene associata la combinazione di 3 bit che ne fa cadere la soglia nella regione di sovrapposizione fra la curva ottenuta per n=0 e quella per n=7

Matrice di configurazione fine della soglia

Scelto il lay-out del rivelatore pixels

Scelto il materiale

Scelto l'asic di lettura

Realizzare l'assembly

Imaging system

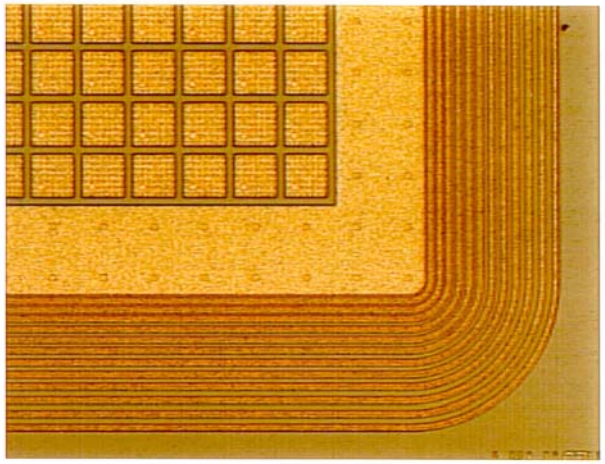

ITC-Irst Detector

- **Si <111>**
- **300-800 μm thick**
- **pixel 170 x 170 μm²**
- **p+ side 150x150 μm²**
- **64 x 64 chs**
- **1.2 cm² area**

Photon Counting Chip
Medipix collaboration

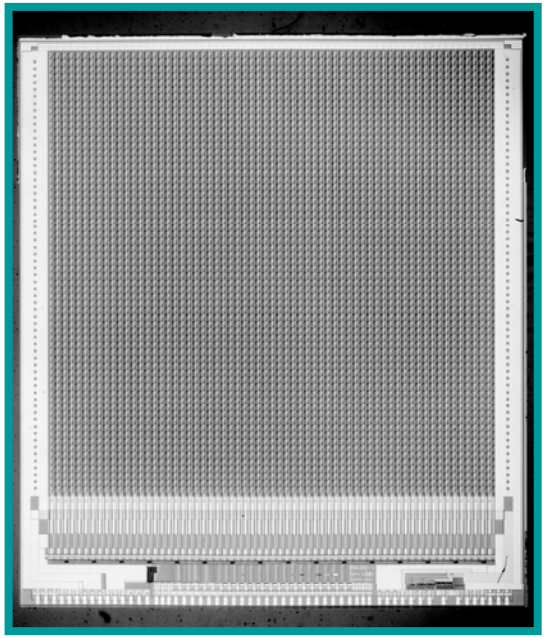

SACMOS 1 μm technology
pixel: 170 x 170 μm²
64 x 64 channels
area 1.7 cm²
threshold adjust 3-bit
15-bit counter

http://medipix.web.cern.ch/MEDIPIX/

Detector of area larger than the electronic chip

Wafer 4 inches in diameter, type of production p+/n, thickness 300 – 500 μm

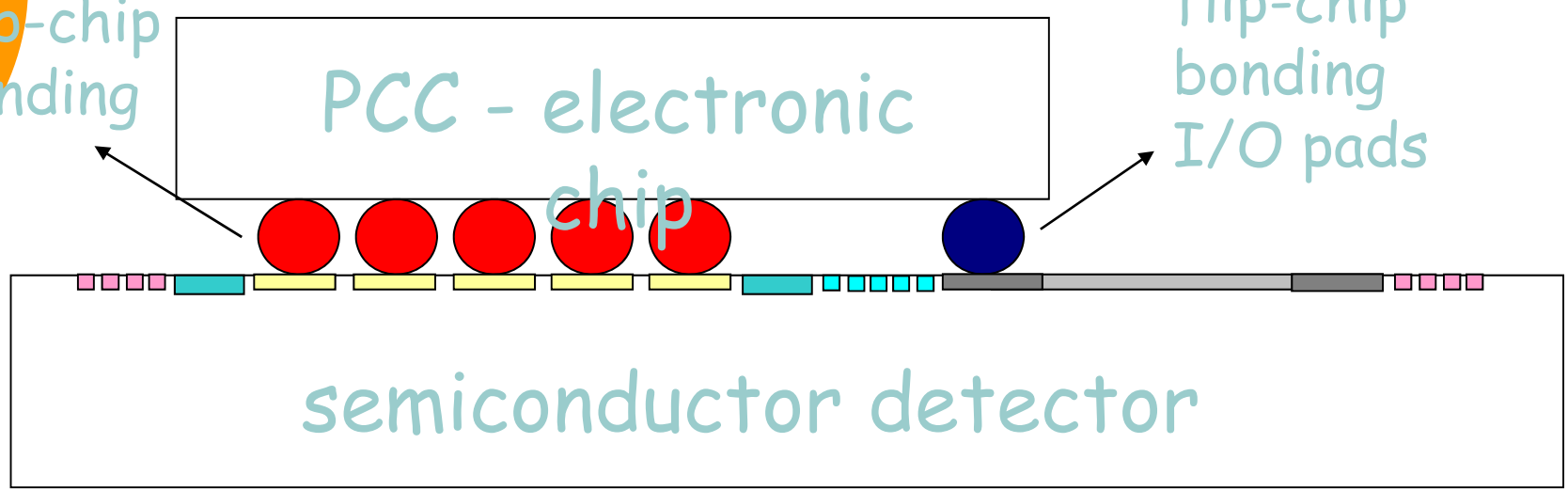

multiguardring around the matrix and the lines for the fanout

guardring around the active matrix of pixels

Series of p+ implantation to isolate the active region from the lines

The Indium Bump Bonding

- The AMS (Alenia Marconi Systems) process
  - Under Bump Metal (UBM): evaporation of a Ti/Al multilayer.
  - Bumps: Indium evaporation on the electronics and the detector pads
  - Bumps: cylindrical 30μm in diameter, 9μm high

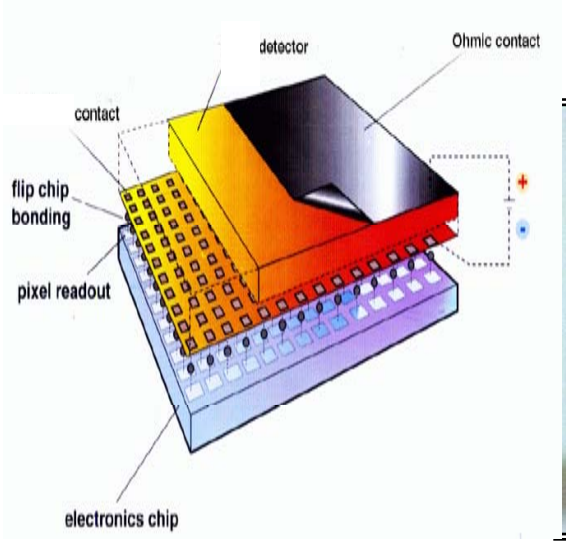

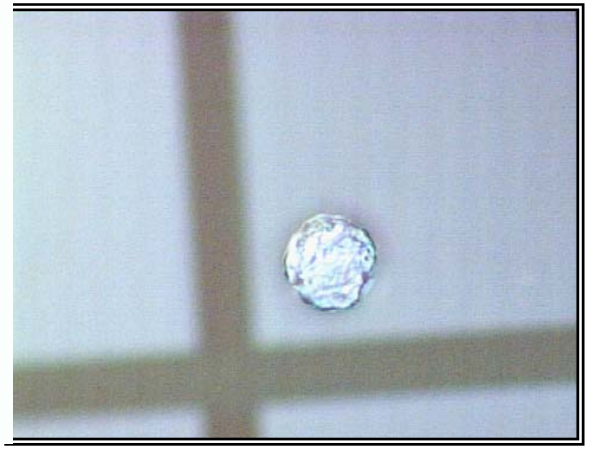

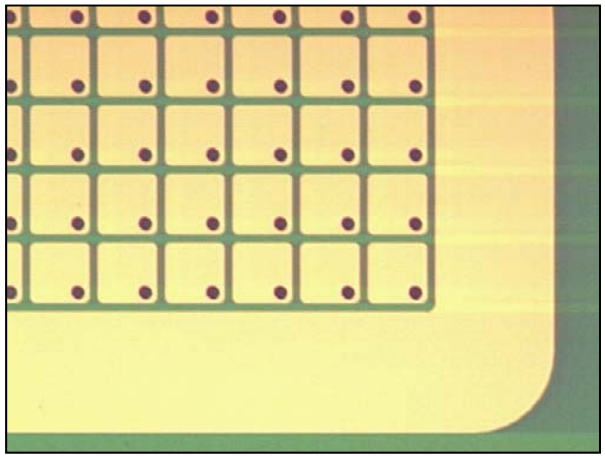

Processes: Indium evaporation process adapted to GaAs
New Au/Sn (10 mm high) galvanic growth

Current stability

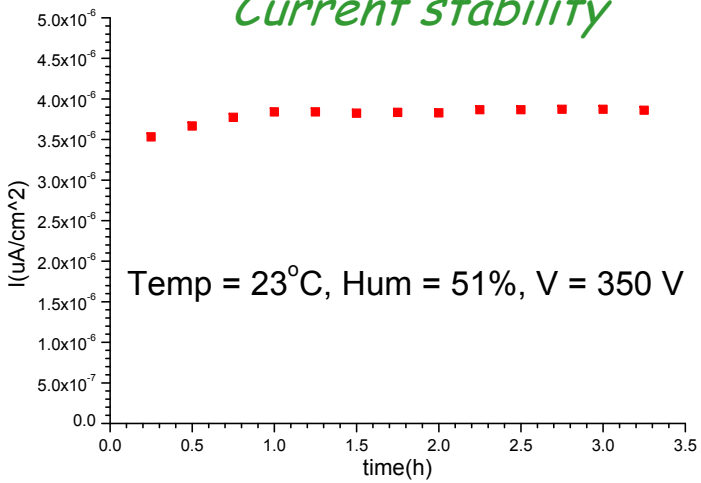

Au/Sn grown without thermic treatment

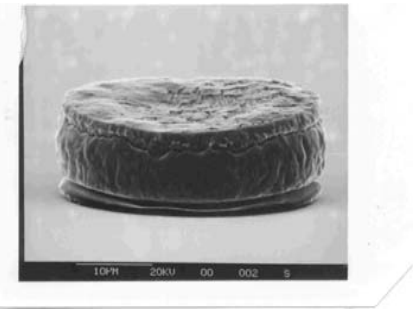

Au/Sn grown with alloy at 320^{0}C

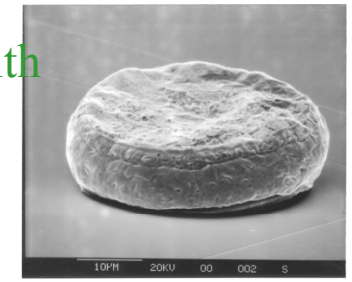

Overall sight of the bumps

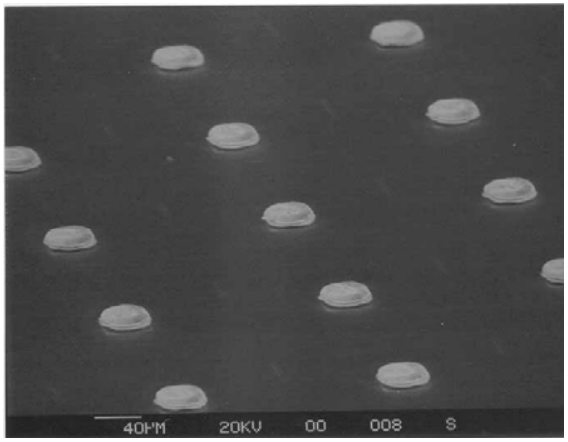

After mechanical breakage ...

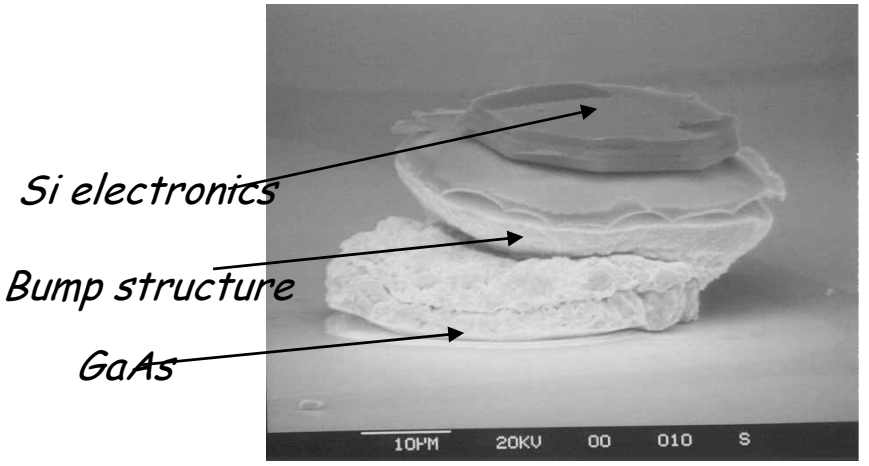

A. Stefanini et al., Nucl Instr Meth, **A518,** (2004), 376-379

Imaging system

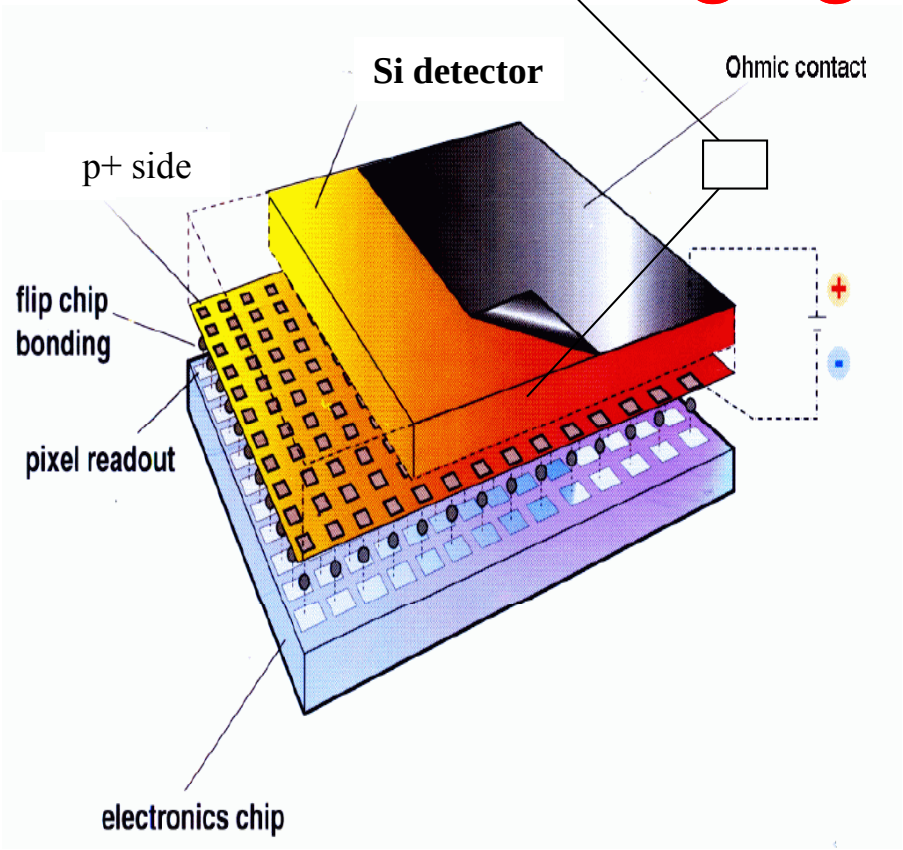

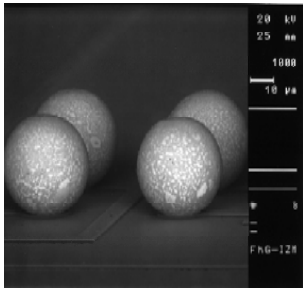

25 µm

VTT Bump-bonding:

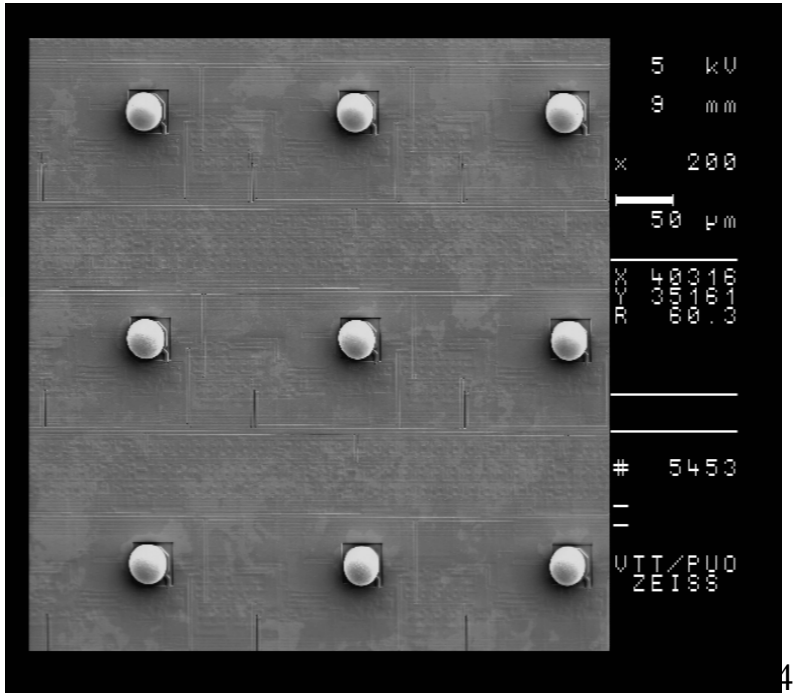

REALIZZATO UN ASSEMBLY VA CARATTERIZZATO

Calibrazione con sorgenti radioattive

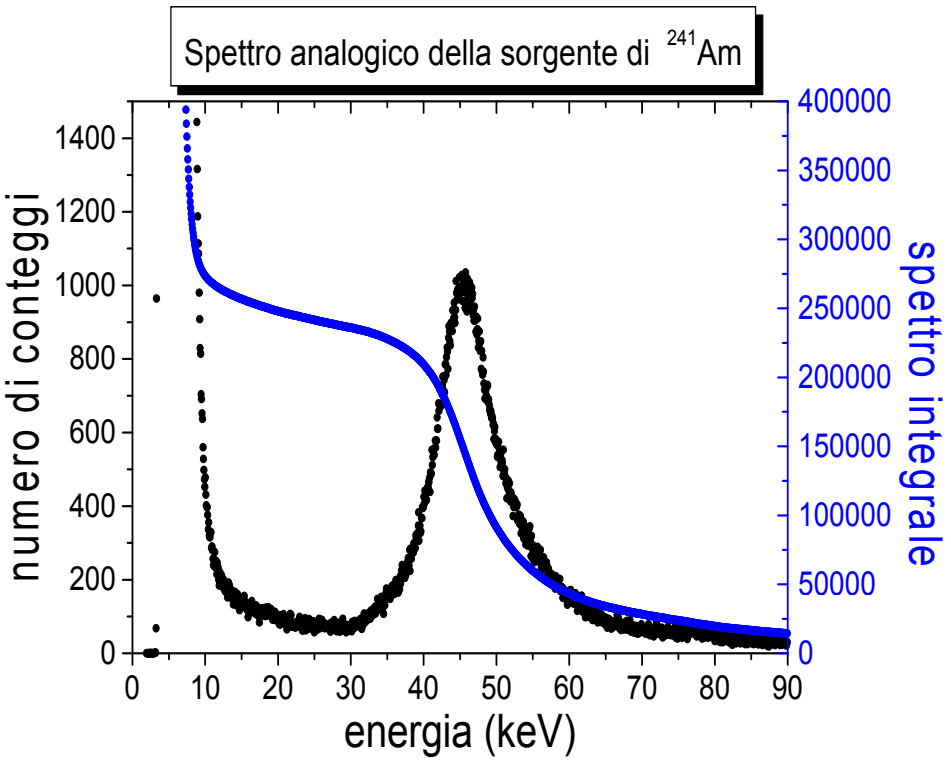

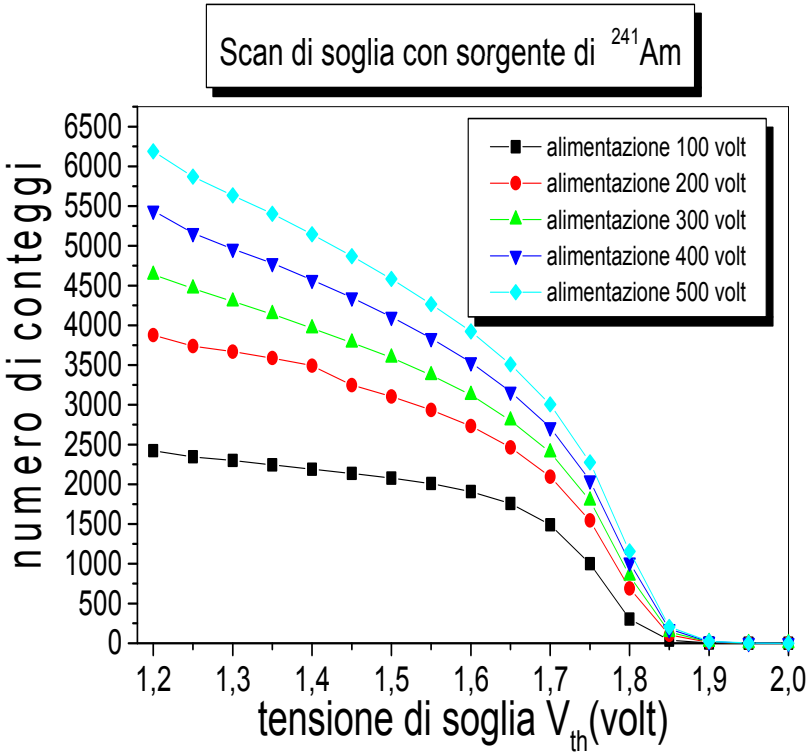

Spectroscopic capability

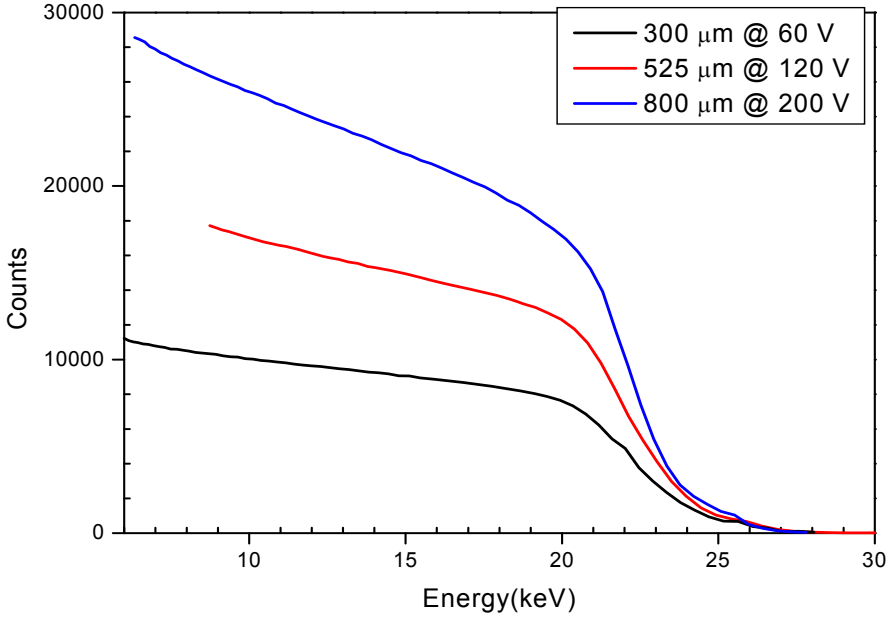

^{109}Cd Integral spectra

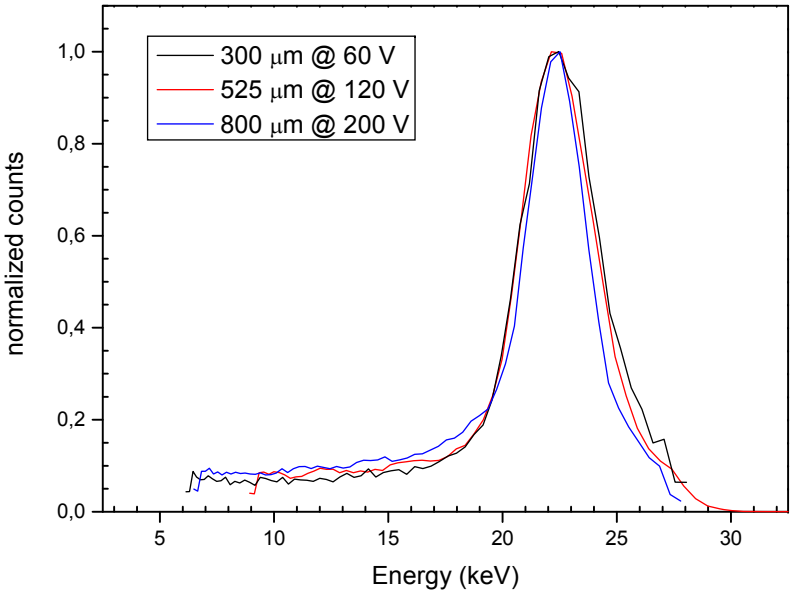

^{109}Cd Differential spectra

Physical Parameters

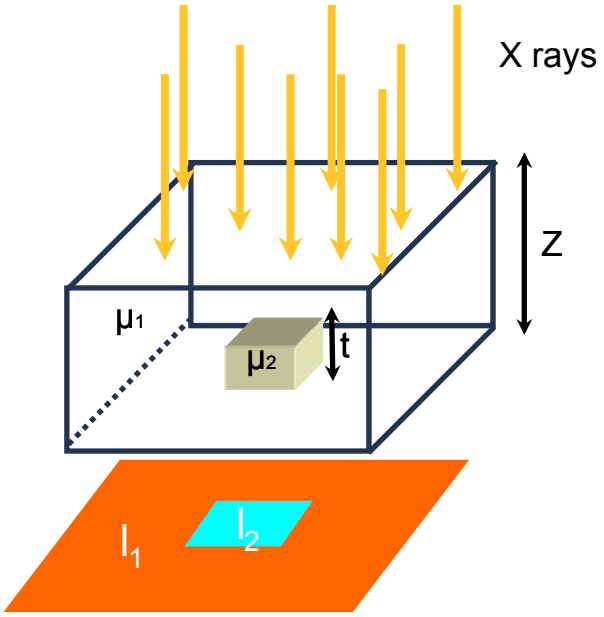

$$C_{rad} = \frac{n_1 - n_2}{n_1} = 1 - e^{-\Delta\mu t}$$

$$SNR = \frac{n_1 - n_2}{\sqrt{\sigma_1^2 + \sigma_2^2}} = \frac{n_1 - n_2}{\sqrt{n_1 + n_2}}$$

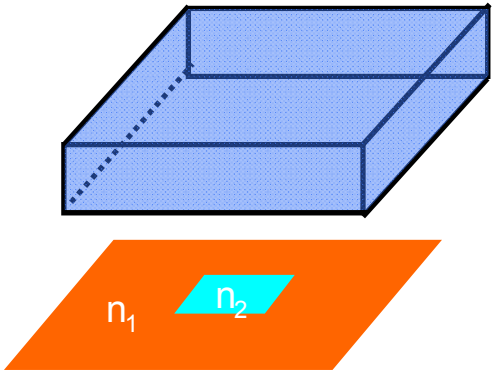

Digital Detector

Detected Image

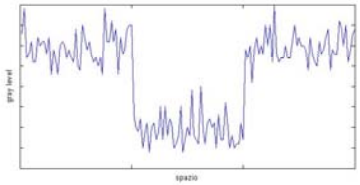

Image line profile

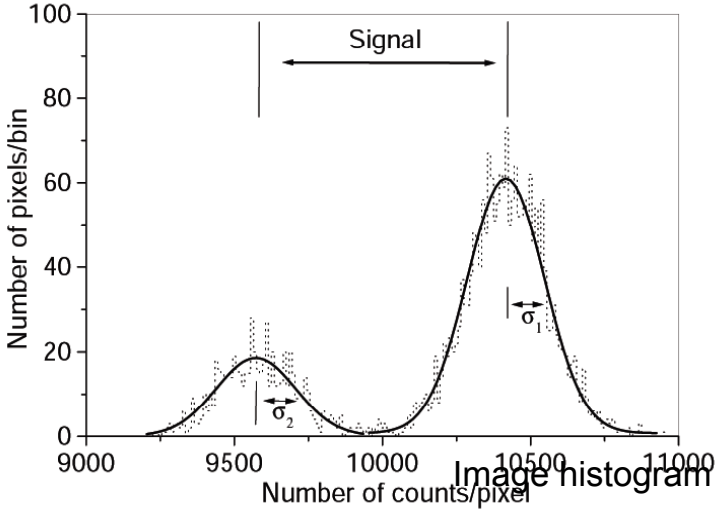

Image histogram

Signal to Noise Ratio

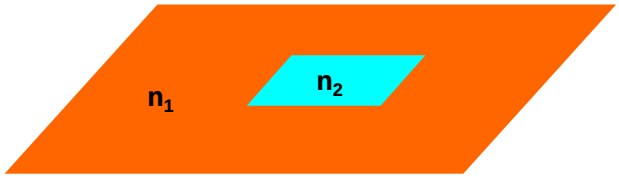

$$SNR = \frac{n_1 - n_2}{\sqrt{\sigma_1^2 + \sigma_2^2}}$$

Only statistics fluctuations

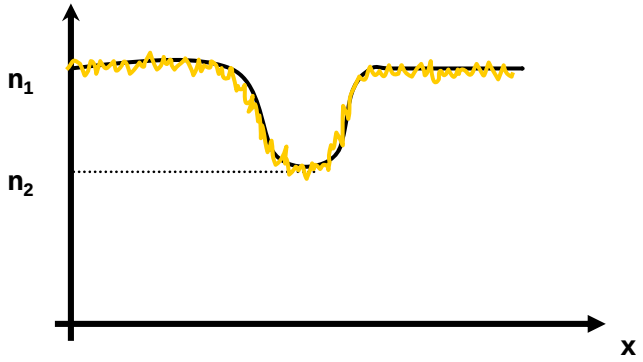

$$SNR = \left(1 - e^{-(\Delta\mu)s}\right)\sqrt{\frac{NAe^{-\mu_1 t}\varepsilon}{1+R}}$$

49

Contrast measurements

X-ray (W-anode) settings : 40 kV, 25 mA, 500 ms

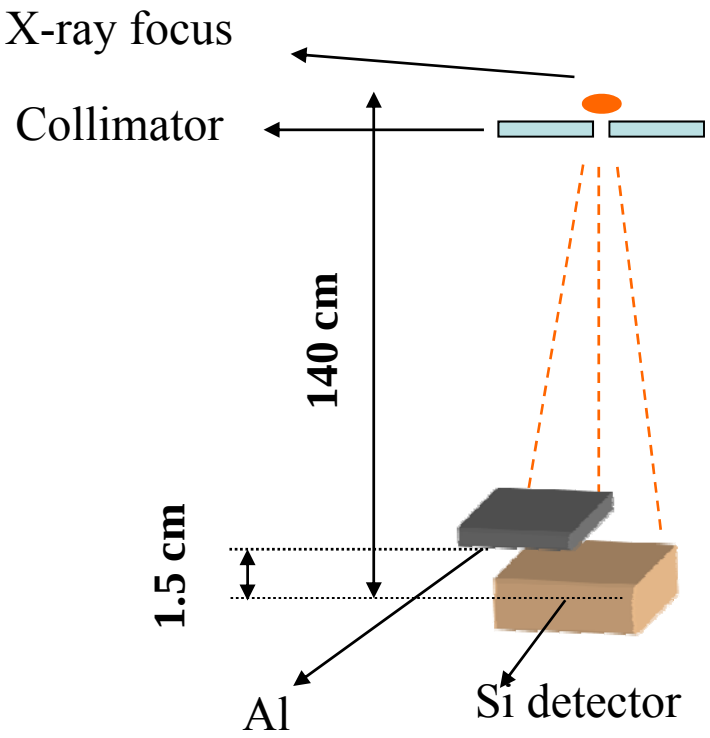

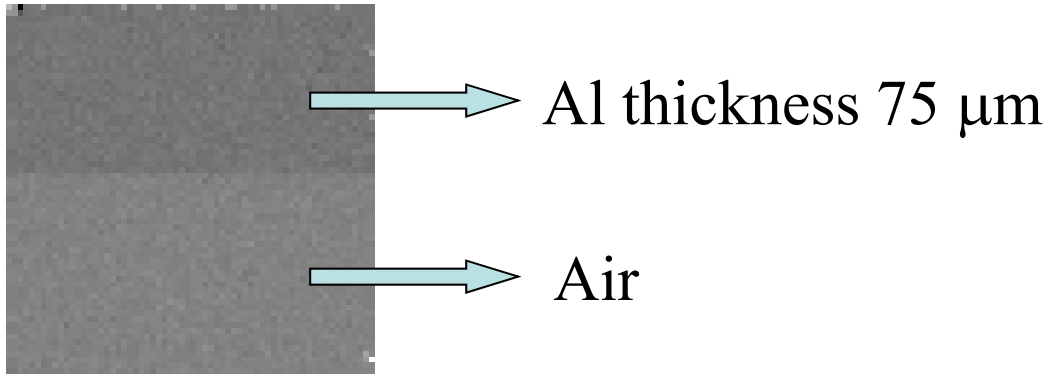

$$C = \frac{N_{air} - N_{Al}}{N_{air}}$$

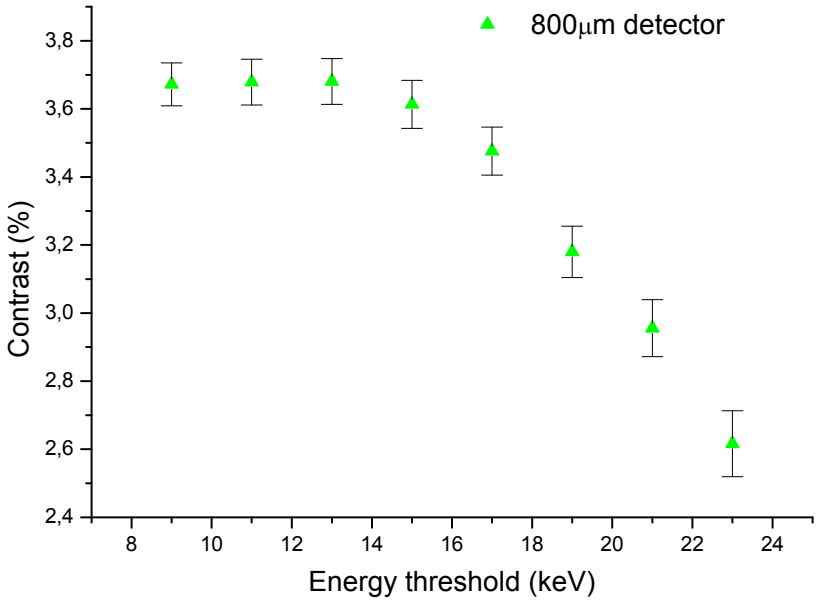

Signal to Noise Ratio

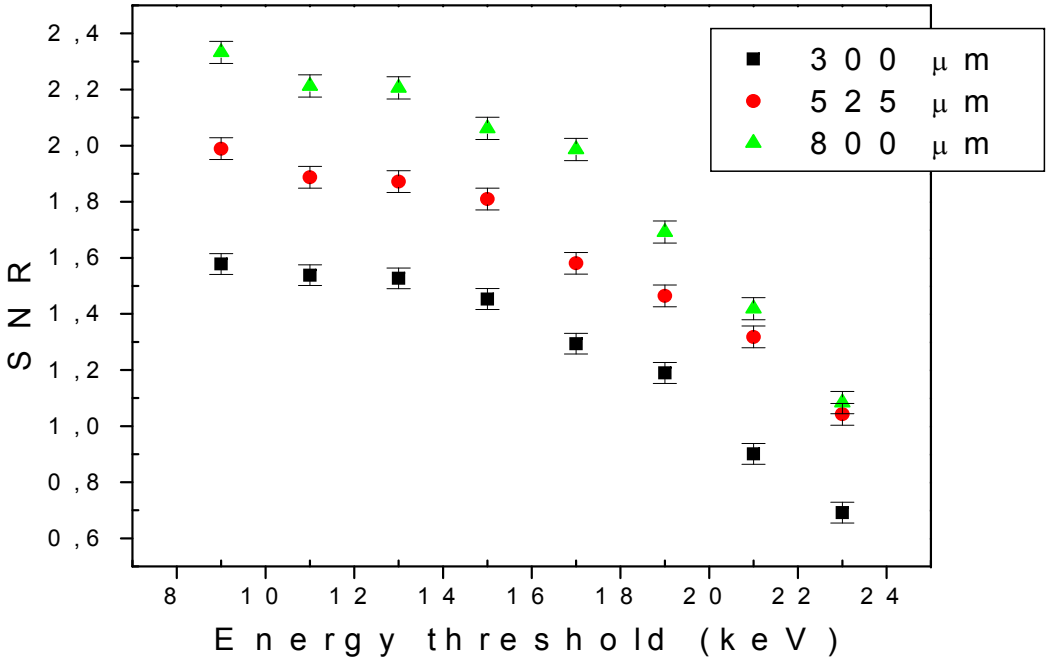

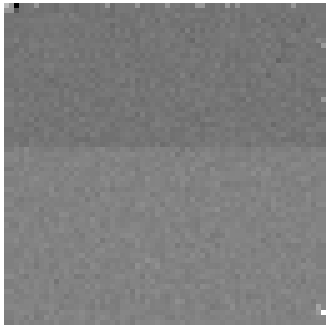

75 μm Al

air

$$SNR = \frac{\left|N_{air} - N_{Al}\right|}{\sqrt{\sigma_{air}^2 + \sigma_{Al}^2}}$$

APPLICAZIONI

- **DIGITAL MAMMOGRAPHY**
- **CARATTERIZZAZIONE DEL FASCIO DI PROTONI A CATANA**
- **DUAL ENERGY**
- **MAMMOGRAFIA A TRIESTE**

A MAMMOGRAPHIC HEAD DEMONSTRATOR WAS DEVELOPED IN THE FRAMEWORK OF THE "IMI" PROJECT

The Integrated Mammographic Project

- The Integrated Mammographic Imaging (IMI) project aims to realize innovative instrumentations for morphological and functional mammography.
- Funded by the Italian Ministry of Education, University and Research (MIUR) and promoted by the INFN for the technological transfer to the national industry

  A. Stefanini, University of Pisa, project-leader

- Research lines:
  - An advanced gamma camera for scintimammography
  - GaAs detectors and bump bonding techniques
  - A prototype of a mammographic head and related developments
  - A high intensity tunable quasi-monochromatic X-ray source

S.R. Amendolia, Nucl Instr Meth, **A518,**(2004), 382-385

Digital Mammography

Principal Mammography task:
✓Detection of the tumor masses (objects with contrast < 1% and diameter ≈ 1-5 mm)
✓Detection of the microcalcifications (objects with high contrast and small dimensions ≈ 100 μm)

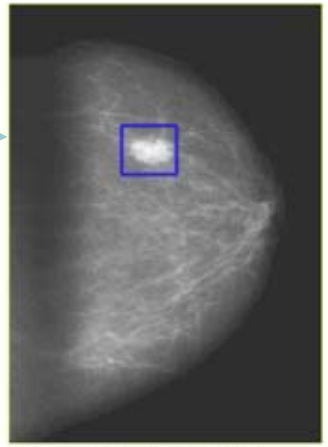

a) Breast carcinoma surrounded by adipose tissue

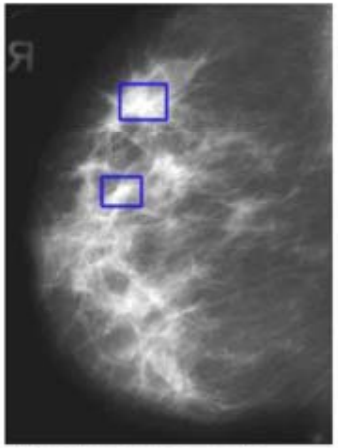

b) Breast carcinoma surrounded by fibroglandular tissue

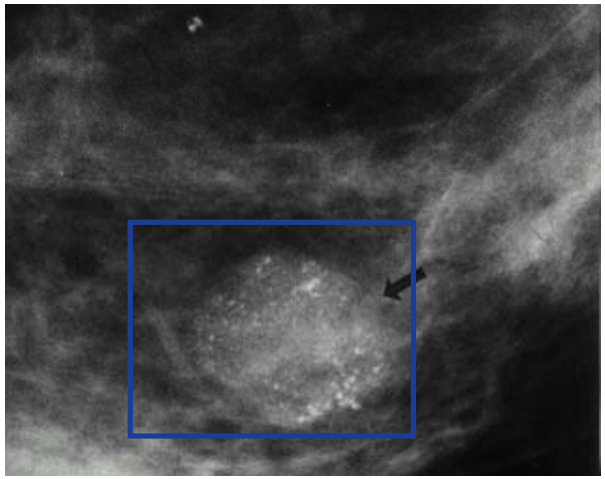

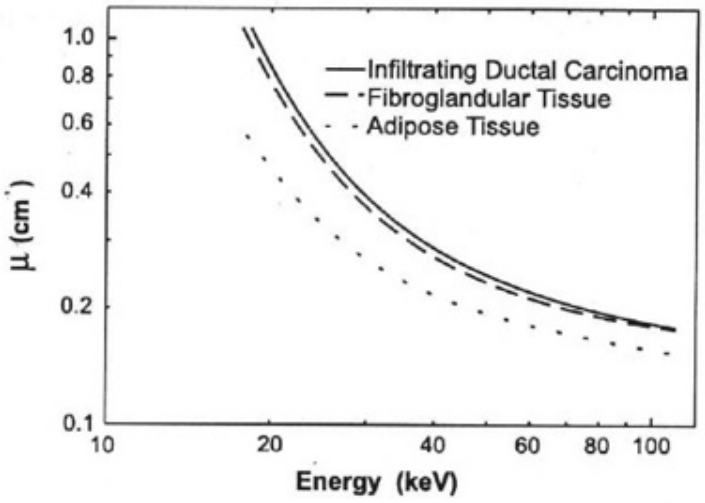

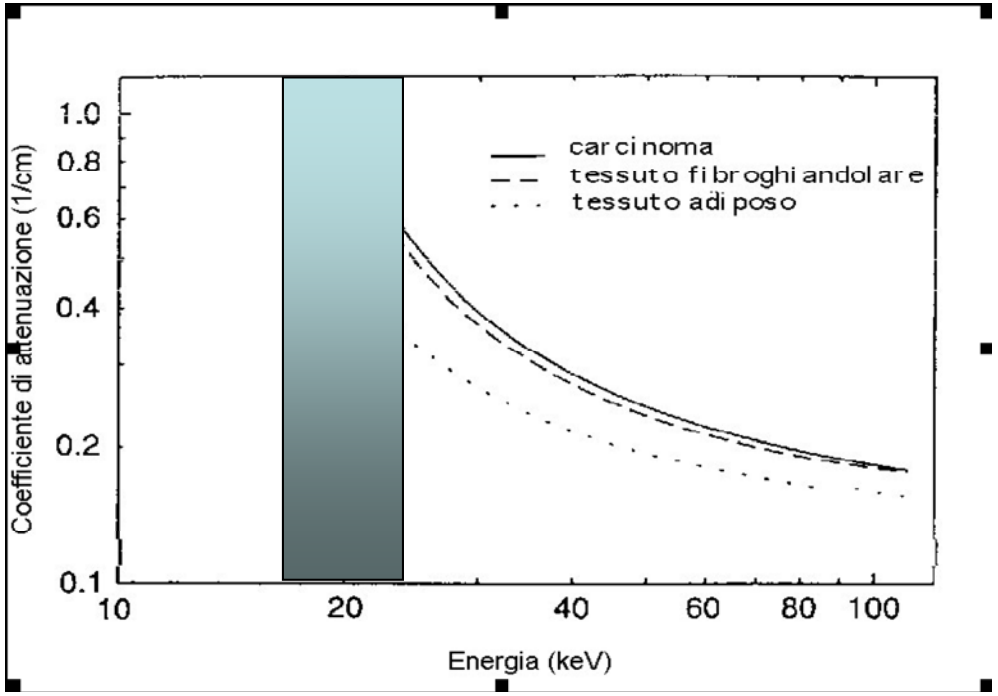

Tumour masses

- Healthy tissue degeneration
- X-ray Attenuation properties similar to healthy tissue
- Size > 5 mm

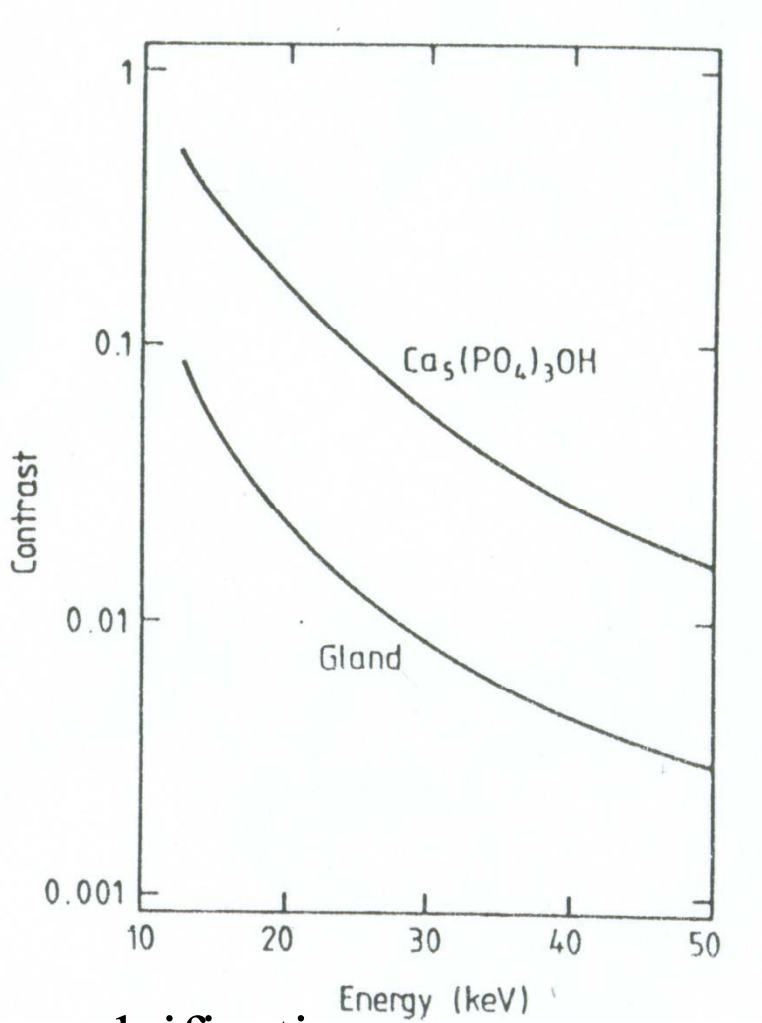

Microcalcifications

- Submillimetric calcium deposits
- Denser than gland and adipose tissues
- Cluster of microcalcificatons are tumour markers

56

The MedipixI/PCC detection unit

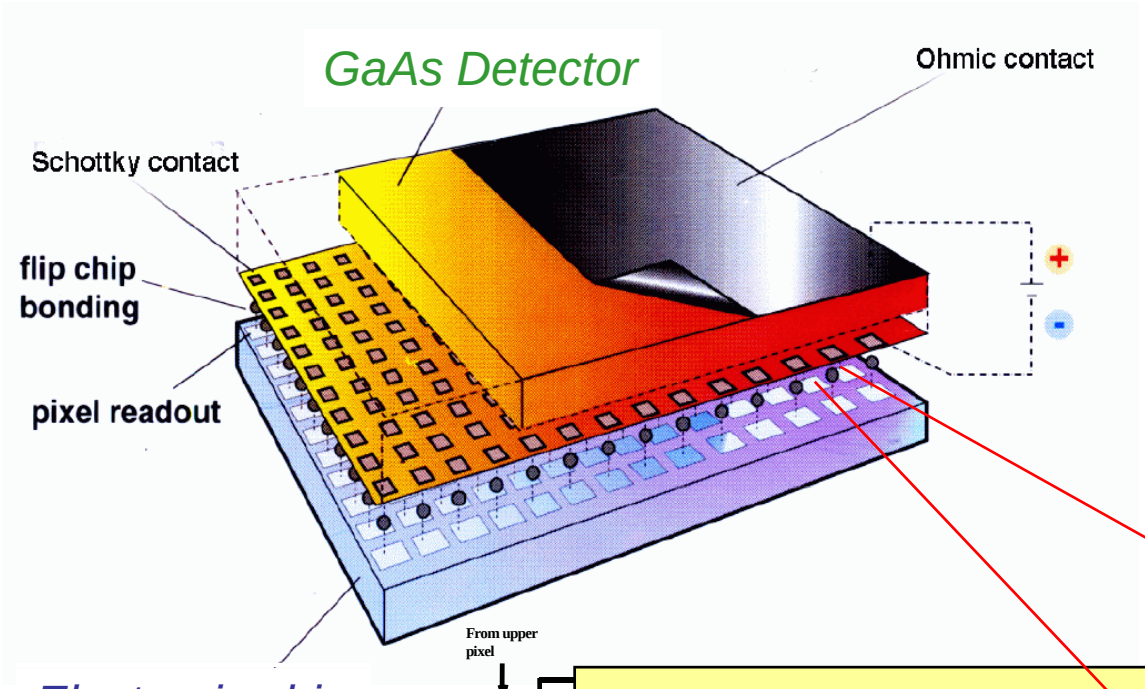

Detectors by AMS Italy

- *semiconductor : GaAs: 200 μm thick*
- *pixel 170 x 170 μm²*
- *Schottky 150x150 μm²*
- *channels 64 x 64*
- *area 1.2 cm²*

Electronic chip

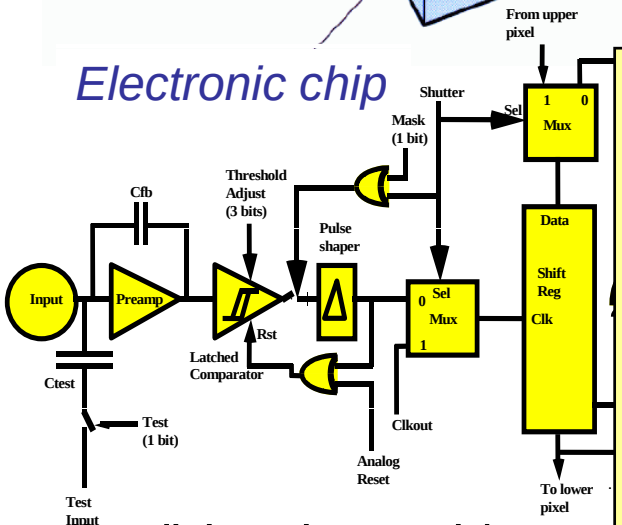

Photon Counting Chip (PCC)
MIC CERN SACMOS 1 μm
FASELEC Zurigo
Pixel 170 x 170 μm²
Channels 64 x 64
Area 1.7 cm²
Threshold adjust 3-bit
Pseudo-random counter 15-bit

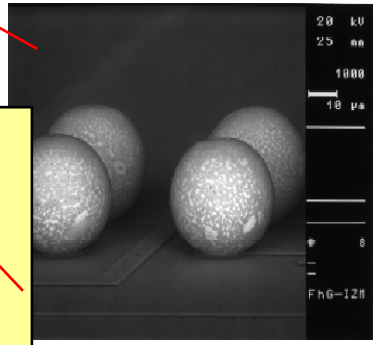

Indium Bump-bonding By AMS Italy

http://medipix.web.cern.ch/MEDIPIX/

Digital Mammography

Imaging detector requirements:

- High efficiency
- Low Noise
- High Spatial Resolution
- Maximization of the contrast information contents

Techical solutions:

- Semiconductor Pixels Detector
- Direct Detection technology
- High Z material (GaAs)
- Single Photon Counting electronics

Conventional Digital Mammography: Indirect detection

Charge Integration

Flat-Panels Phosphor Systems
Scanning Phosphor-CCD Systems

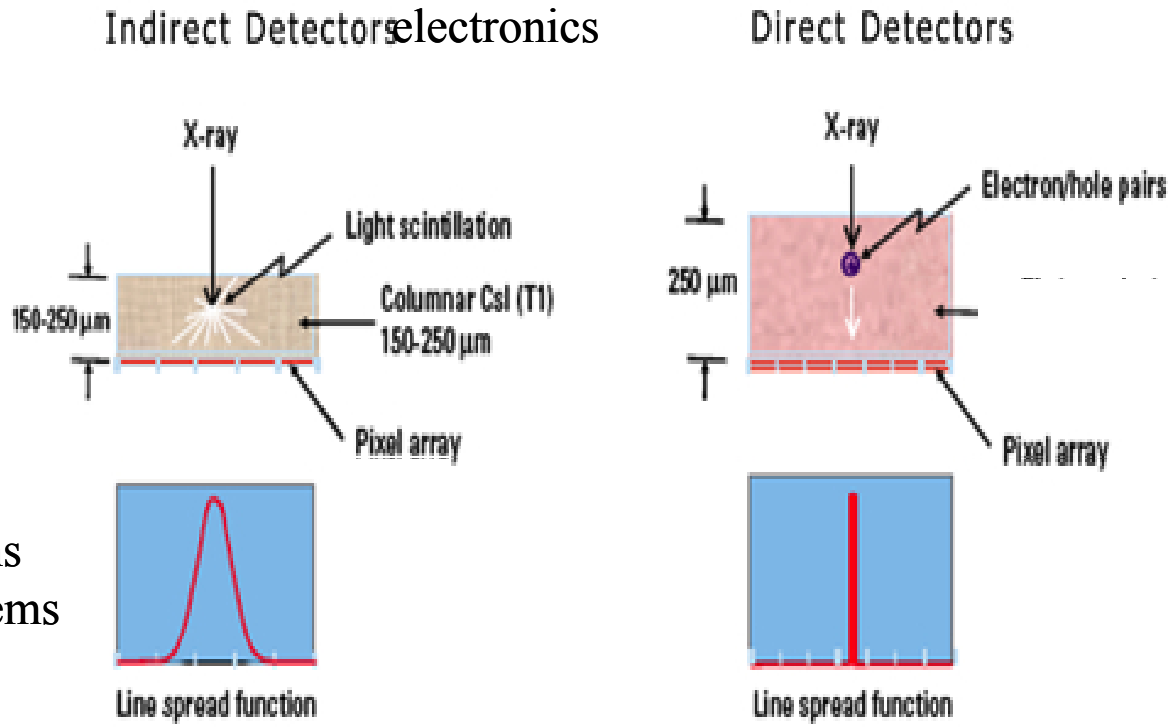

Why Single Photon Counting?

- Good noise discrimination
- Improvement of the Spatial Resolution
- Maximization of the contrast information contents

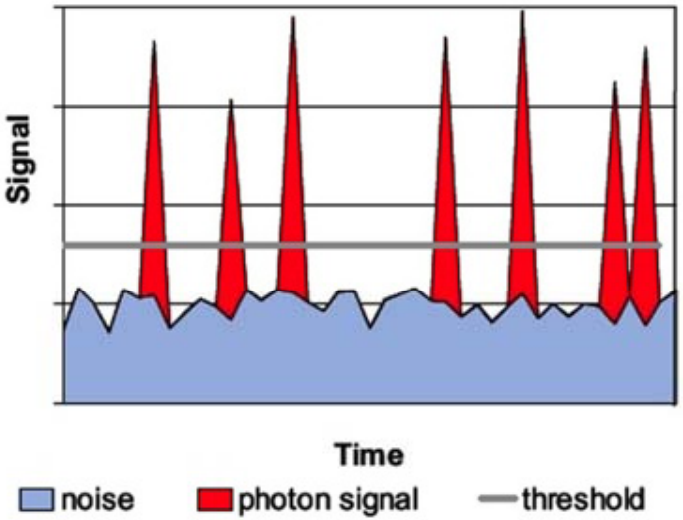

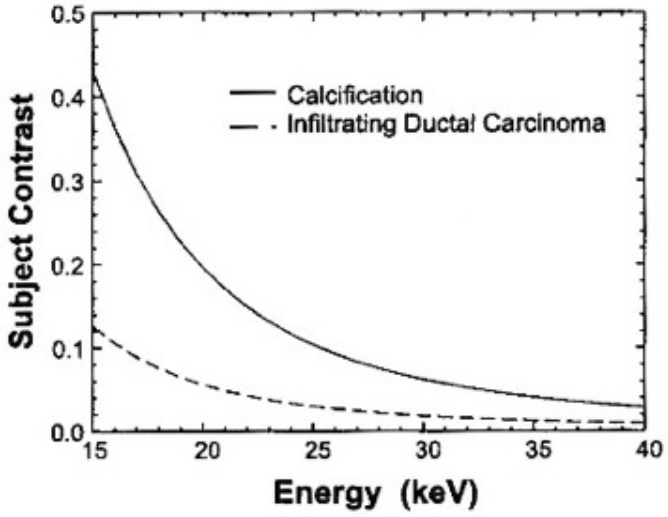

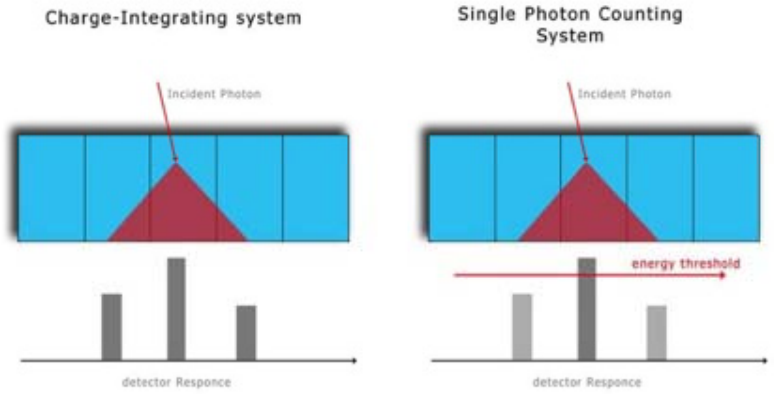

The IMI demonstrator

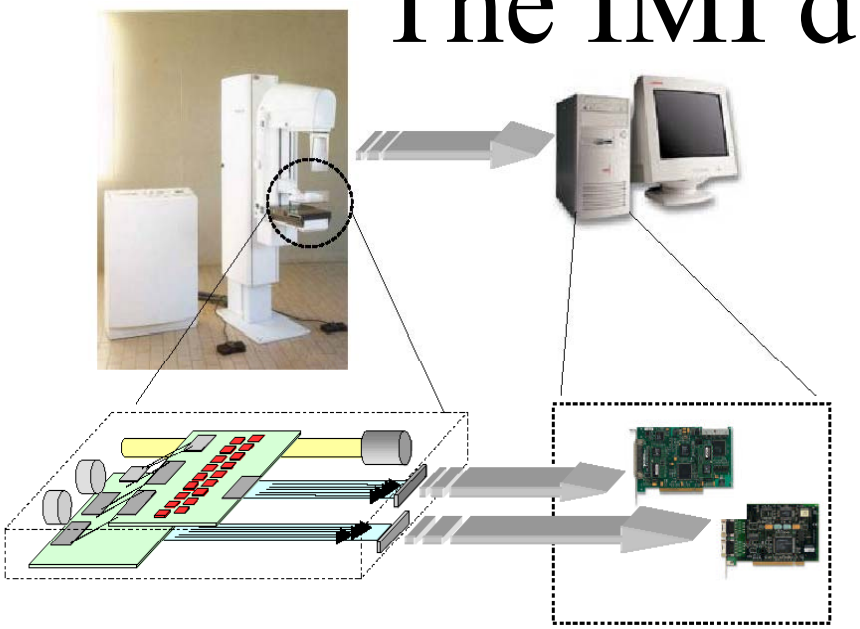

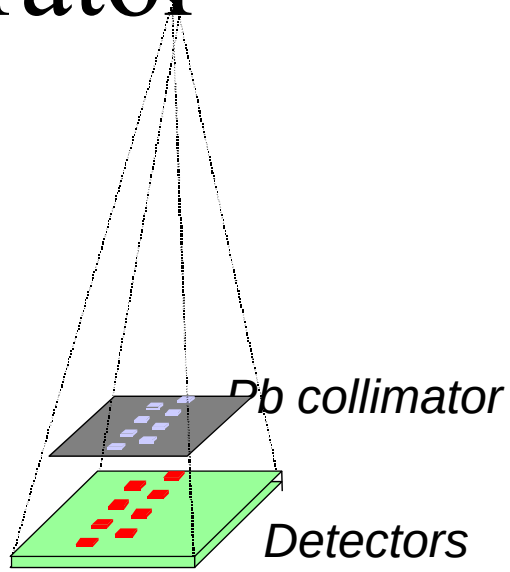

- Mosaic geometry with staggered rows of nine assemblies each one,
- Scanning across the exposure field by means of a stepper motor.
- The read-out system MMRS (Multichip Medipix Readout System) (LABEN)
  - custom designed chipboard
  - interface board (IB), connected to the chipboard, implements all the logic functions of the MMRS
  - PCI board commercial board (NI 6533) that interfaces the IB to the PC.
- The BIAS Board (CAEN) provides the analog and digital biases of the chips.
- The X ray tube (Gilardoni) is the clinical mammographer SYLVIA adapted to host the collimator and the detection head.
- A controller PC handles the whole image acquisition process by means of a software program written in LabWindows CVI.

The IMI Demonstrator

X ray tube

Mammographic Head

LEAD COLLIMATOR

Scanning simulation

- 18 x 24 cm2 exposure field
  - 1D scanning
  - 9 x 2 assemblies
  - 26 exposures
- “off-line” image reconstruction

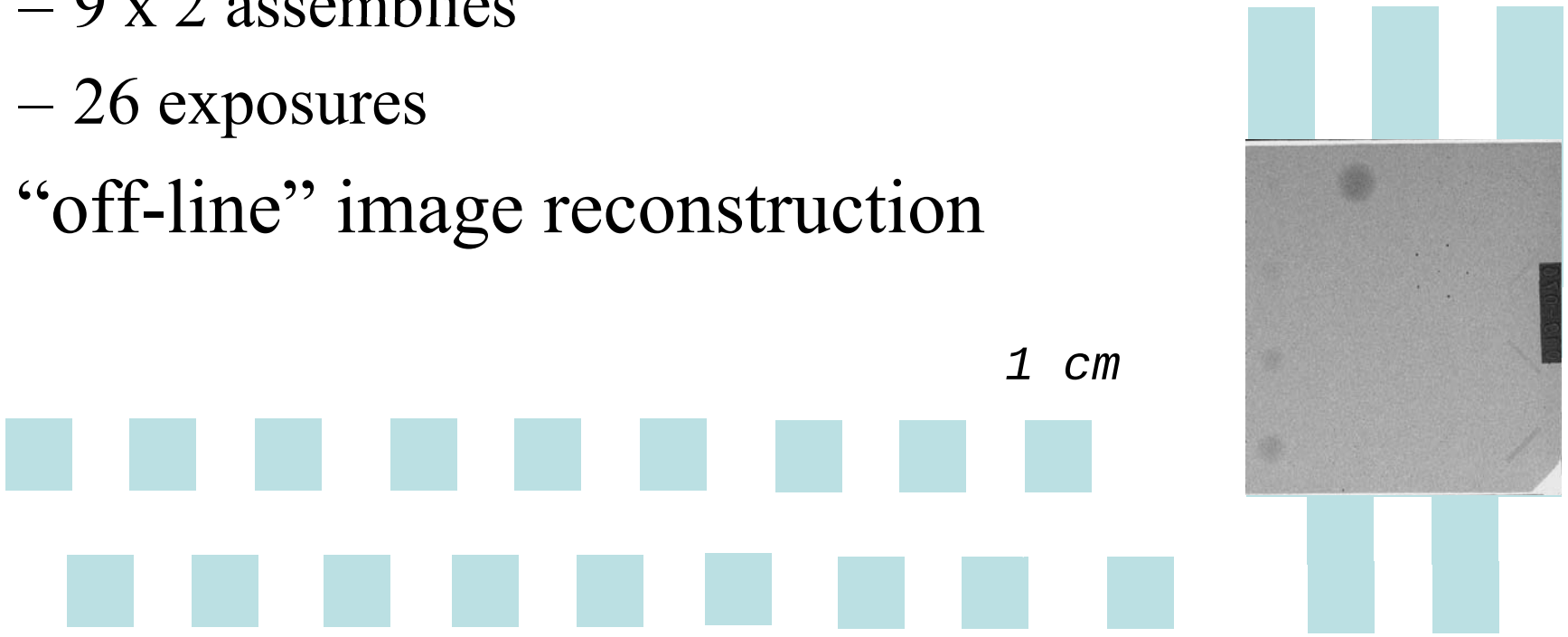

The Detection head

- The Detection Unit
  - The assemblies have been produced and bump bonded by Alenia Marconi Systems (Roma)
  - Each detection unit has been mounted in a protective case.

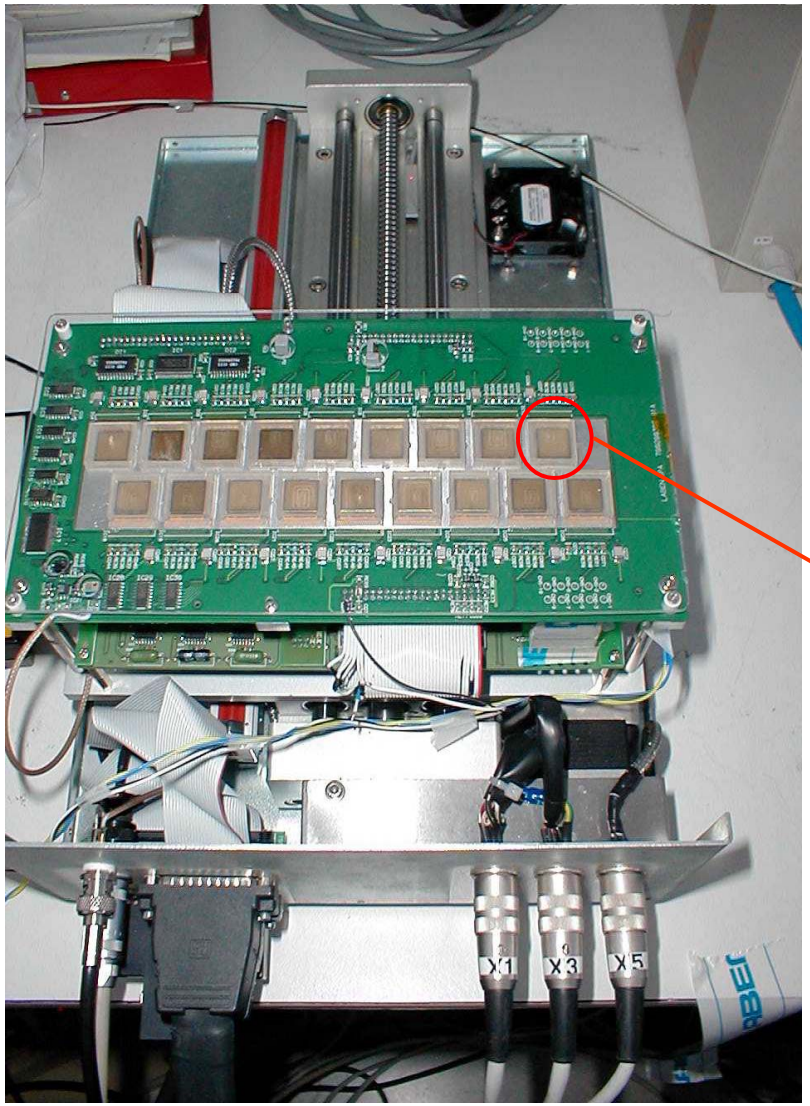

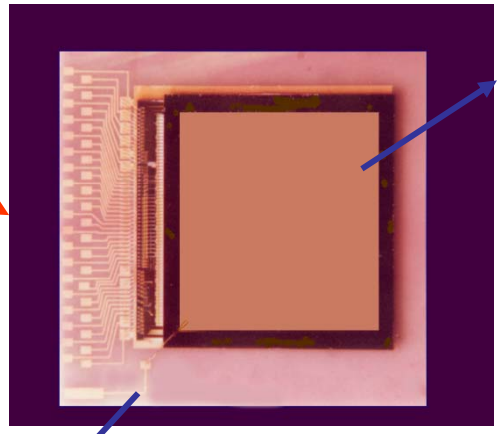

GaAs MPXI/PCC assembly

Aluminum nitride (AlN) substrate,
LEXAN cover on top (not shown)

Calibration of the IMI system

Threshold equalization:

Fine pixel threshold adjustment (3-bit resolution)

Electrical calibration

Absolute energy calibration

Energy threshold = 11 keV
(spread 1keV)

1

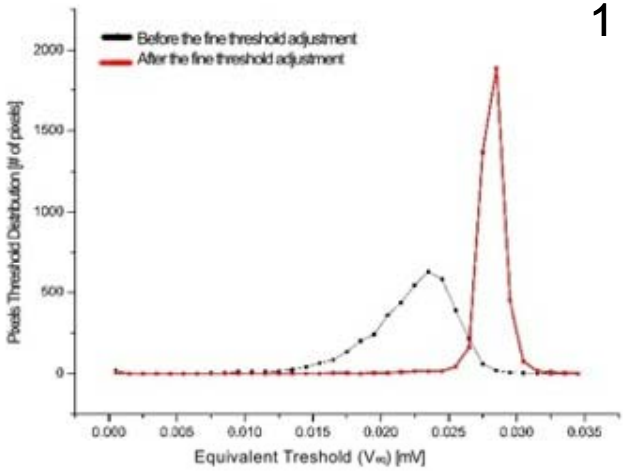

2

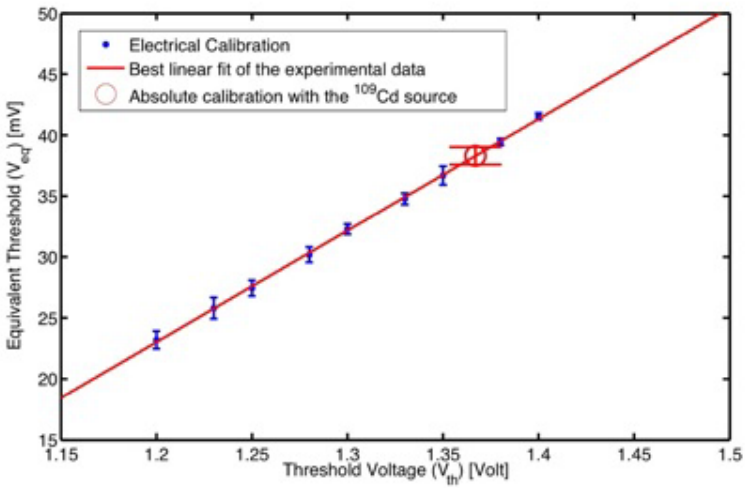

3

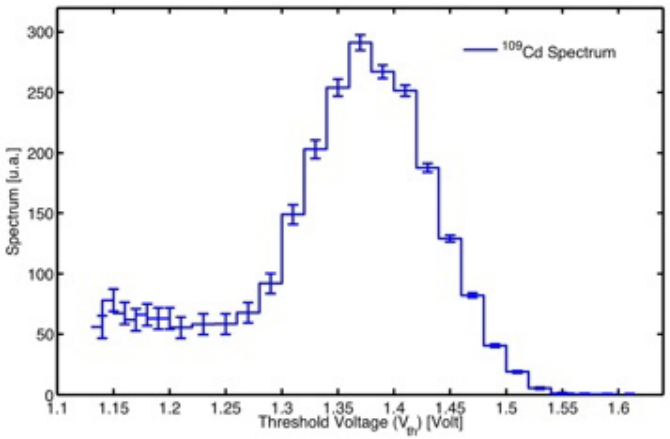

Calibration of the IMI system

Gain equalization:

- Flat-field equalization
- Noise pixels removing procedure

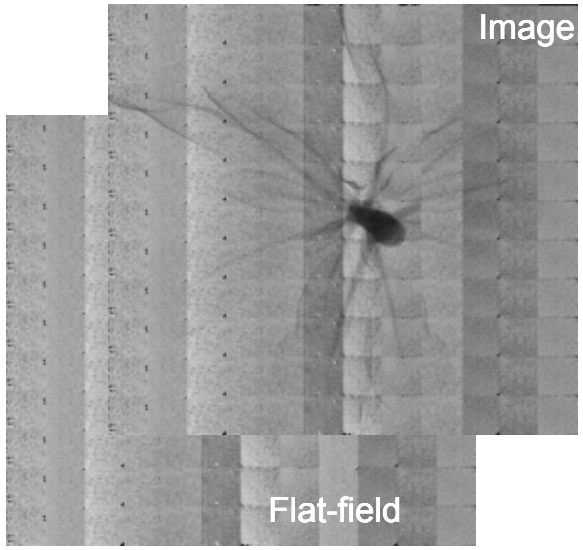

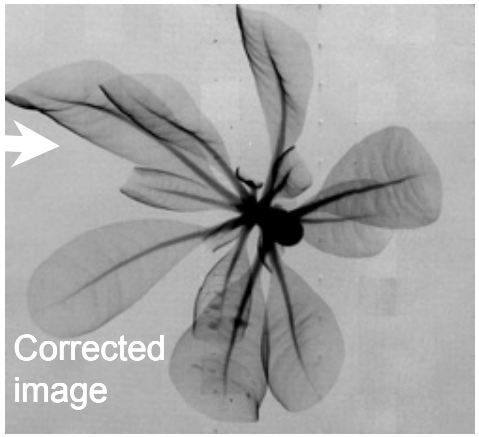

The IMI Prototype
(firsts acquired images)

12cm x 20cm

12cm x 17cm

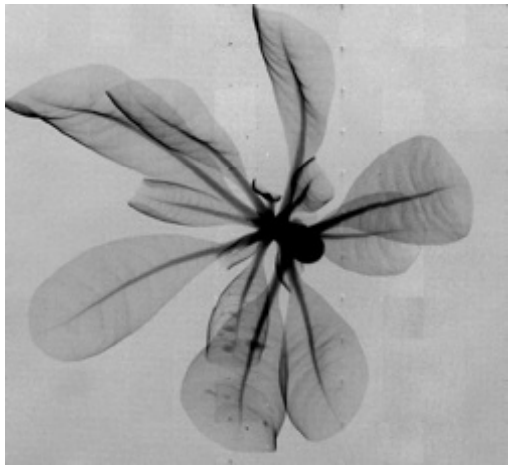

12cm x 11cm

Mo/Mo, 28kVp, 20 mAs

Assessment of the Imaging Quality of the IMI Prototype

Two different strategies have been followed:

1. Transfer Functions analysis:

(Protocol IEC 62220-1-2: "Medical electrical equipment - Characteristics of digital X-ray imaging devices - Part 1-2: Determination of the detective quantum efficiency - Detectors used in mammography")

- Presampling Modulation Transfer Funtion (PMTF)
- Detective Quantum Efficiency (DQE)

1. Contrast-Threshold Analysis:

•EUREF Protocol: Perry N, Broeders M, de Wolf C, Törnberg S, Holland R, von Karsa L (eds), " European Guidelines for quality assurance in breast cancer screening and diagnosis – Fourth Edition", Luxembourg (2006)

- •Thickness-Threshold diagrams (CDMAM phantom)

S.R. Amendolia, Med. Phys. **36**, 4, (2009), 1330-1339

experimental results:

Presampling MTF

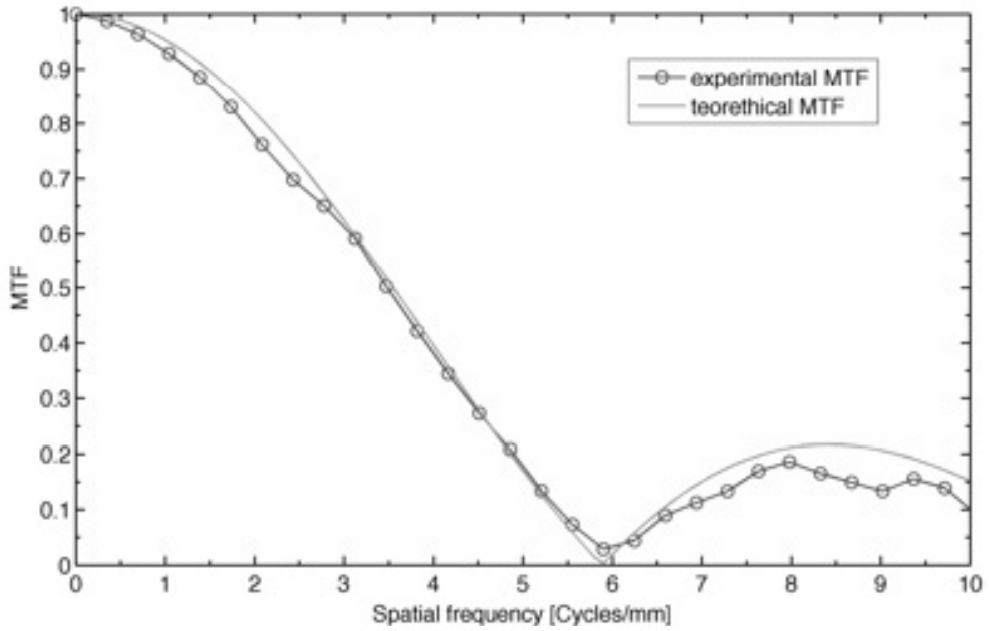

Experimental Presampling MTF.

maximum uncertainty = 3%

Low frequency Drop effect.

Fit wit the function |sinc(πau)|:

a = 170 μm ± 5μm.

Perfect agreement with the physical pixel dimensions!!!

Tilted edge

- Tungsten Edge: 80mm x 13mm
  70μm thick
- Edge angle: ϑ = 3.05° ± 0.05°
- N=1/tanϑ=18.8 ± 0.4
- Oversampling distance = 9 μm

experimental results:

Detective Quantum Efficiency

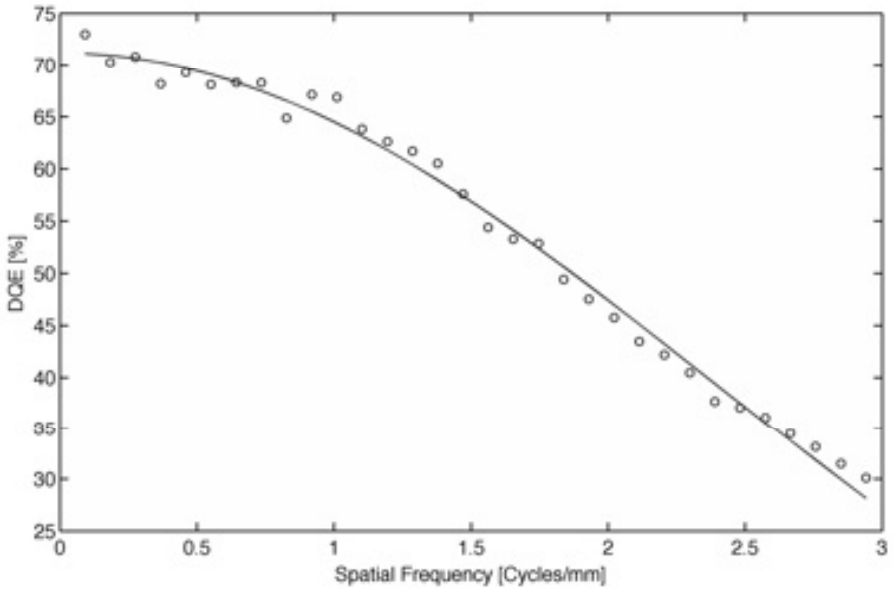

DQE(u) for a single detection unit working in stationary mode.
a flat- field with high statistics has been used to correct the image

experimental detection efficiency

$$G = \bar{I}/\bar{q} = 74\% \pm 2\%$$

DQE(0) as a function of the incident dose on the flat-field

The DQE(0) grows up to the 74% ± 1.6%

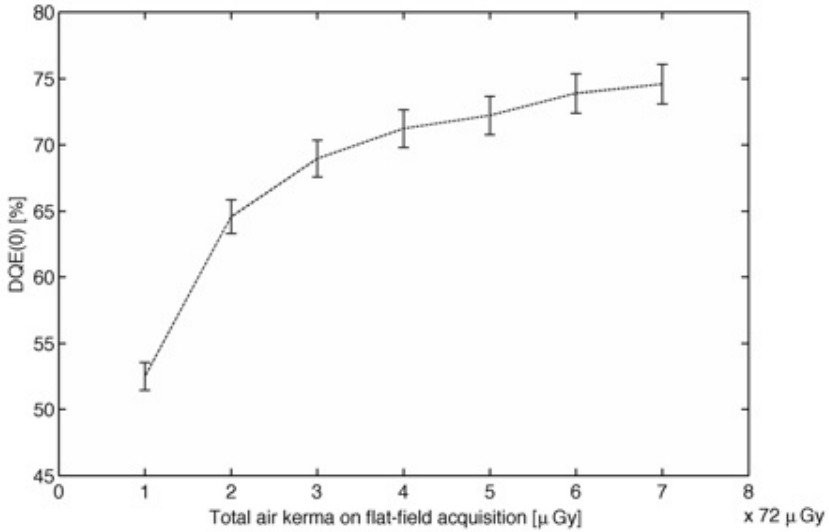

experimental results:

Detective Quantum Efficiency

Comparison of the DQE of the IMI Prototype with the most common digital mammographic systems

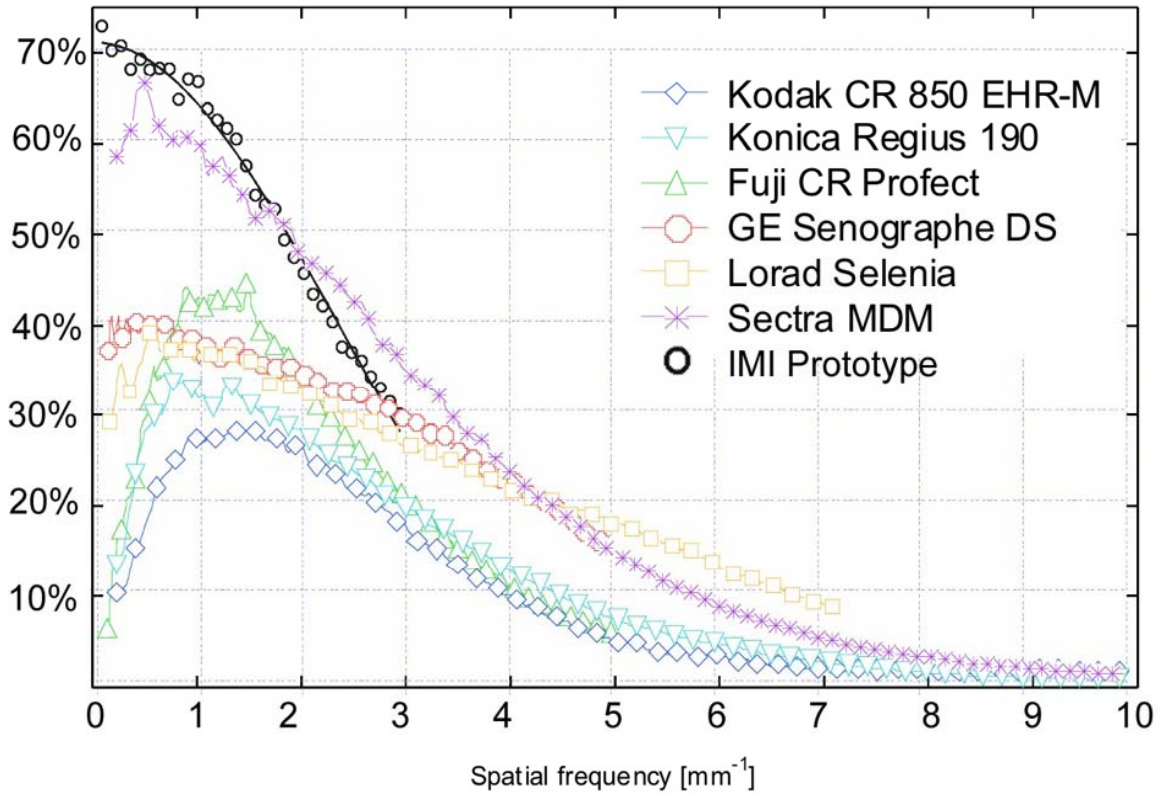

* Monnin et al. Medical Physics, March 2007, Volume 34, Issue 3, pp. 906-914

experimental results:

Thickness-Threshold curves

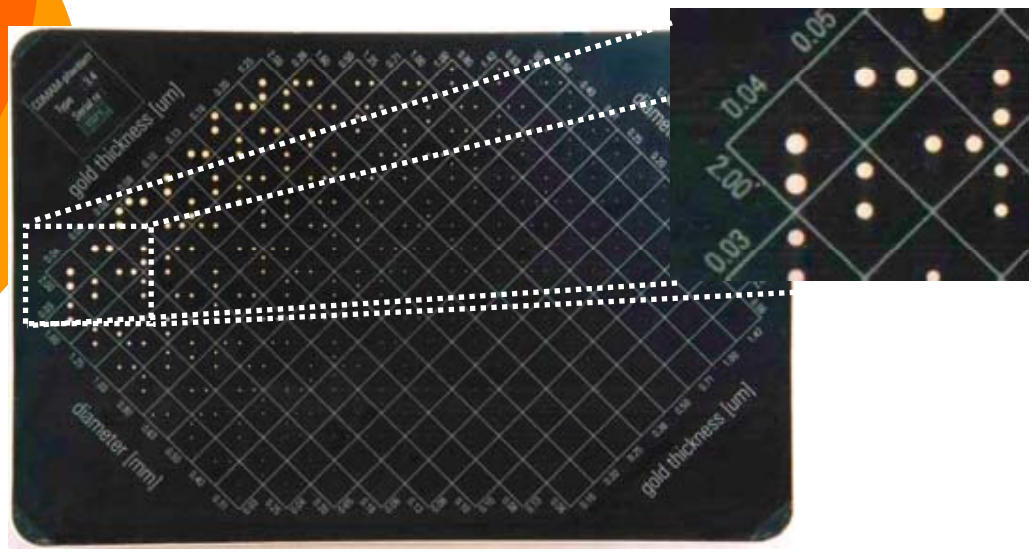

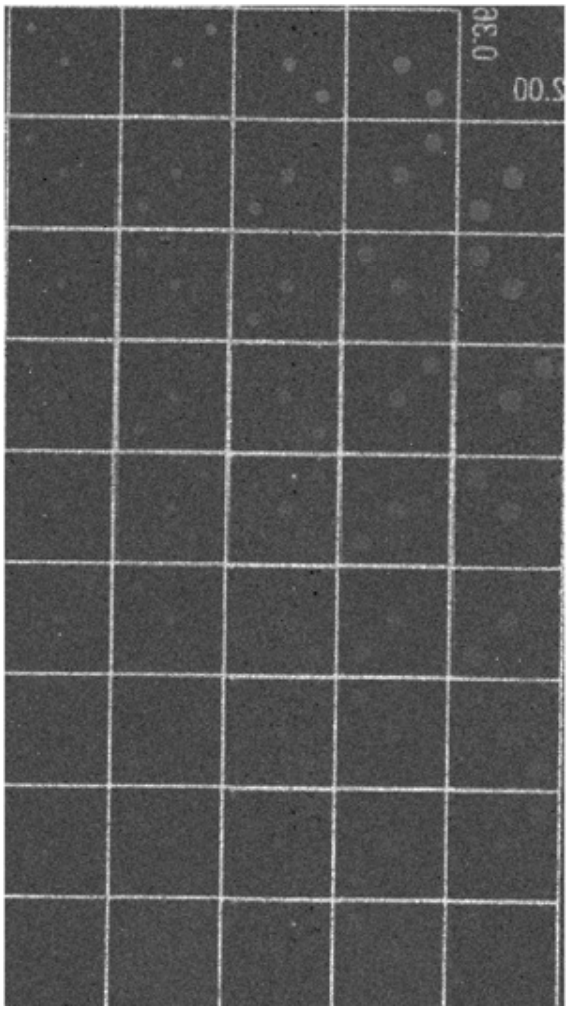

CDMAM Phantom

aluminum base 0.05 mm thick
gold disks (99.99% pure gold),
with diameter and thickness in the rang:
diameter: 0.01 mm to 2 mm
thickness: 0.03 μm - 2μm
16 x 16 rows. Each row has constant diameter
and each columns constant thickness

experimental results:

Thickness-Threshold curves

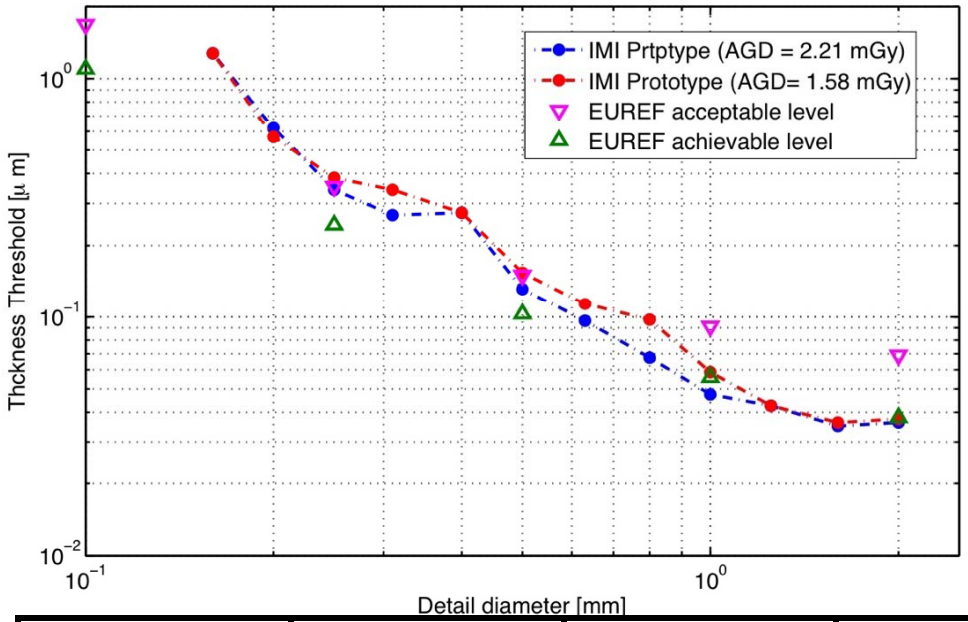

Thickness-Threshold for details of 1.6 mm of diameter = 35 nm of gold, corresponding to an intrinsic contrast of 0.49%

Disk diameter (mm)	EUREF Acceptable value (μm)	EUREF Achievable value (μm)	IMI Thick.-Tresh, (μm) 1.58 mGy	IMI Thick.-Tresh., (μm) 2.21 mGy
2 mm	0,069	0,038	0,0375	0,0362
1 mm	0,091	0,056	0,0588	0,0475
0.50 mm	0,15	0,103	0,1537	0,1312
0.25 mm	0,352	0,244	0,3833	0,3417
0.1 mm	1,68	1,1	-	-

Conclusions

Transfer Functions Analysis: MTF DQE

- The transfer functions are in accord with the model of the ideal SPC detector
- The spatial resolution is limited only by the pixel size:
- The pixels are uncorrelated and there are not additive or multiplicative noise: the system is quantum limited

Thickness-Threshold Analysis

- The system comply with the EUREF limits for details bigger than the pixel size. The system shows the best performance in the detection of detail in the range 2mm - 1mm

proton beam characterization

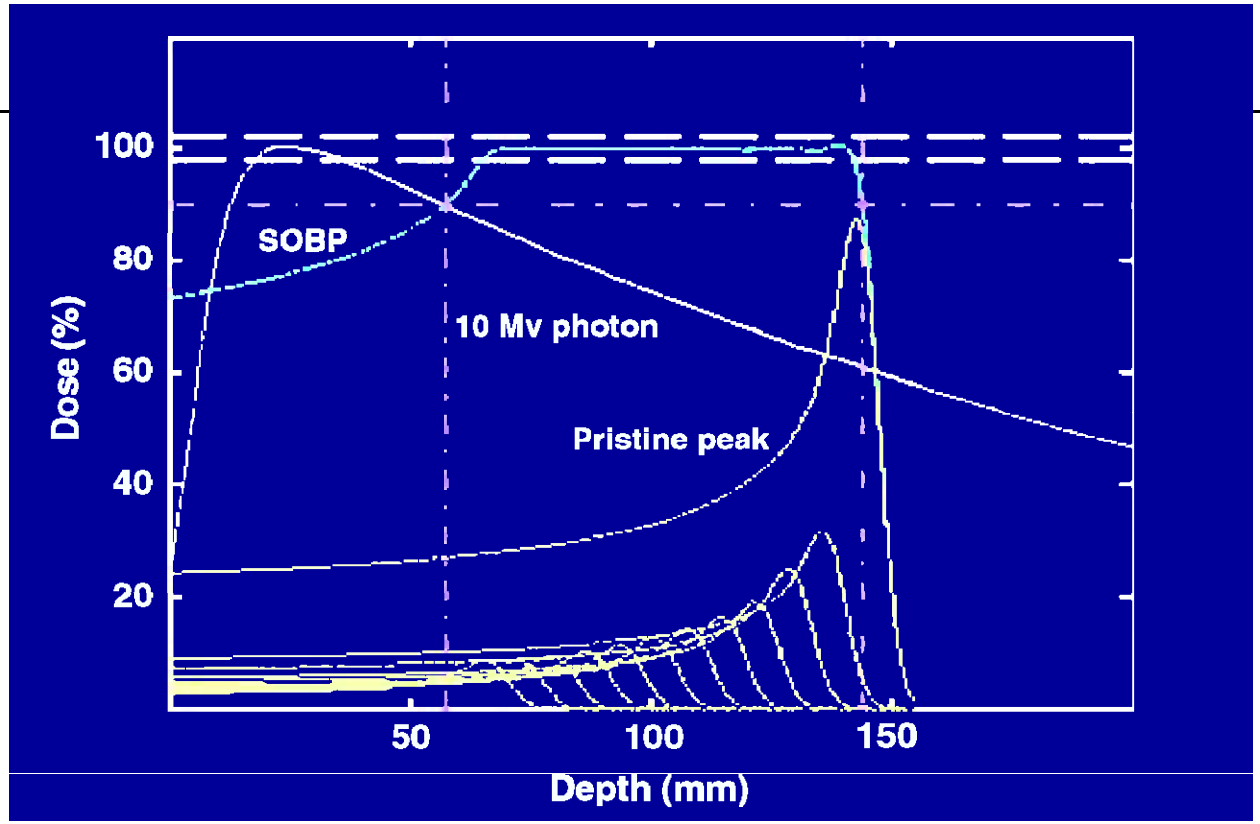

- The tumors are still one of the main cause of death reason in Europe
- **Light ion beams**, as proton, can overcome the limitations of conventional electromagnetic radiation due to the more selective energy deposition in depth.

- Proton-therapy is a technique used to deliver a highly accurate and effective radiotherapy for a variety of tumor diseases.
- To characterize the proton beam an instrument able to give on-line information on the beam penumbra and the flatness will be useful.

Contents

- Monte Carlo simulations
- Experimental measurement with MPX2 system
  - broadening of the proton beams as the beam passes throw a medium
  - the beam penumbra and flatness
  - the dose and dose rate of the incident proton beam

Monte Carlo simulations:

⑩ GEANT-4

1. - Uniform irradiation of a Ø 5mm area with 62 MeV protons
2. - Silicon detector 300 μm thick
3. - a 55 μm mash was superimposed to the silicon detector
   - Vth= 120keV
   - different PMMA specimen as absorber

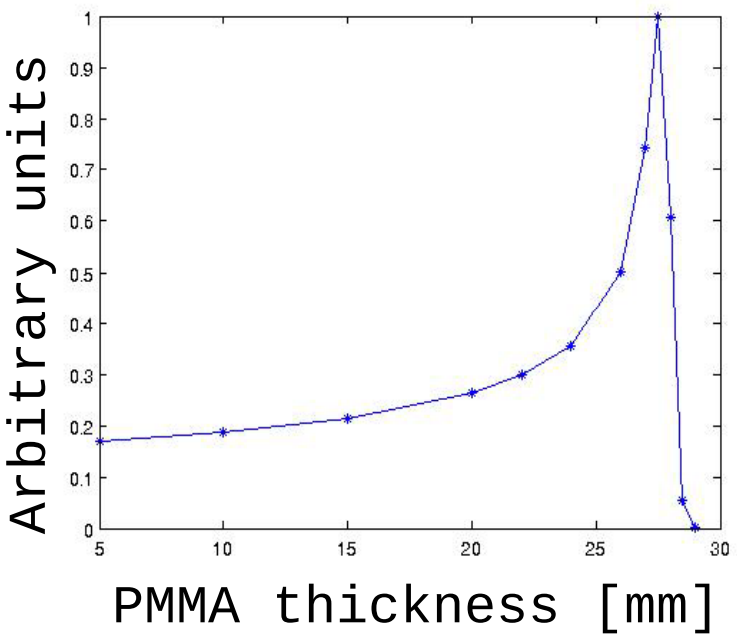

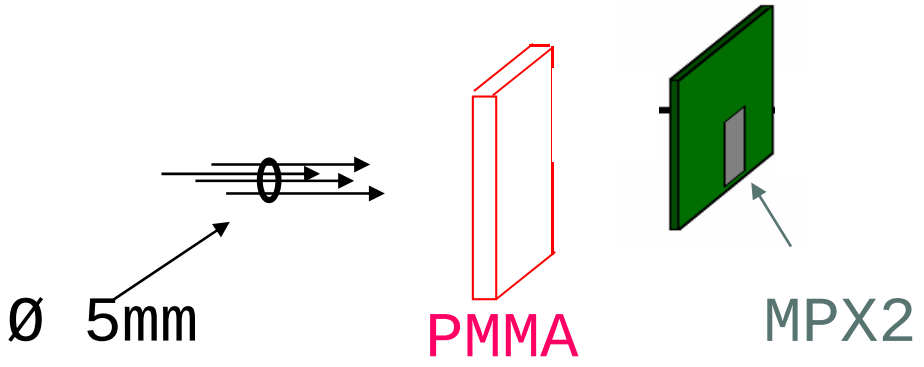

DETECTION SYSTEM

300µm Si detector

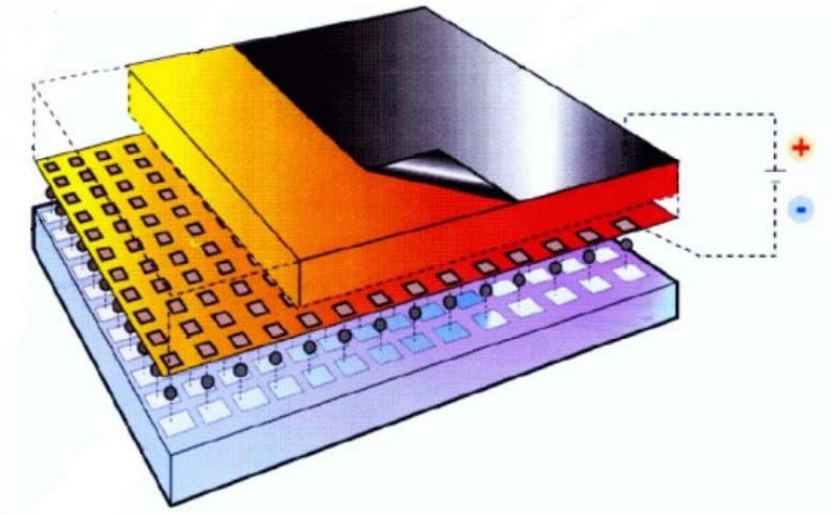

MPX2 read-out chip

- 256 x 256 square pixel matrix (size 55 µm)
- 13 bit pixel counter
- Max. count rate per pixel 1 MHz
- Electronic noise (sigma) 105 e-
- Window threshold discriminator (low and high level)
- 8bit conf. reg. (mask, enable, 3-bit thrs. adj. per each discriminator)
- Radiation tolerance <200 krad (10 keV X-ray)

A 62 MeV low flux proton beam. Due to the small detector surface collimators were used

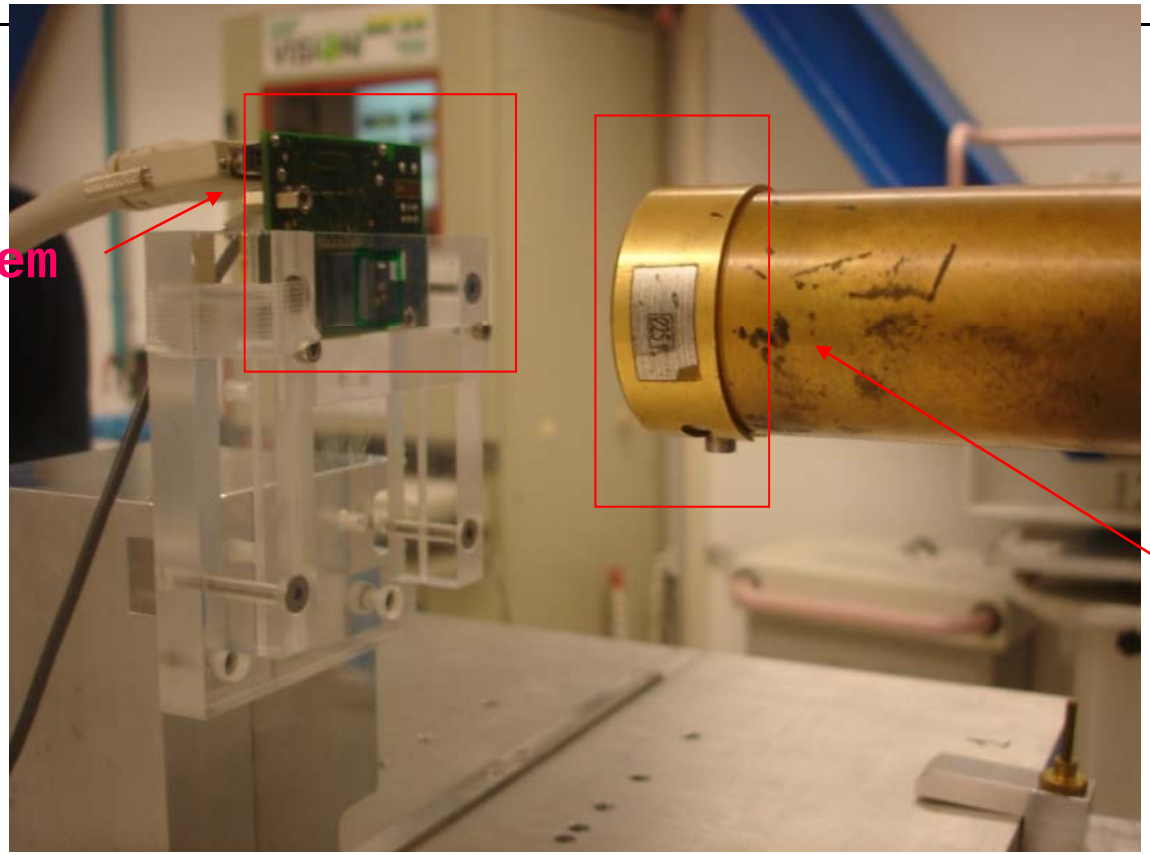

Experimetal set-up @ Catana: Laboratori Nazionali del Sud- INFN Catania, Italy, were a Superconducting Cyclotron is used for the treatment of the choroidal and iris melanoma (in Italy about 300 new cases for year) with 62 MeV proton

To check the MPX2 counts , with no PMMA, a different detection system was used in cascade to our MPX2 system

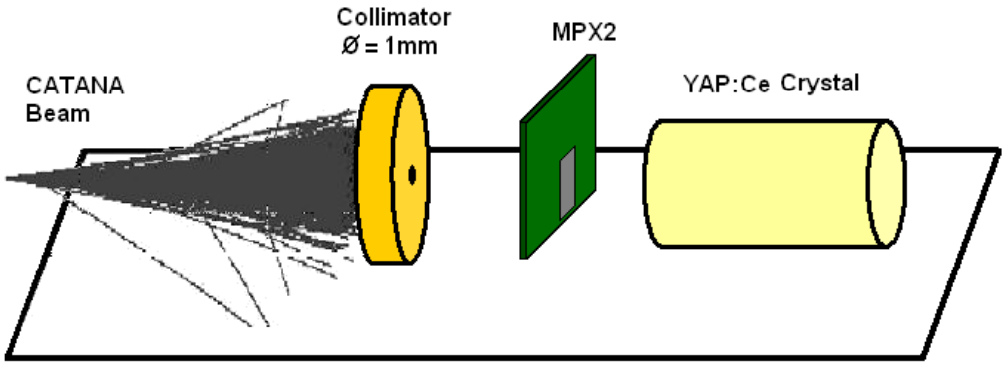

YAP:Ce Crystal	
Length	10 cm
Diameter	2,5 cm
Time constant	30 ns
Light yield	15 10^3 ph / MeV
Energy Resolution @ 60 MeV	2,6 %
Linearity (range 30-60MeV)	1 %

Data acquisition system

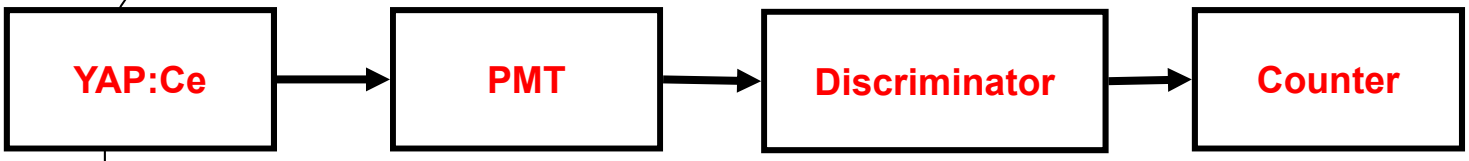

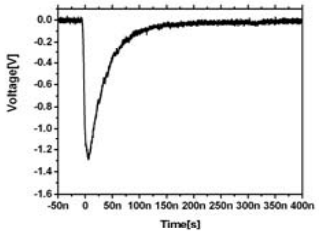

Typical PMT output

Amplitude= 1.2V

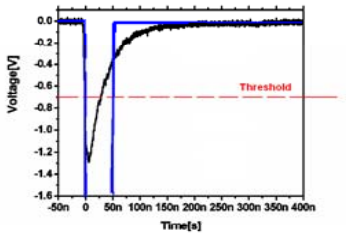

Threshold = -700mV

Dark current < 10 Hz

The two systems were operated together at a cyclotron current of 3pA, measuring the **same rate of 1.6 protons/(second*pixel).**

Beam broadening

experimental beam image after several PMMA thicknesses

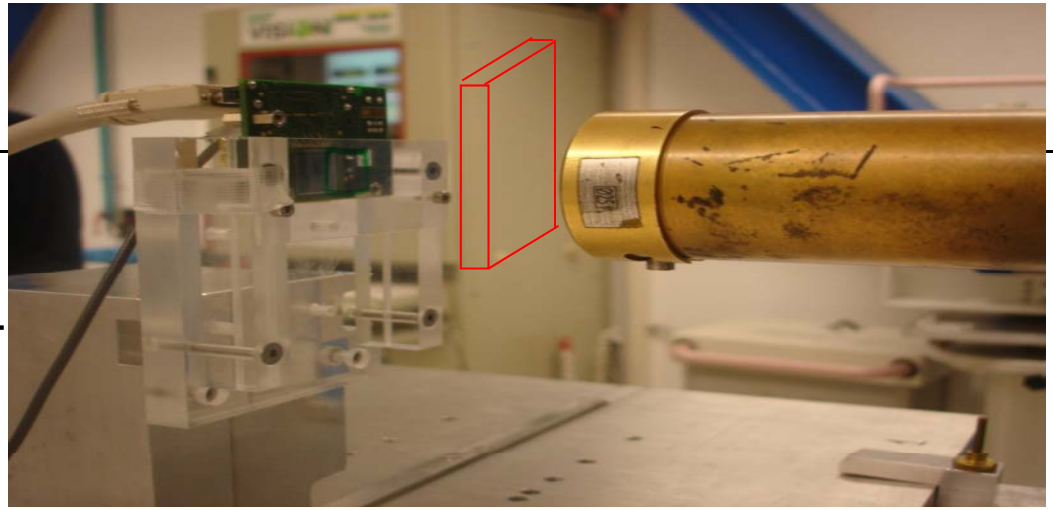

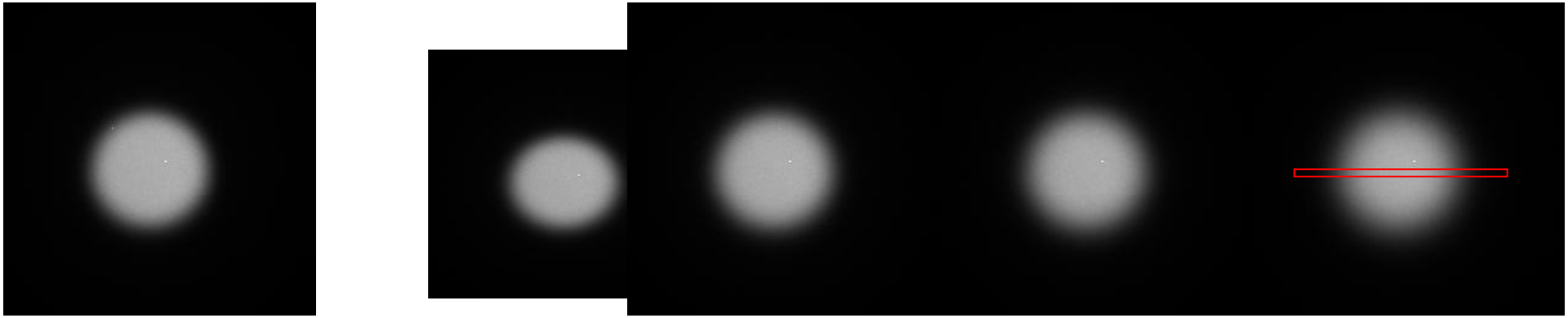

0 mm 5 mm 10 mm 15 mm 20 mm

Vth= 120 keV
Input dose 30 cGy
Cyclotron current of 1nA (about a factor 6 lower than the current used during treatments)

Beam broadening: experimental and simulated profiles

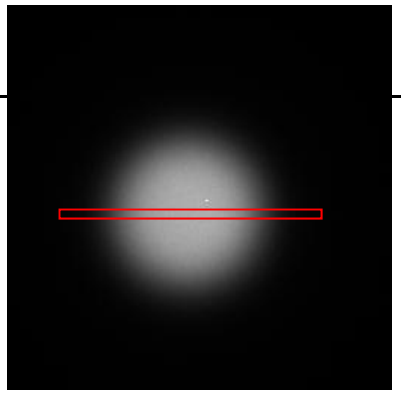

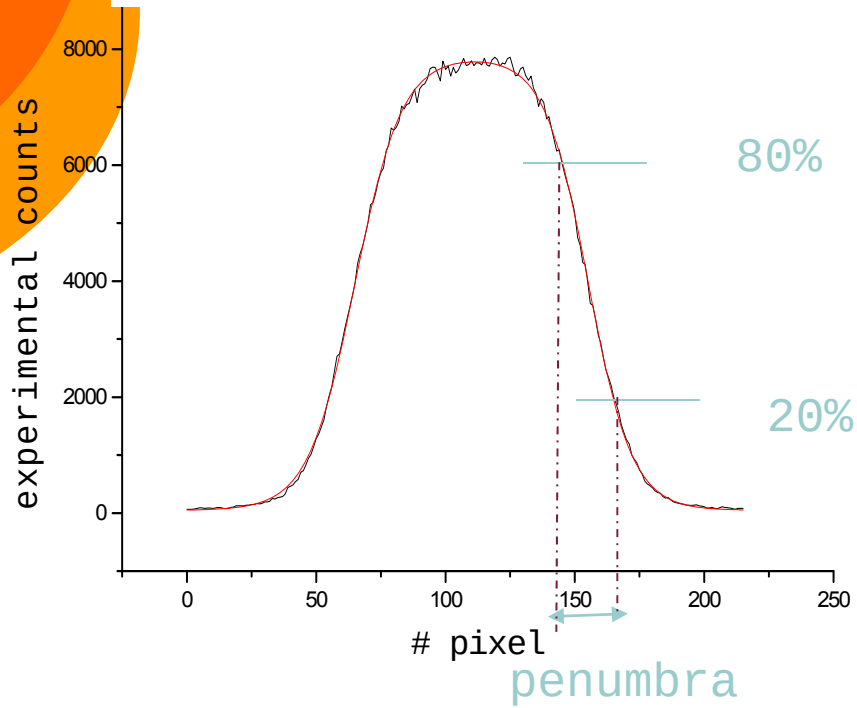

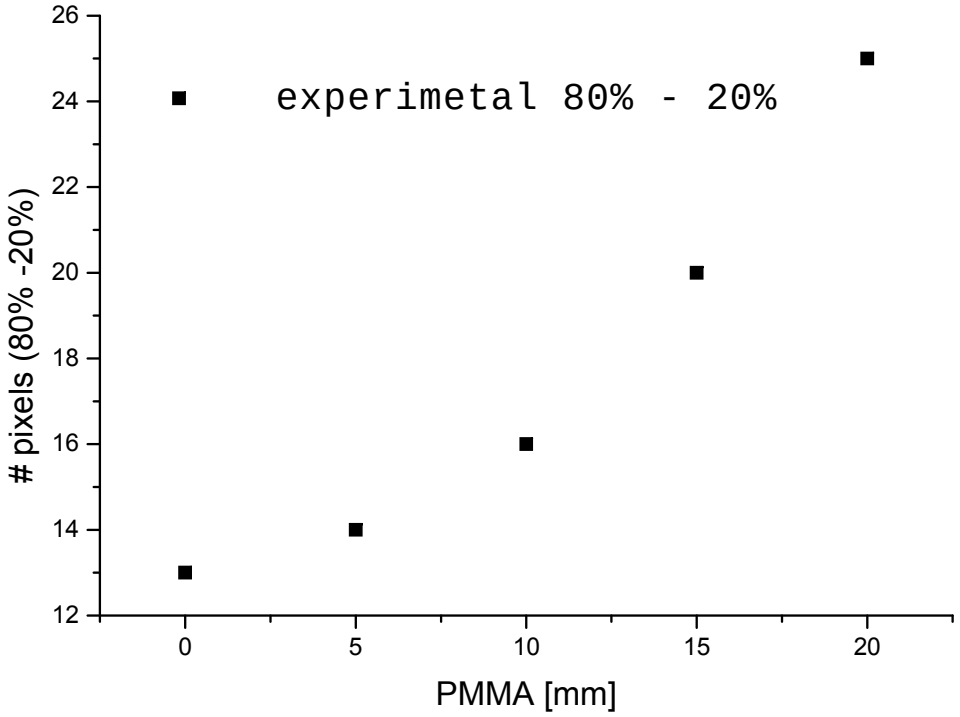

A double-Boltzman function was used to fit the rise and the fall of the profiles

Beam broadening

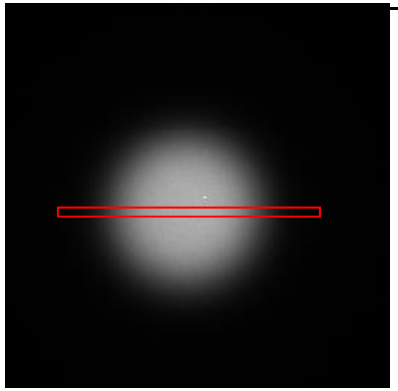

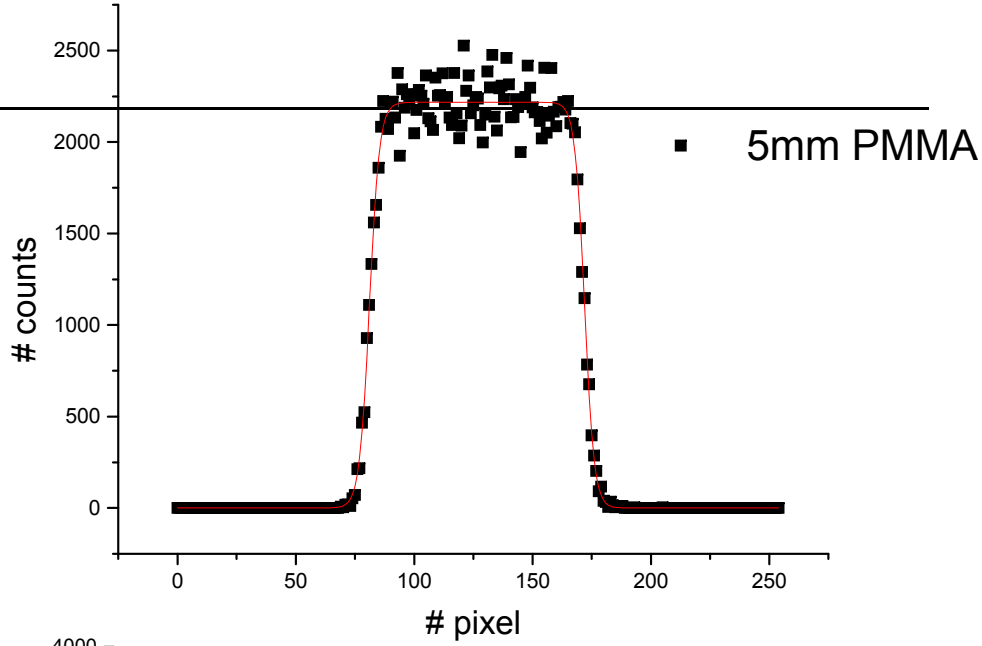

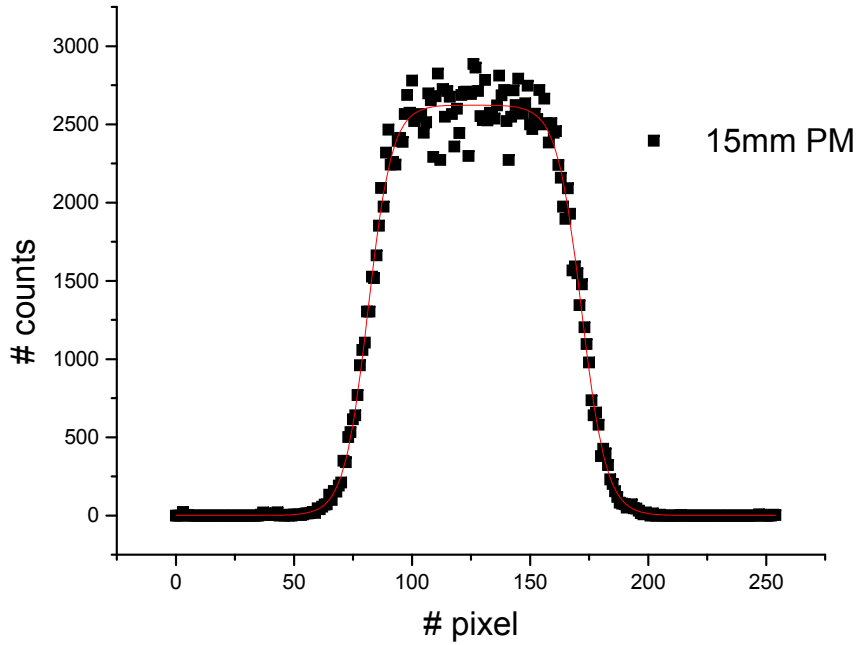

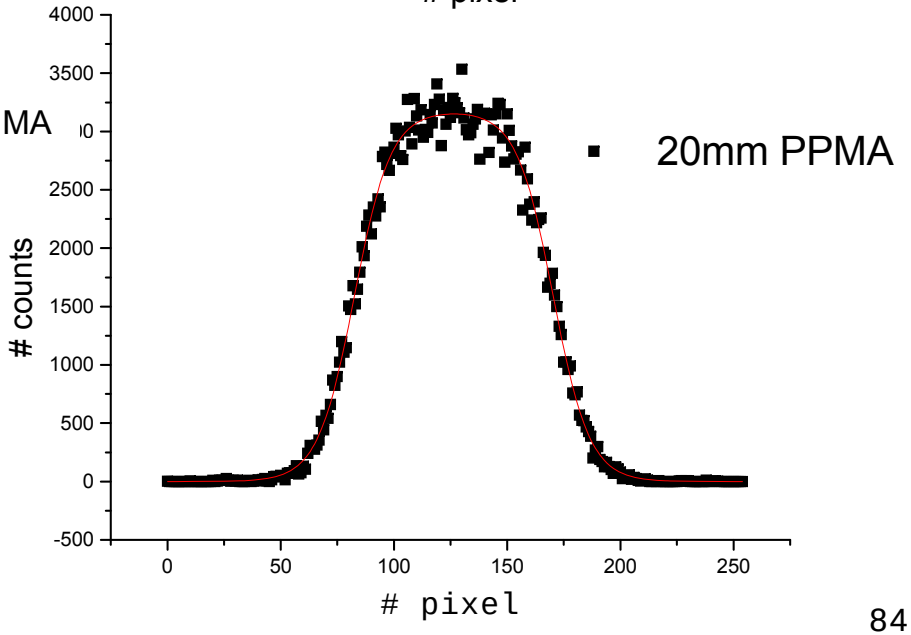

Beam broadening: experimental and simulated penumbra

- experimental 80%-20%
- simulated 80%-20% no divergency
- ca… …ency

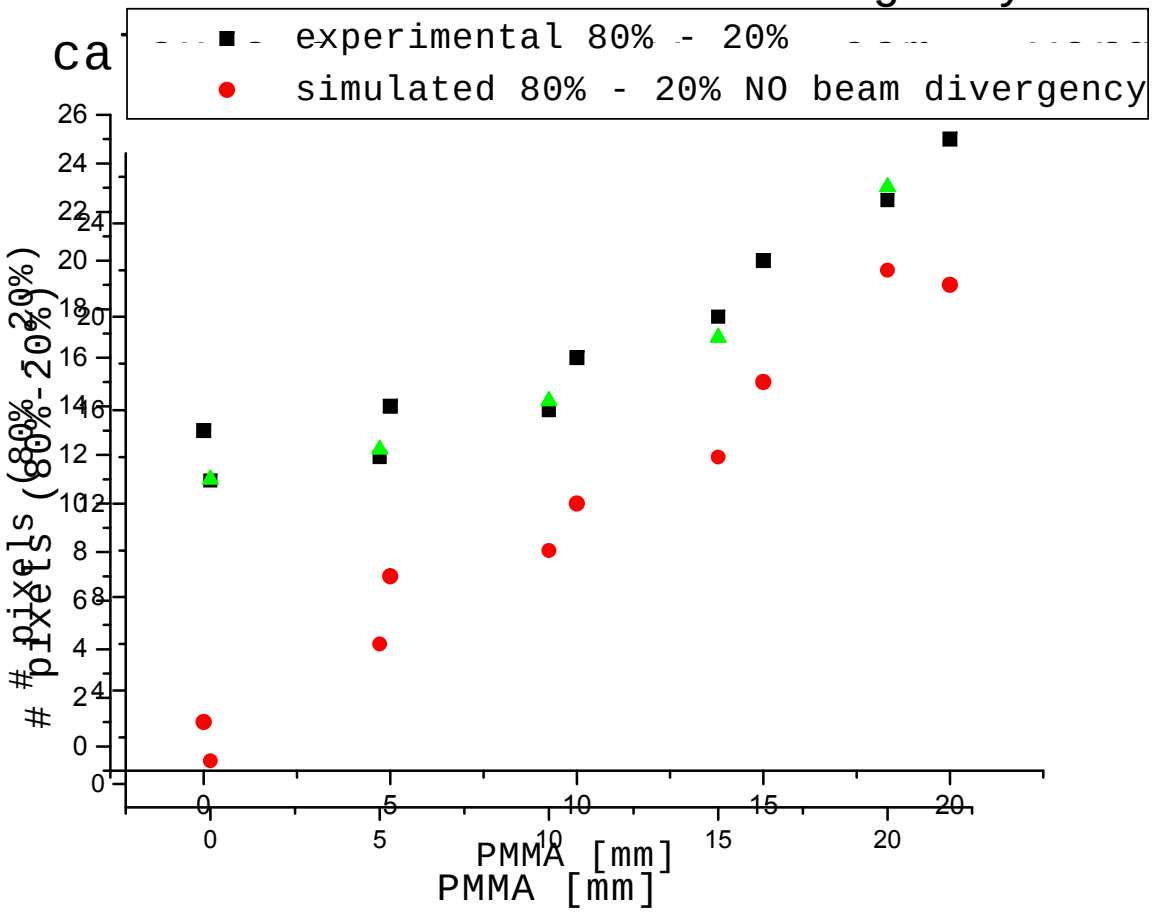

$$P_{\_calculated} = \sqrt{(P_{\_exper0mm}^2 + P_{\_simul}^2)}$$

Beam penumbra and flatness

MPX2
(55μm)

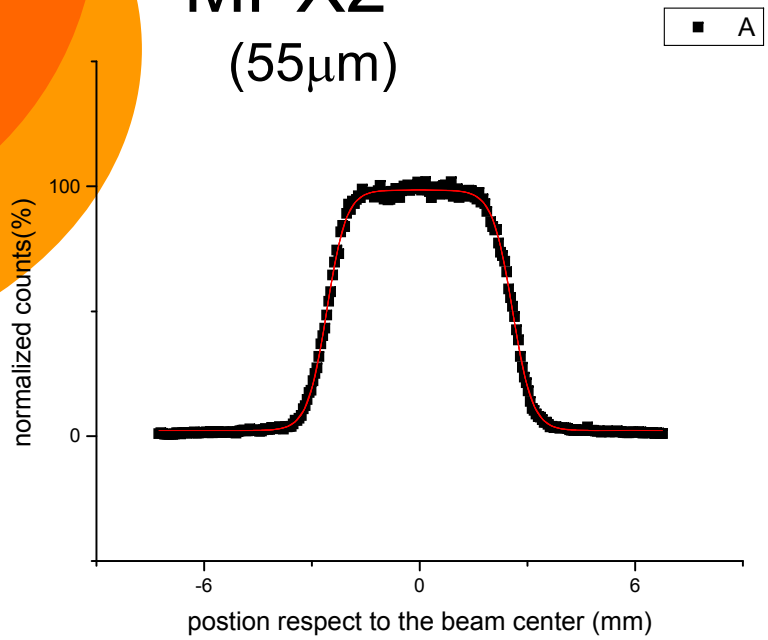

Gafchromic
(200 μm)

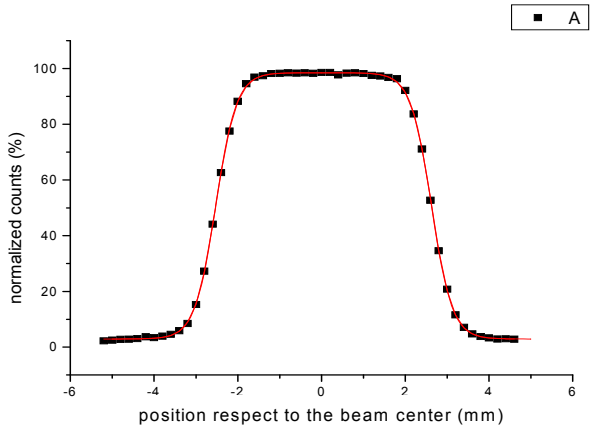

Mpx2_penumbra_rise = 0.79mm

Mpx2_penumbra_fall = 0.81mm

Gaf_penumbra_rise = 0.73mm

Gaf_penumbra_fall = 0.73mm

Beam flatness

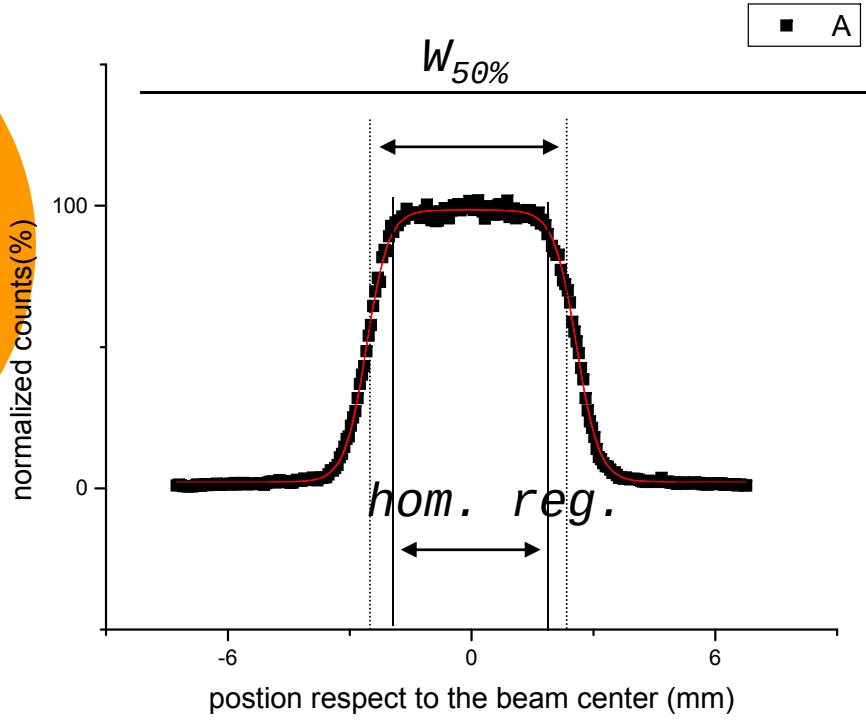

Gaf $R_T\%$ = 6.3%

MPX2 $R_T\%$ = 6.3%

$$R_T\,\% = \frac{P_{\max} - P_{\min}}{P_{\max} + P_{\min}} \times 100\%$$

Count rate as a function of the dose for different dose rates

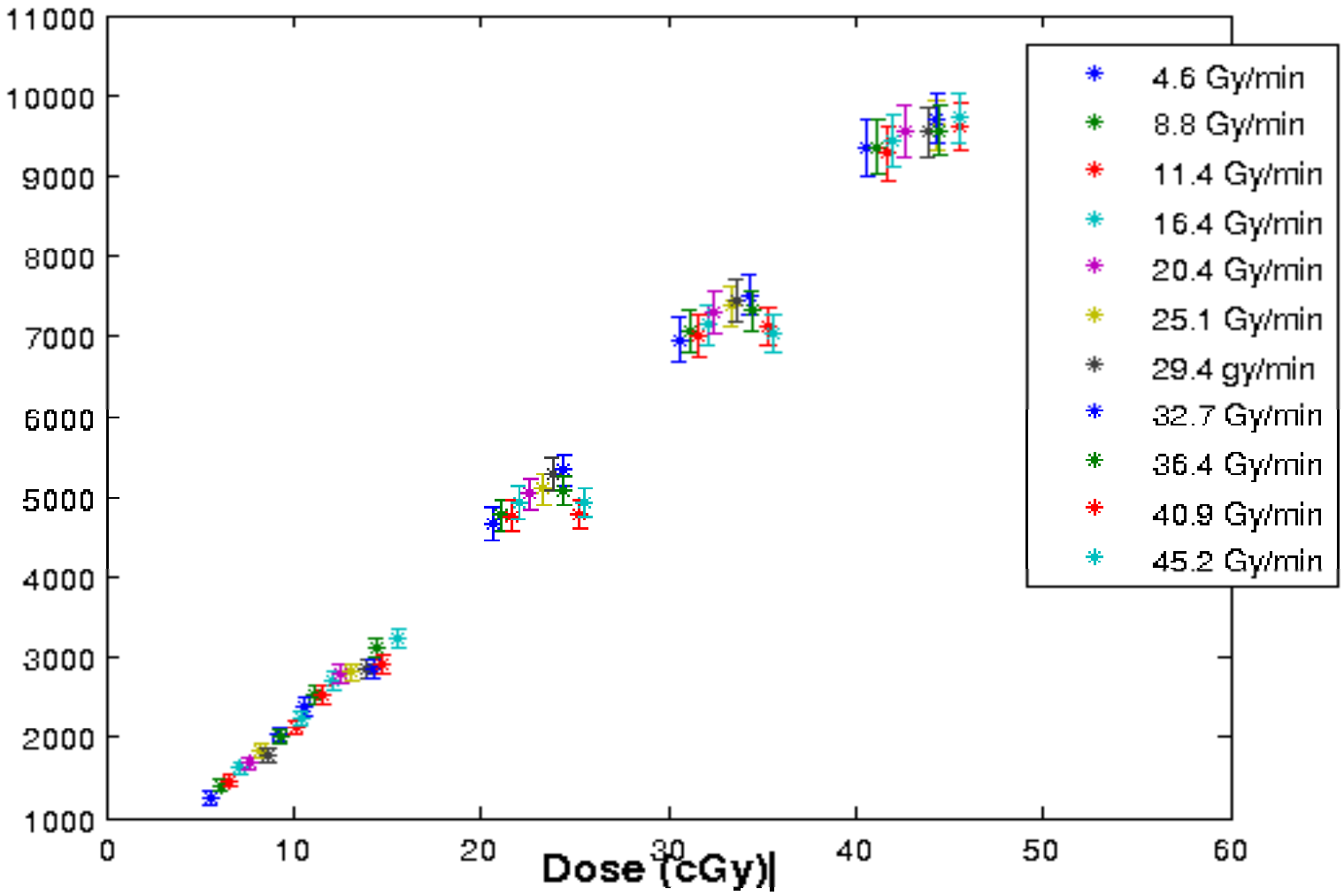

Linear and independent on the dose rate up to 35 Gy/min
Clinical dose rate 15 Gy/min

Count rate as a function of the exposure time and reproducibility

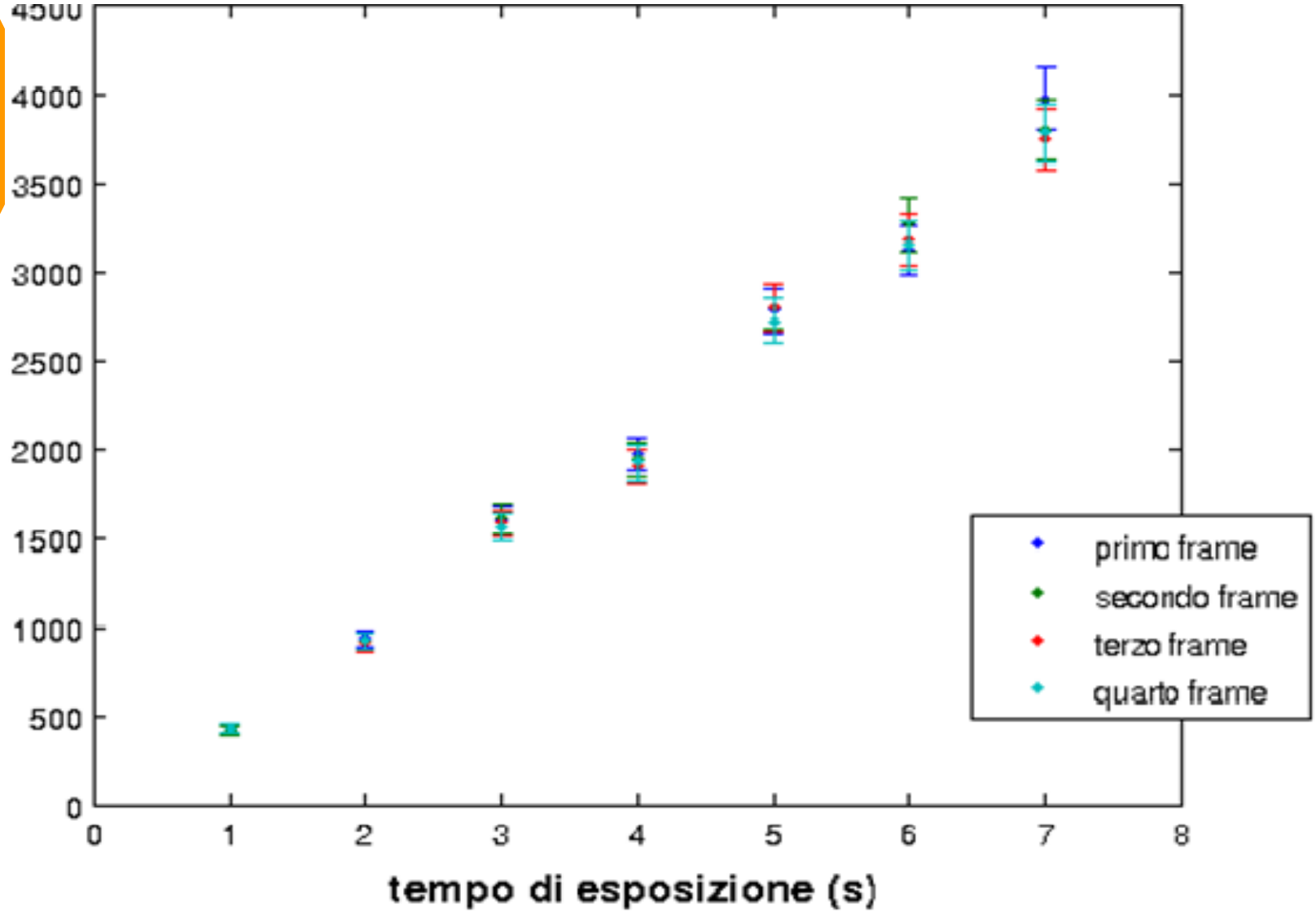

Conclusions

MPX2 can measure the beam characteristics on-line: very good agreement with reference systems measurements

Linearity as a function of the dose, independence on the dose rate above clinical dose rates and reproducibility of the measurements have been assessed.

The proposed detection system can be suitably applied in the monitoring and characterization oof the beam and of the dose in hadrontherapy and it can be considered as a valid alternative to the systems currently used for the beam characterization.

Spettro energetico

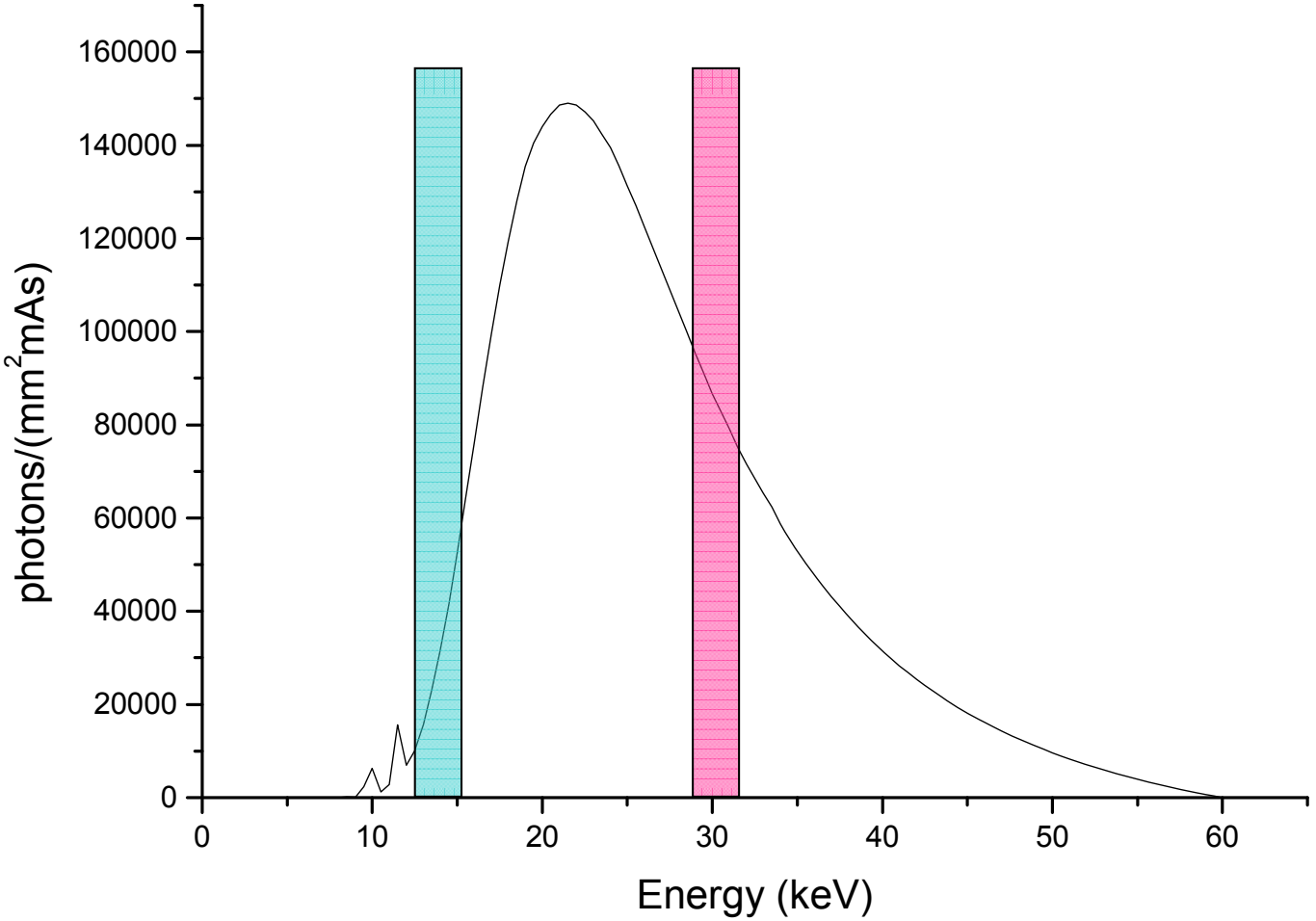

Fantoccio

- *Cilindro di plastica Ø = 1 cm riempito con:*
- *Polistirene: pezzi ~ 3 mm³;*
- *PMMA: pezzi ottenuti da rod Ø =3 mm*

Quarzo: rod Ø =1 mm

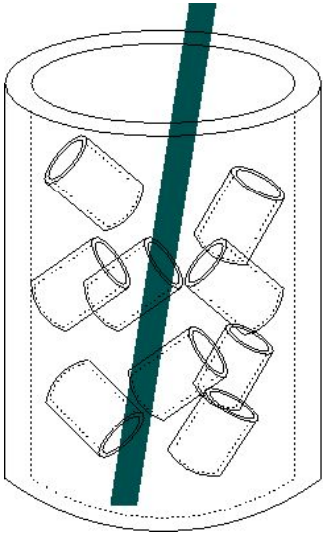

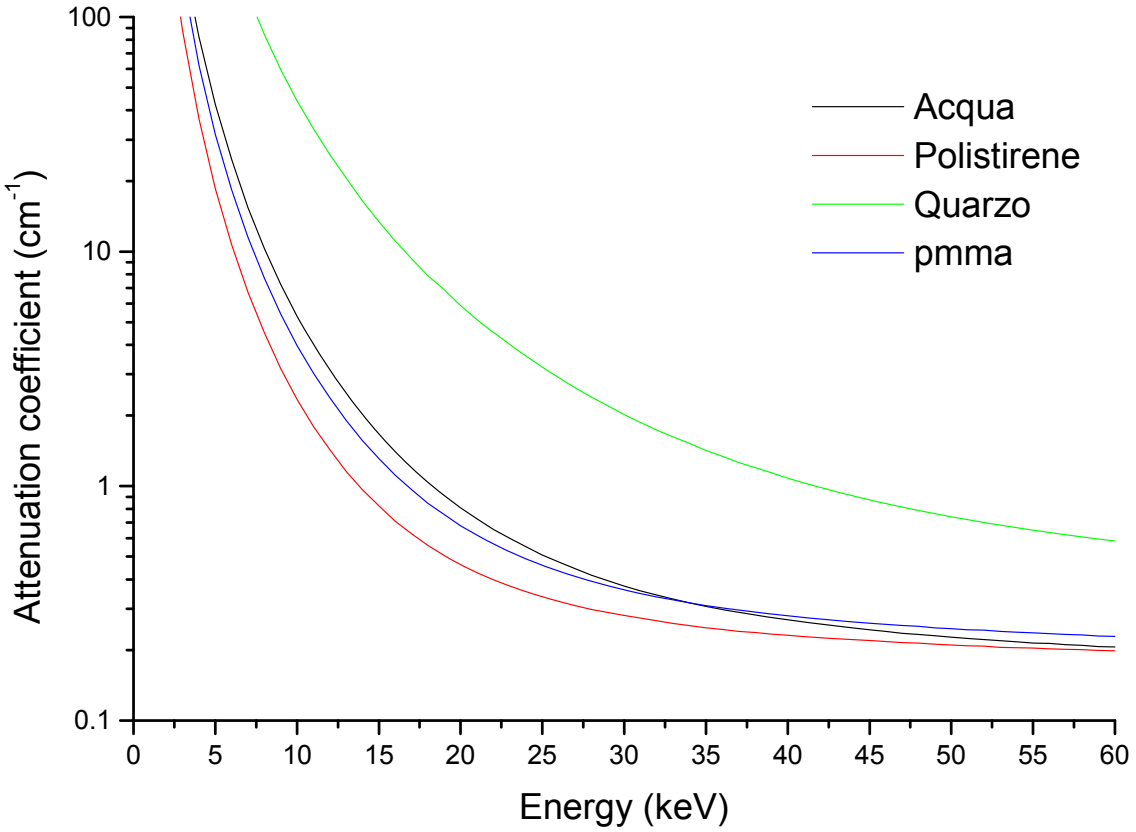

12.1-15.3 keV

26.7-30.1 keV

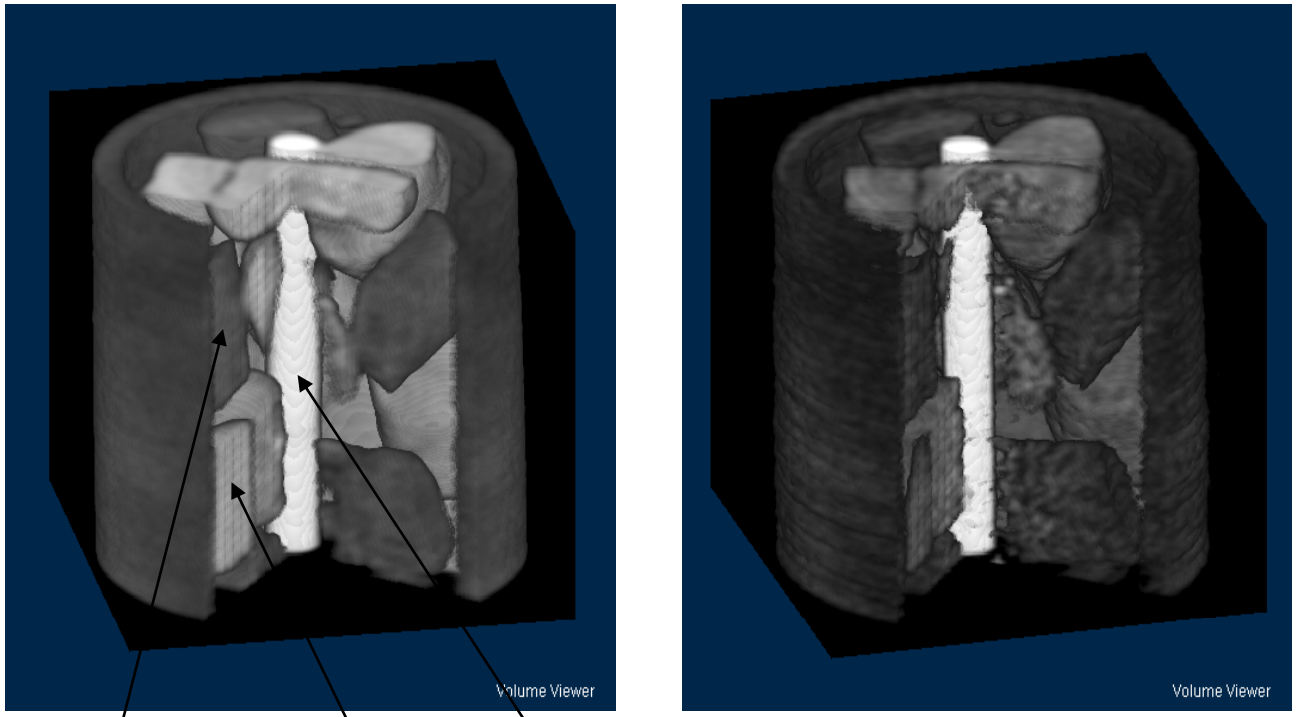

Polystyrene

Polyethylene Terephthalate

Silicon dioxide

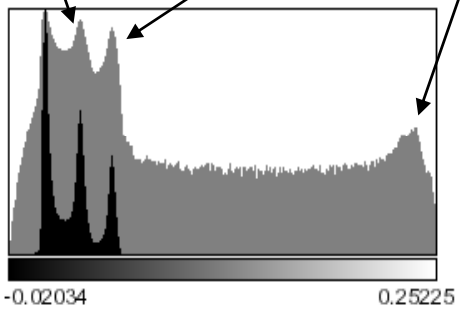

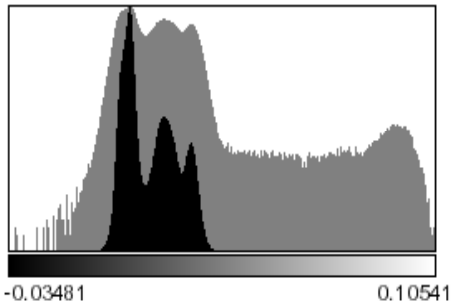

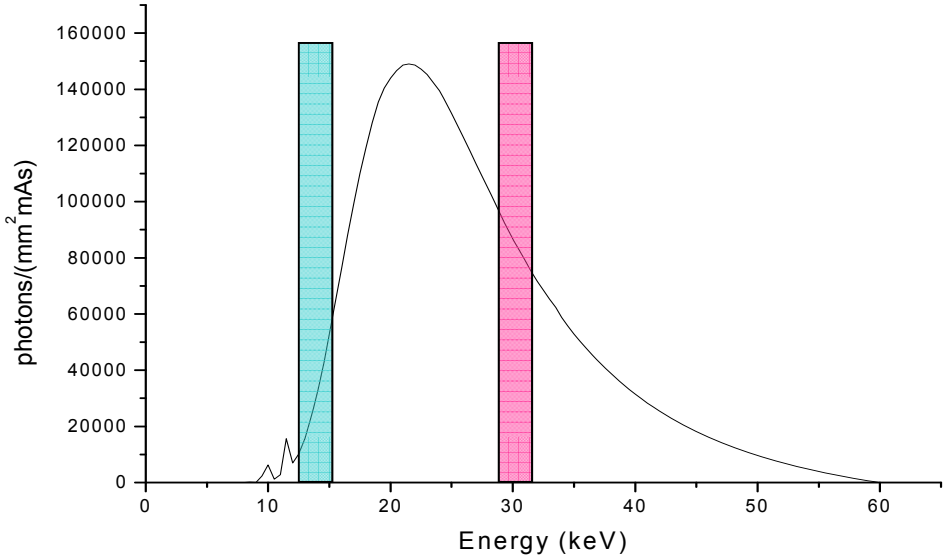

<E> = 13.21 keV

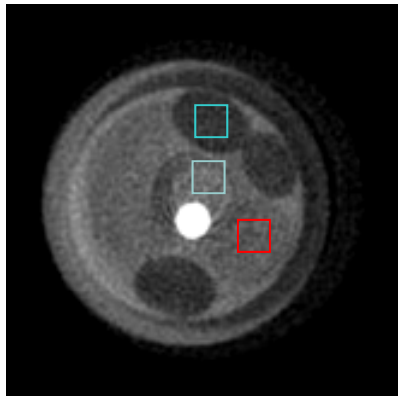

Cps = 34.4 ± 0.2 %

Cpmma = 11.5 ± 0.2 %

<E> = 27.01 keV

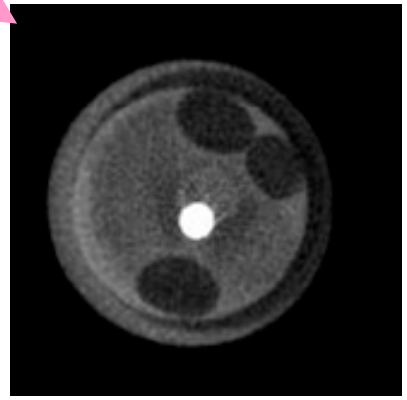

Cps = 28.6 ± 0.1 %

Cpmma = 8.2 ± 0.2 %

We have shown the good energy selection capability of our detection system also in CT applications: the SNR has a different maximum in energy for different thickness materials. For example for 3.1 mm Al thickness the SNR in the range 18.7-21.9 keV is 1.2 times the corresponding value for the whole spectrum. This improvement in SNR will lead to a better detectability of low contrast details as shown in the images below.

This study is preliminary for a future development of a dual-energy CT that could add functional information to the morphological information that is obtained in a CT examination.

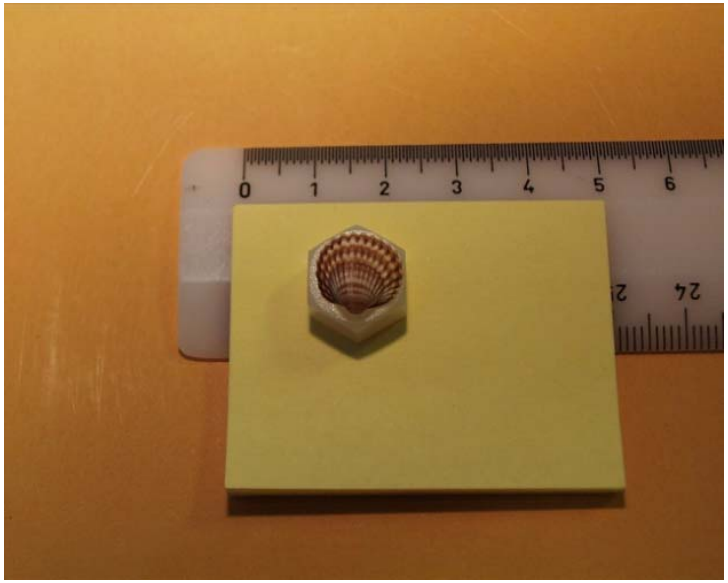

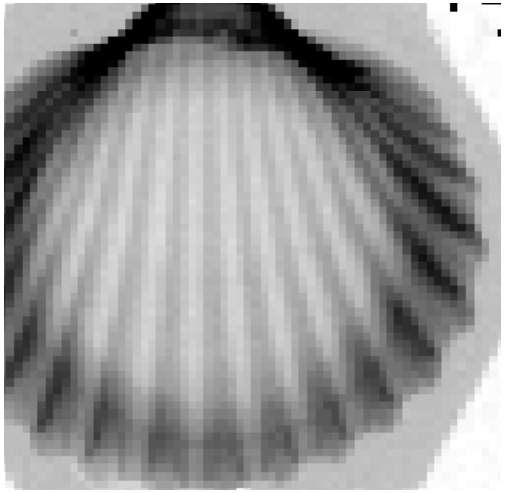

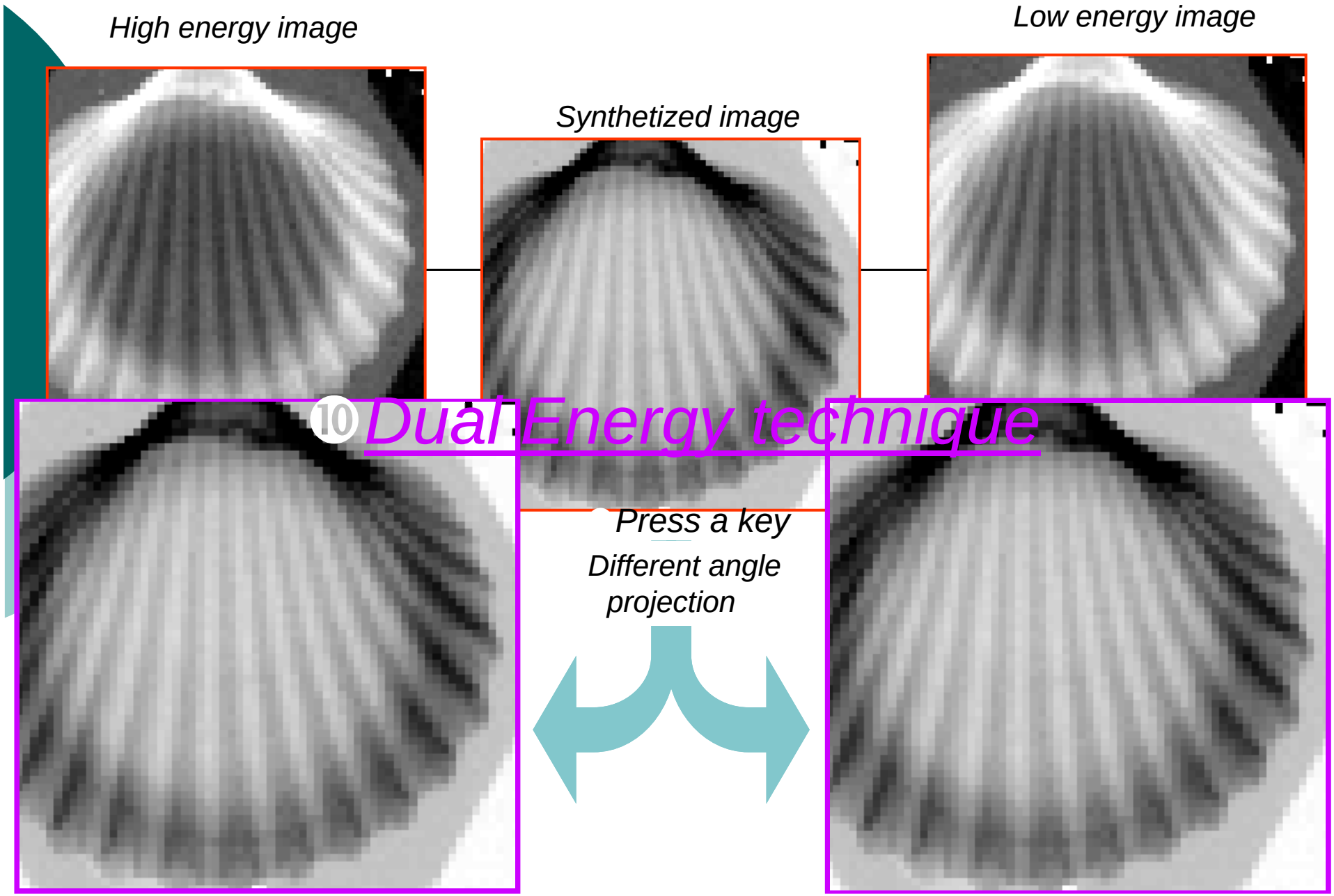
High energy image
Low energy image
Synthetized image
10 Dual Energy technique
Press a key
Different angle projection

Imaging con raggi X da luce di sincrotrone: metodi e applicazioni

Renata Longo
University of Trieste & INFN
Italy

Characteristics of synchrotron radiation (SR)

- High x-ray intensity on a broad energy range
  - Tunable monochromatic beam
    - Choose the optimum energy for a specific examinati
    - Dose optimization/reduction
    - Allow double energy subtraction techniques
    - No beam hardening effects or artifacts (tomography

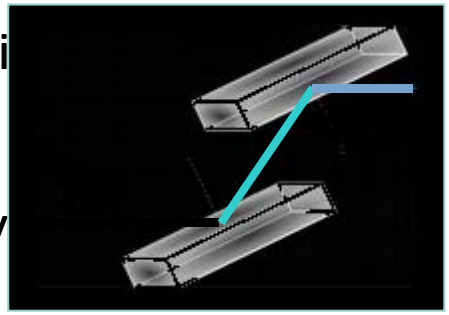

- Laminar beam geometry:
  the beam is naturally collimated
  - Images are acquired by scanning the object through the fan beam
  - High scattering rejection

- Small source size and
  large source-to-sample distance
  - High degree of lateral coherence
  - Phase contrast (PhC) imaging

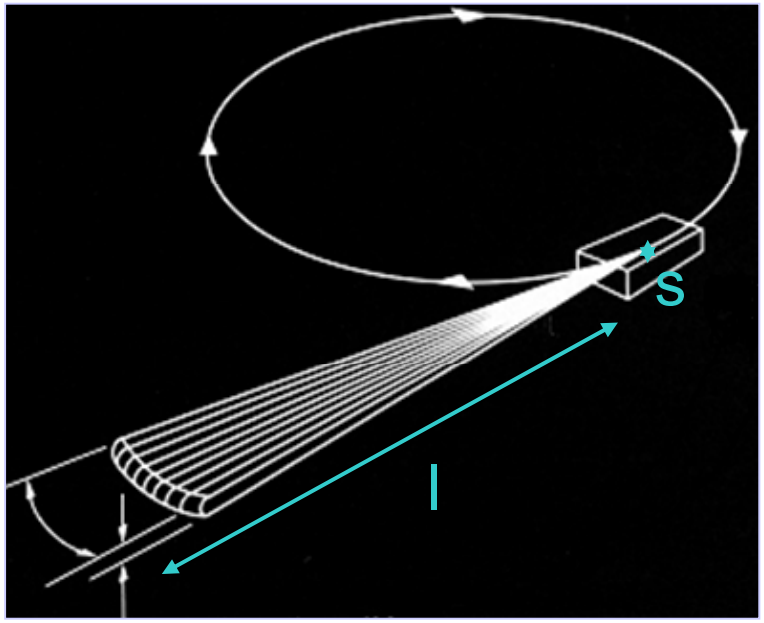

The SYRMEP Beamline (I)

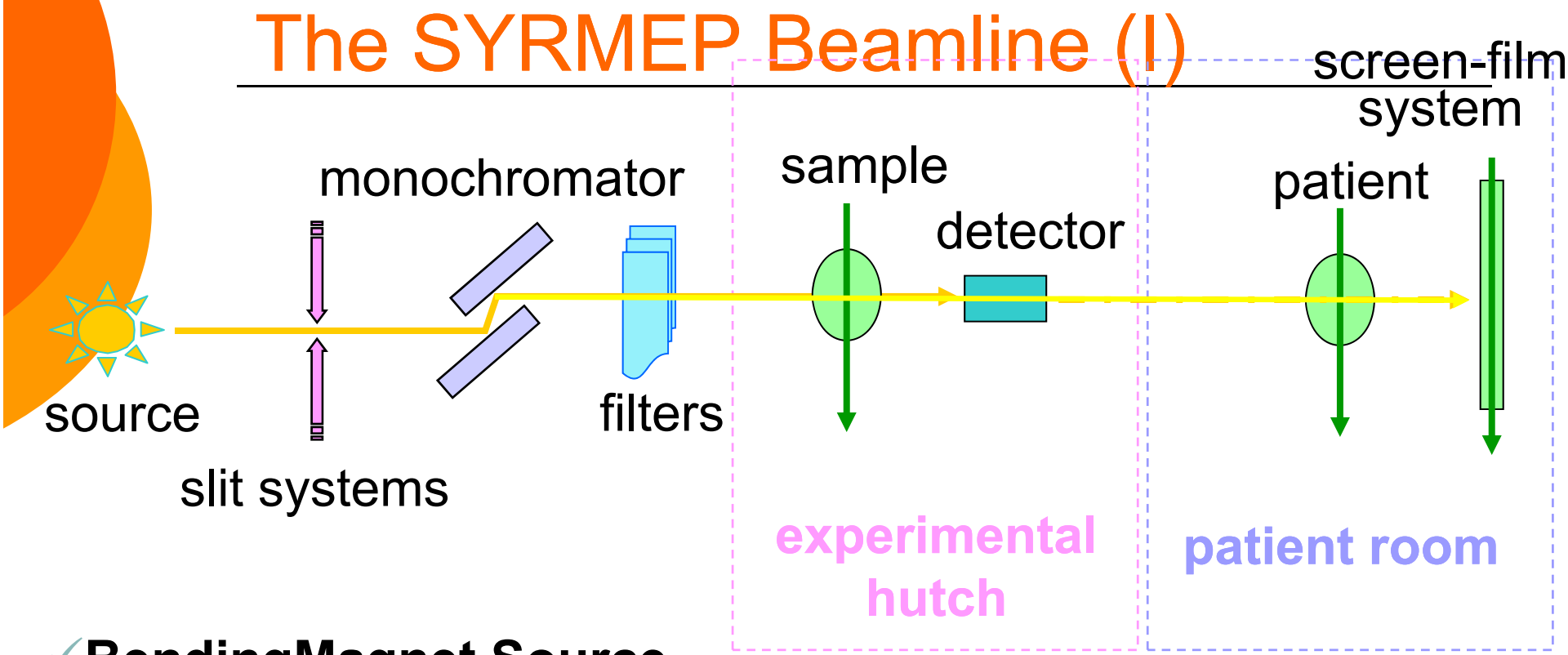

- ✓ **BendingMagnet Source**
- ✓ **Source size ~ 1.1 (horizontal) x 0.1 (vertical) mm^2**
- ✓ **Monochromatic beam with tuneable energy (8.5 - 35 keV)**
- ✓ **Bandwidth: $\Delta\lambda/\lambda \sim 2 \times 10^{-3}$**
- ✓ **Divergence: ~ 7mrad (horizontal) x 0.2 mrad (vertical)**

The SYRMEP Beamline (II)

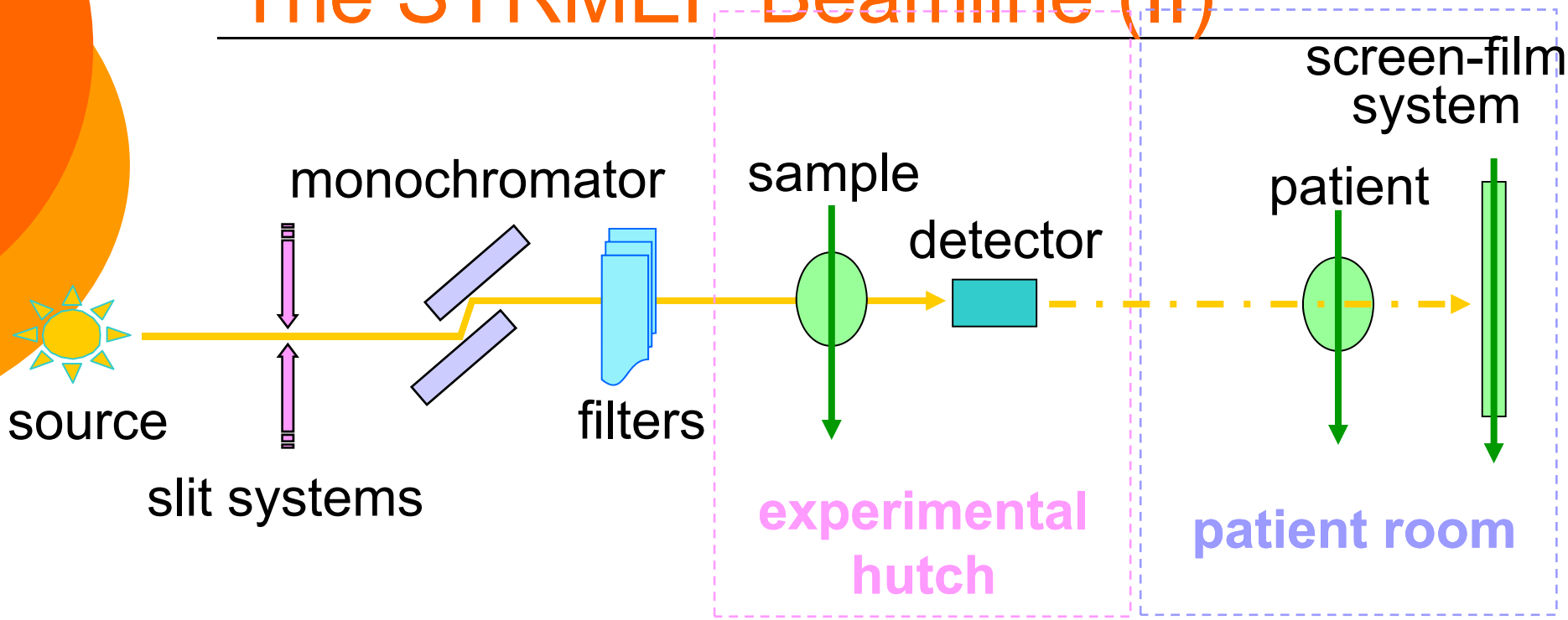

- **Source-to-Sampledistance:** ~ 23 m ~32 m
  Laminar beam cross section 4x 150 mm^2 4x 210 mm^2
- **Flux available at 17 keV (Elettra operated at 2.4 GeV, 140 mA ring current):** 6 10^8 ph/mm^2/s 2 10^8 ph/mm^2/s
  length at 17 keV ($L_c = \lambda R_1 / 2s$)
- 8 µm 11 µm

PICASSO Detector Requirements

- Laminar geometry
  - Matching beam cross section
    - 21 cm
  - Scatter Rejection
- High efficiency
  - Low dose
- High spatial/contrast resolution
- Wide dynamic range
  - Detect both high and low contrast
- Fast Rate Capabilities and Read-Out
  - Image acquisition in a few seconds

The SI microstripdetector: "edge-on" geometry

- Advantages of "edge-on" geometry:
  - High absorption efficiency
  - Matching the laminar geometry of the beam with a natural pixel array
- Problems:
  - Dead (undepleted) volume in front of the sensitive region that reduces the detection efficiency (~70-85% @20keV)

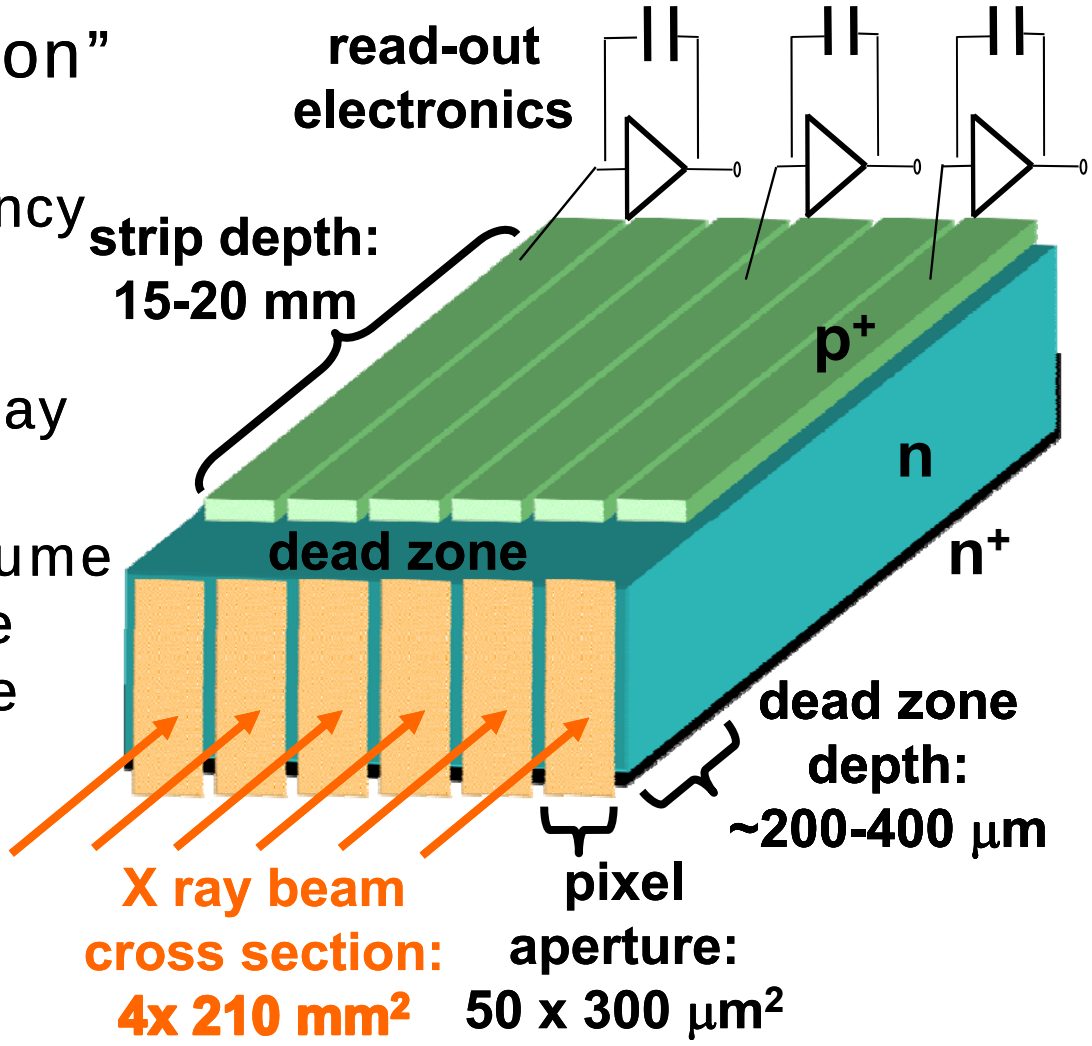

Single Photon counting

- Each strip is bonded to a channel of the read-out electronics. Each channel features:
  - Charge sensitive preamplifier
  - Shaper
  - Discriminator
  - Counter

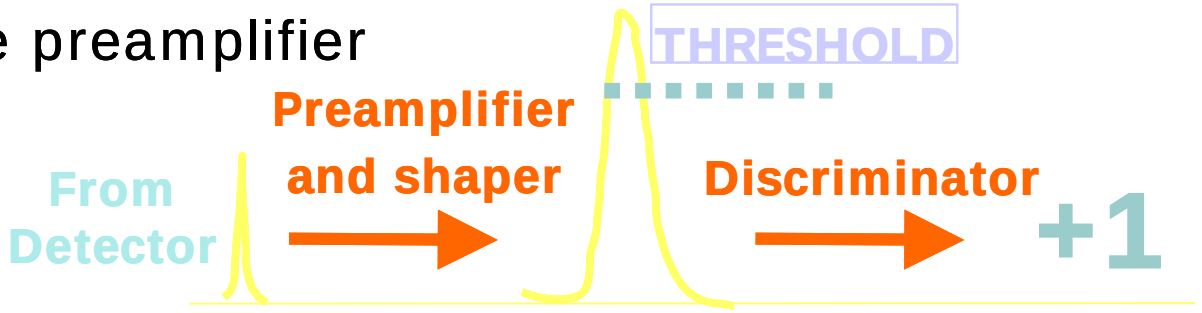

- Advantages
  - The quantum nature of the information carried by the photon beam is preserved
  - High (virtually infinite) dynamic range
- Challenges
  - Can we have a uniform response over all channels?
  - Can we have a low noise AND high acquisition speed (~MHz)?
  - Can we have all channels (pixels) counting simultaneously at full rate (when contrast is in the order of 1%)?

Photon counting electronics

- Mythen–II ASIC developed by the SLS detector group of the Paul Scherrer Institute (PSI, Swiss) for photon counting ASIC for powder diffraction studies
- Features:
  - 0.25 µm UMC technology
  - 128 channels, 50 micron pitch
  - 24 bit counter
  - 50 µm pitch
  - low noise preamplifier (noise about 230 e-)
  - 6-bit threshold trim DAC for each channel
  - Count rate: 1 MHz per channel

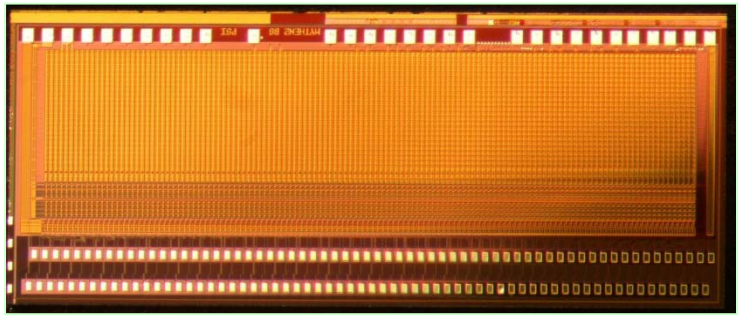

- Collaboration between INFN and PSI to apply the Mythen modules to SR imaging

Single layer design

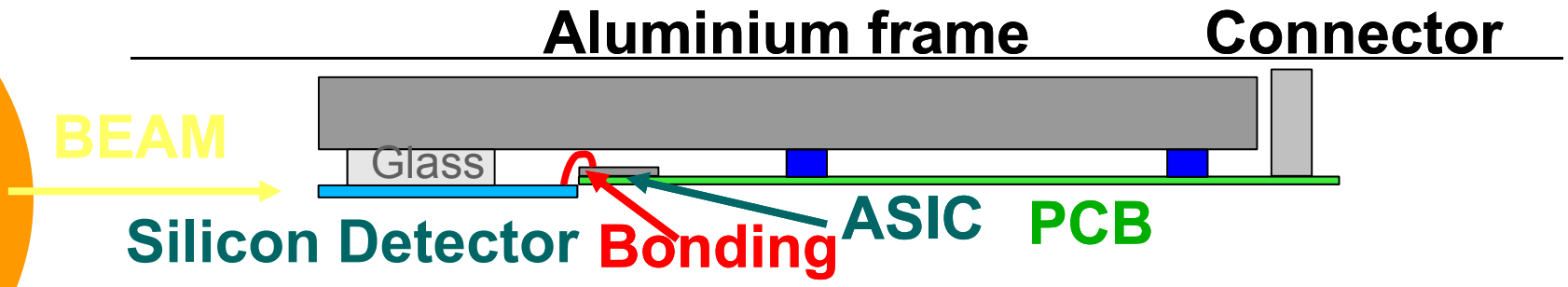

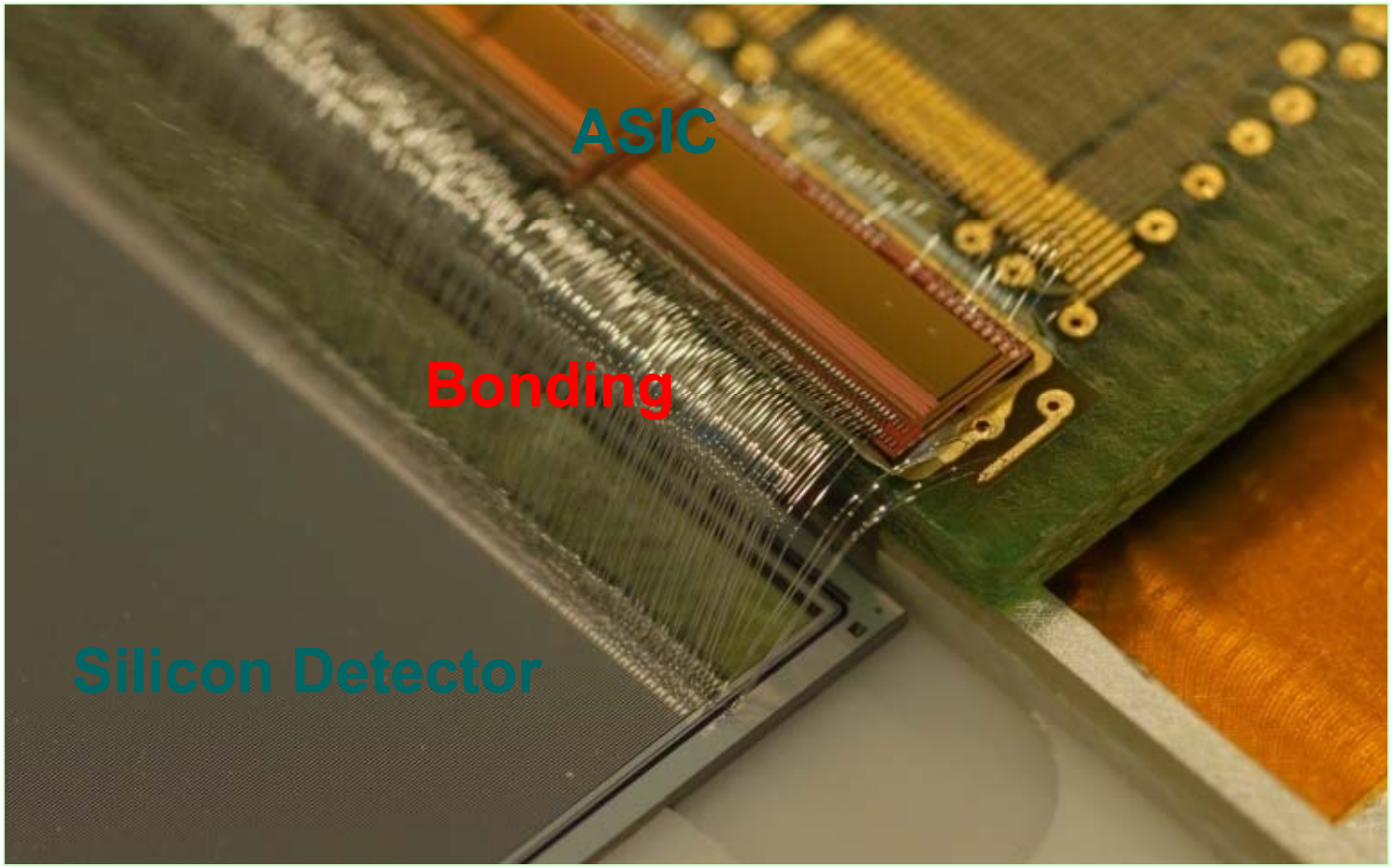

Double layer prototype

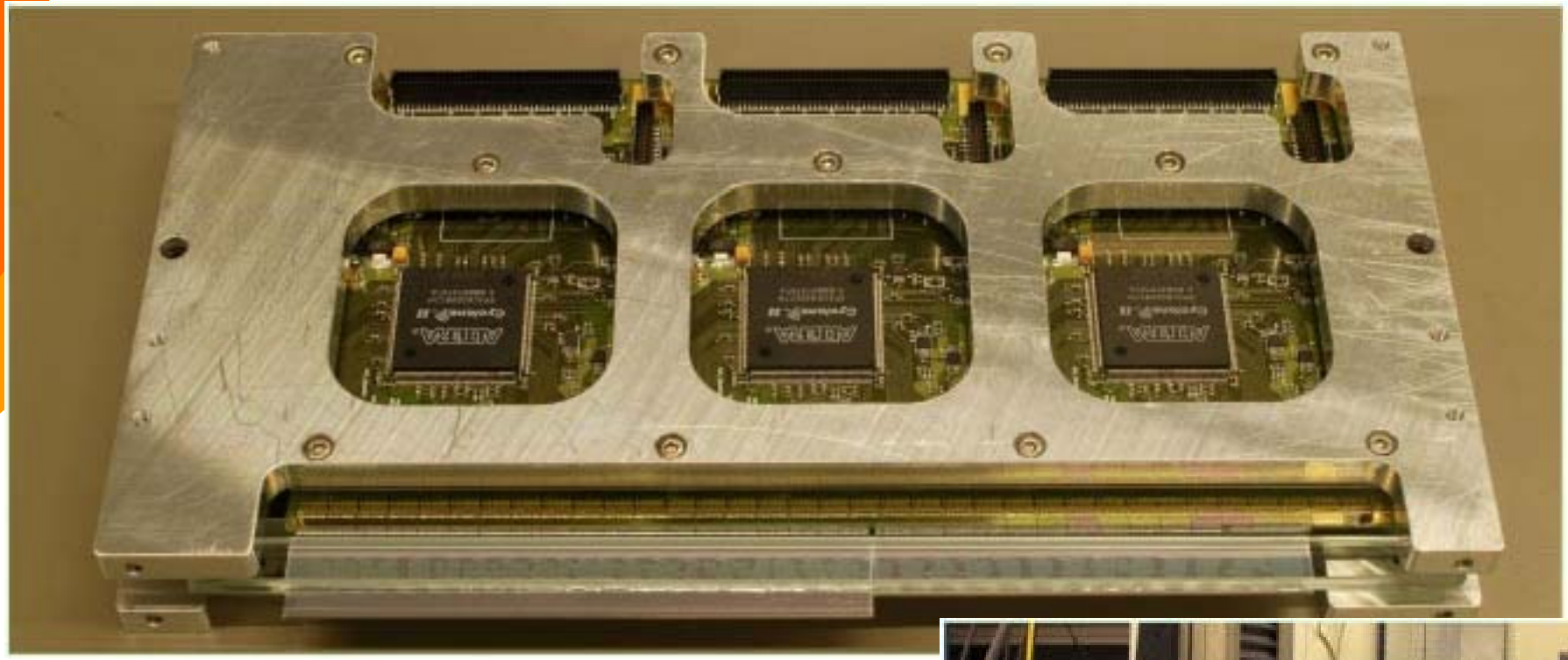

Double layer silicon detector prototype:

- Active area 210mm x 0.3 mm each layer

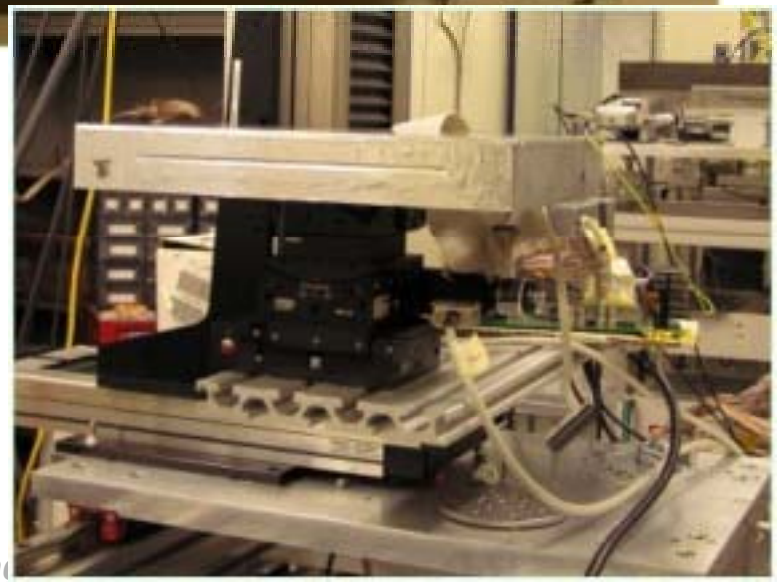

Quantitative tomography

- PICASSO detector was used
- The voxel values measured from the CT images were calibrated against the theoretical linear attenuation coefficients of 3 reference samples.
- The breast samples were histologically cut and evaluated
- Linear attenuation coefficients of different breast tissue components were measured from the tomographic slices.

Histology and Tomography selected images

- 23 keV
- 26 keV

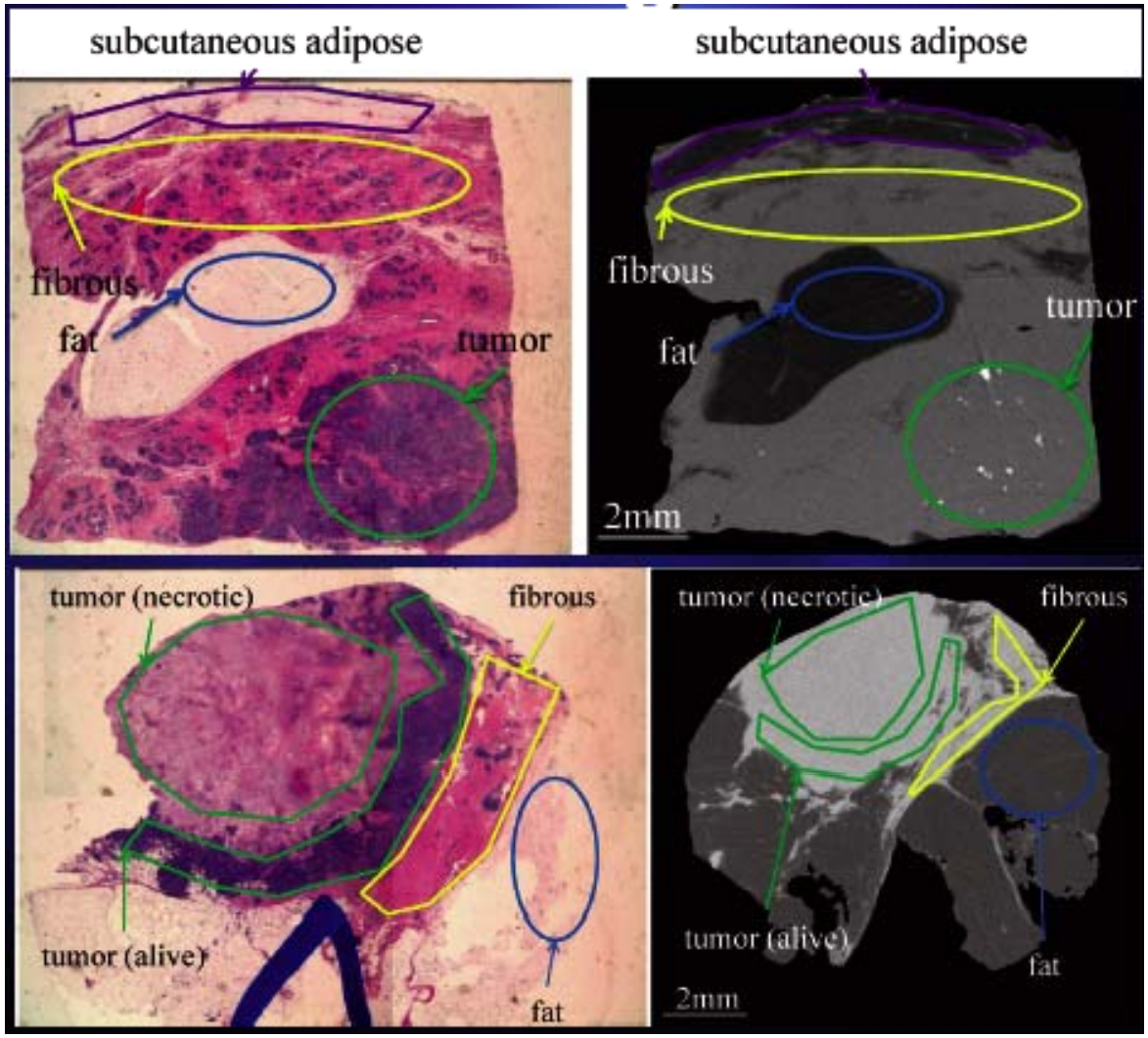

By courtesy of Renata Longo

Linear attenuation coefficient

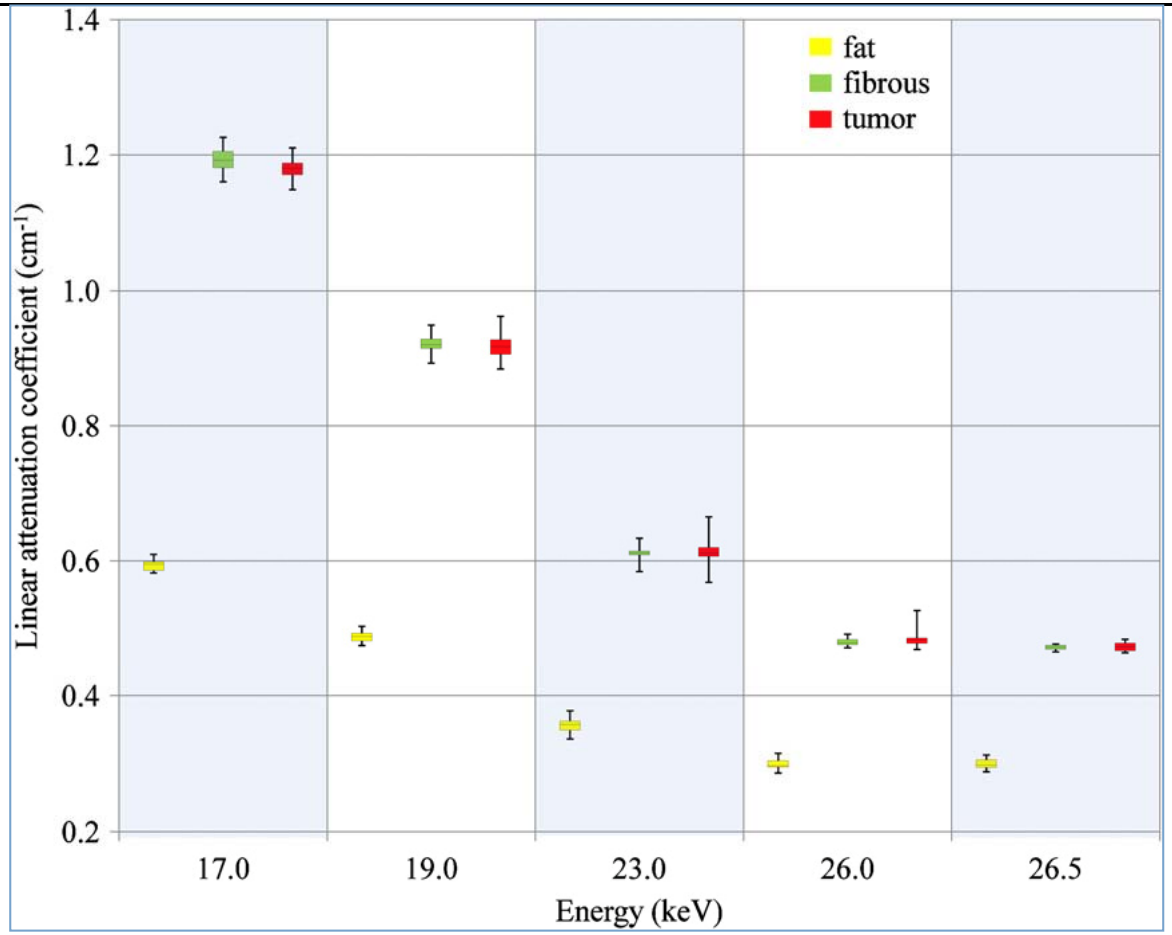

✓ ***No significant differences between fibrous tissue and tumor***

- ***Chen R.C., Longo R, Rigon L et al. Phys Med Biol 2010 55, 4993***

A violin tomographic study

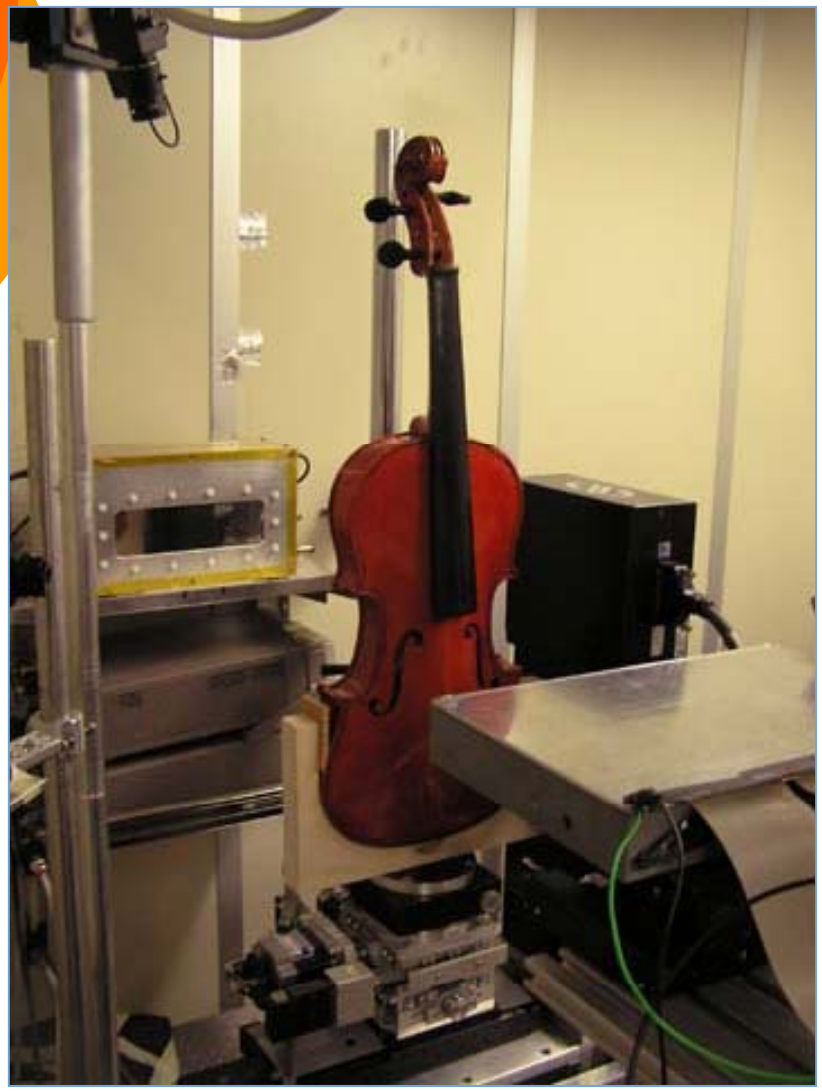

The main limitation in the use of synchrotron radiation is related to the reduced dimensions of the samples under investigation.
The development of new X-ray detectors designed for the particular characteristics allows the researchers to overcome this kind of problems.

Courtesy of Franco Zanini

A violin tomographic study

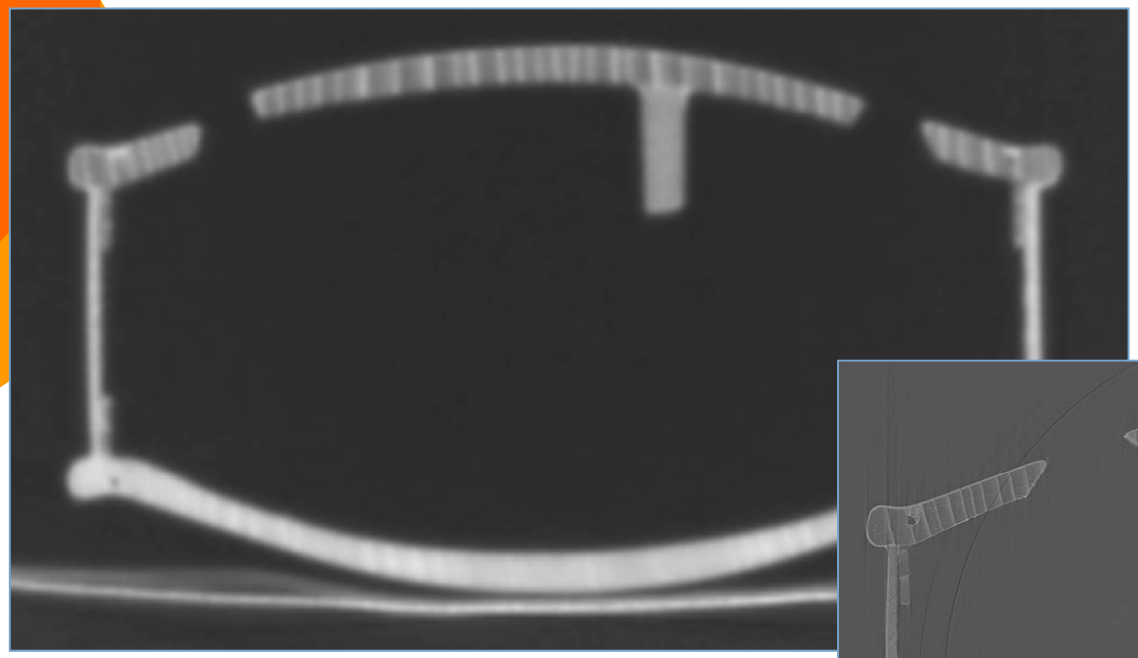

CT image acquired using a state-of-the-art clinical instrument

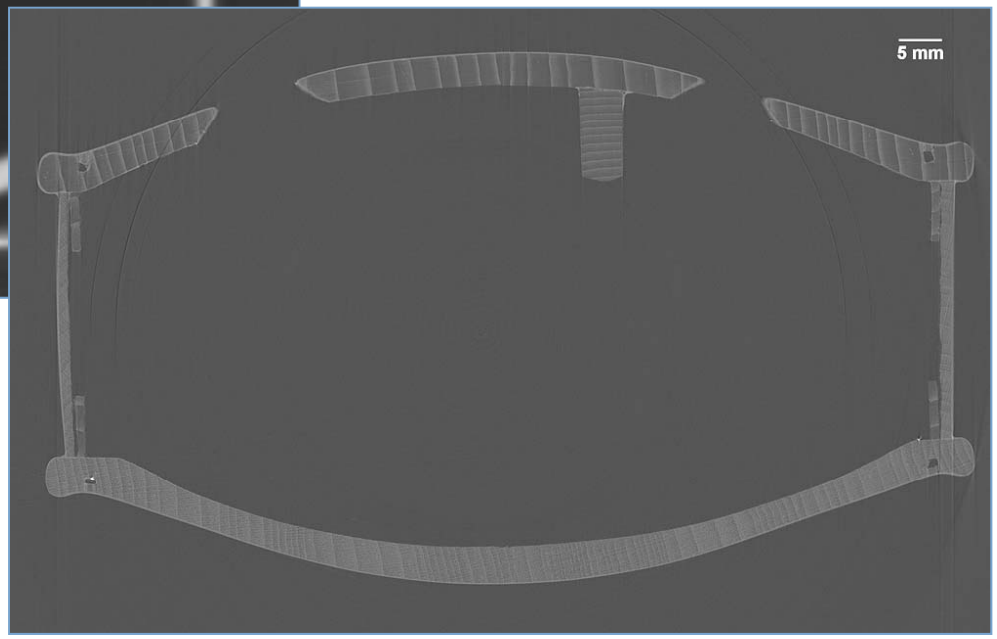

μCT acquired at SYRMEP (E = 23 keV)

A violin tomographic study

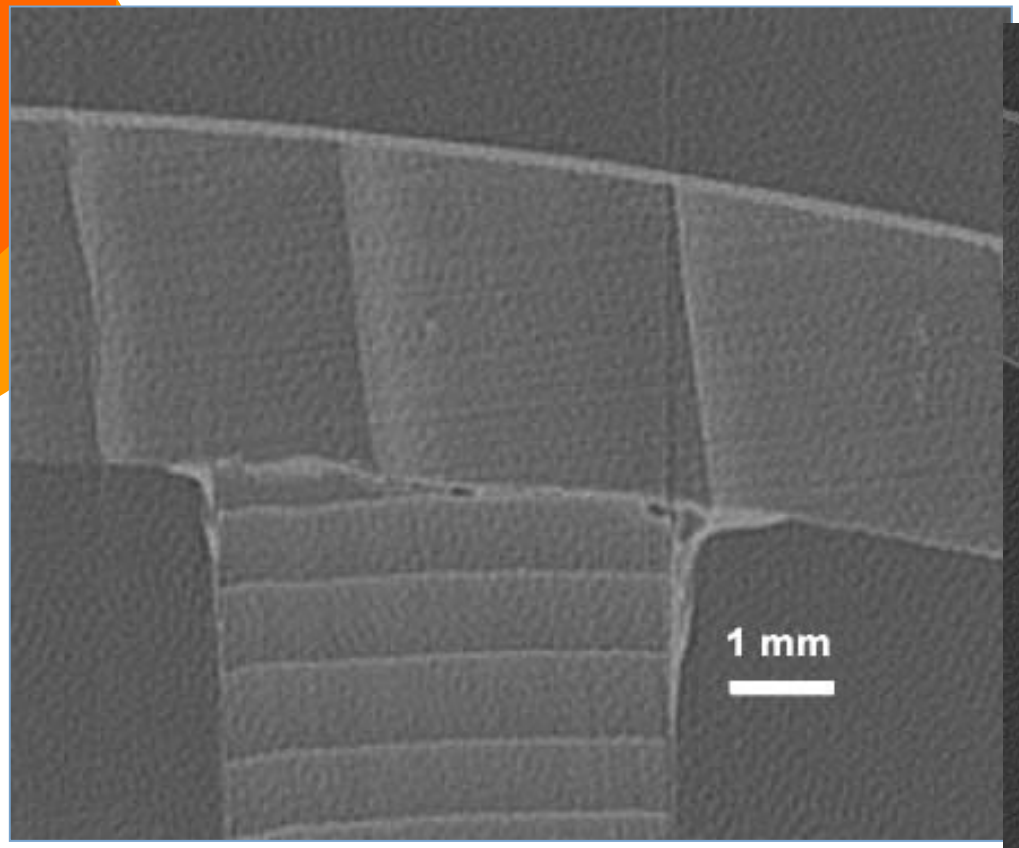

Detail showing the bass bar and the glue used to attach it to the front plate.

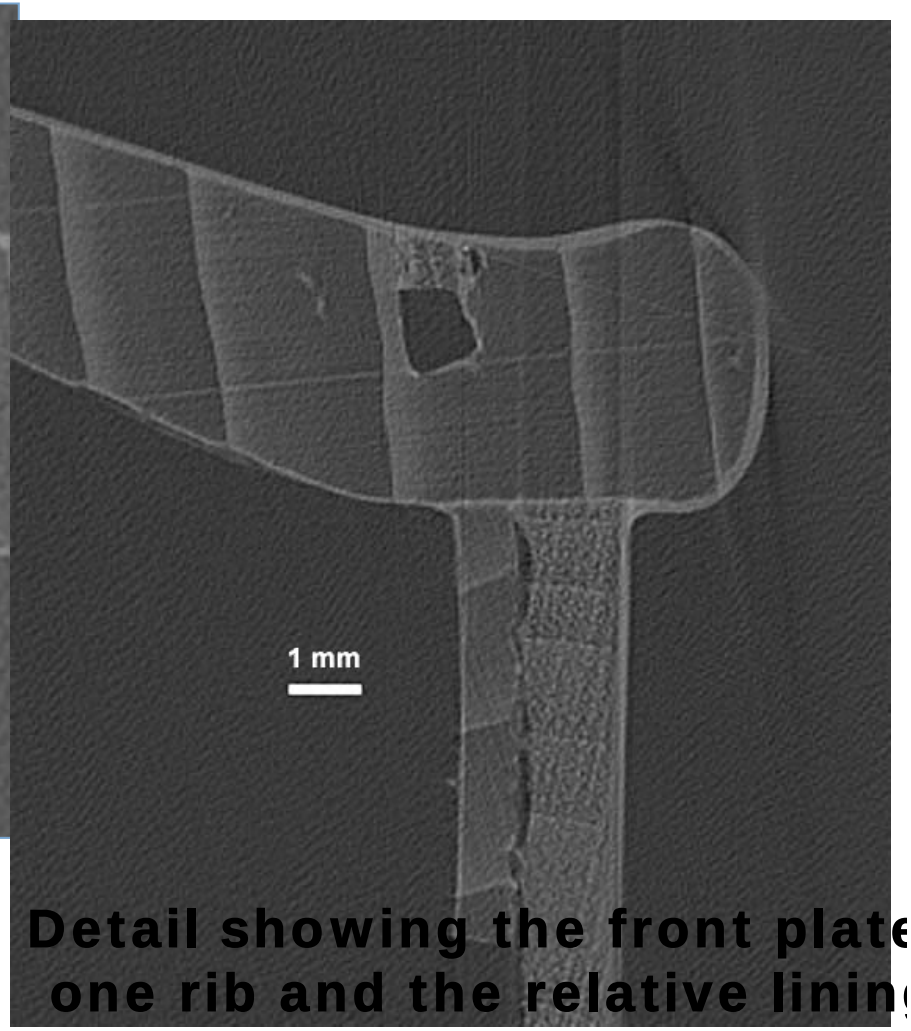

Detail showing the front plate one rib and the relative lining

Rigon L. et al. e-PS, 2010, 7, 71-77